SPECTRO-TEMPORAL BASED QUANTIFICATION OF BRAIN FUNCTIONS IN NEUROLOGICAL DISORDERS

BY

ROOHOLLAH JAFARI DELIGANI

A DISSERTATION SUBMITTED IN PARTIAL FULFILLMENT OF THE REQUIREMENTS FOR THE DEGREE OF

DOCTOR OF PHILOSOPHY

IN

ELECTRICAL, COMPUTER AND BIOMEDICAL ENGINEERING

UNIVERSITY OF RHODE ISLAND

2021

DOCTOR OF PHILOSOPHY IN ELECTRICAL, COMPUTER AND BIOMEDICAL ENGINEERING DISSERTATION

OF

ROOHOLLAH JAFARI DELIGANI

APPROVED:

Dissertation Committee:

Major Professor: Yalda Shahriari

Kunal Mankodiya

Walter Besio

Susan D'Andrea

Brenton DeBoef

DEAN OF THE GRADUATE SCHOOL

UNIVERSITY OF RHODE ISLAND

2021

ABSTRACT

Human brain studies that quantify neural functions using neuroimaging techniques have many applications related to neurological disorders, including characterizing symptoms, identifying biomarkers, and enhancing existing brain computer interface (BCI) systems. The first major goal of this dissertation is to quantify the neural functions associated with neurological impairments, specifically in amyotrophic lateral sclerosis (ALS), using two neuroimaging modalities, electroencephalography (EEG) and functional near-infrared spectroscopy (fNIRS), that respectively characterize electrical and hemodynamic neural functions. The next major goal is to integrate these modalities using state-of-the-art techniques including time-frequency based decompositions and functional and directional connectivity methods, and to use the quantified neural functions to classify different brain states through leading edge techniques, including information theory based fused feature optimization and deep learning based automatic feature extraction. In this dissertation, we explored the non-motor neural alterations in ALS patients reflected by simultaneously recorded EEG-fNIRS data both during task performance and in the resting state. Our results revealed significant neural alterations in ALS patients compared to healthy controls. Moreover, these neural signatures were used to classify data as coming from ALS patients versus healthy controls. For this purpose, we used mutual information-based fused feature optimization for EEG-fNIRS to select the best features from all the extracted neural markers, which considerably improved classification performance in classifying data as from people with ALS vs. healthy controls based on mental workload. These results support the idea of using complementary features from fused EEG-fNIRS

in neuro-clinical studies for the optimized decoding of neural information, and thus, improving the performance of relevant applications, including BCIs and neuro-pathological diagnosis. In addition, we examined our findings in motor imagery classification, another fundamental processing step in applying BCIs for people with neurological disorders, including ALS patients. To do this, we proposed a convolutional neural network-based classification architecture for automatic feature extraction from EEG-fNIRS data, which outperformed conventional classification methods using manually extracted features. These outcomes suggest promising improvements in BCI performance using multimodal EEG-fNIRS and deep learning classifiers with automatic feature extraction, which can be utilized in clinical applications for people with neurological disorders including ALS patients. These findings can be further developed to automate the optimal quantification of neural functions in neurological disorders, with less dependence on prior knowledge, and thereby facilitate BCIs and other clinical applications for patients with neurological disorders.

ACKNOWLEDGMENTS

First, I would like to thank my major professor, Dr. Yalda Shahriari, for her support throughout my time in the Biomedical Engineering program, helping me to become a better scientist. Her support enabled this dissertation.

I would also like to thank my committee members. Dr. Besio has supported me in this way by providing feedbacks for my work. Dr. Mankodiya and Dr. D'Andrea broadened my horizons during my graduate career with their course programs at URI. I look forward to continue their ways by what I learnt from them.

Truly, I would like to thank my entire academic community: all my lab mates, past and present, my fellow graduate students at URI, my professors, and the scholars I may never have taken a class from but who nevertheless influenced my work. I look forward to being able to see you again.

Finally, I would like to thank my family and friends for their support and encouragement, so I could finish and enjoy the life on the way.

PREFACE

This dissertation is written in manuscript format. The first chapter serves as an introduction to the dissertation as a whole, providing an overview of the main topics and a justification for the research. The first chapter additionally notes the four primary aims for the research described in this dissertation. The remaining chapters are the manuscripts. The first manuscript, Multimodal exploration of non-motor neural functions in ALS patients using simultaneous EEG-fNIRS recording, was published in the *Journal of neural engineering*. This manuscript primarily addresses the first research aim. The second manuscript, Electrical and hemodynamic neural functions in people with ALS: an EEG-fNIRS resting-state study, was published in the *Journal of IEEE Transactions on Neural Systems and Rehabilitation Engineering* and primarily addresses the second research aim. The third manuscript, Multimodal fusion of EEG-fNIRS: a mutual information-based hybrid classification framework, was published in the *Journal of Biomedical Optics Express*. This manuscript primarily addresses the third research aim. The fourth manuscript, Multimodal fusion of EEG-fNIRS: a mutual information-based hybrid classification framework, addresses the fourth research aim and is in preparation for submission to *Neurocomputing*.

TABLE OF CONTENTS

Page

ABSTRACT……...……..…….ii

ACKNOWLEDGEMENTS……...…….……iv

PREFACE……...…...……...v

TABLE OF CONTENTS…….……...……vi

LIST OF FIGURES……..……...…..…..…….x

LIST OF TABLES…….…….……..…….xiv

1. INTRODUCTION……..…….1

1.1 Motivation……...……1

1.2 Recording Modalities……...……...3

1.2.1 Electroencephalography (EEG)……3

1.2.2 Functional Near-Infrared Spectroscopy (fNIRS)….……6

1.3 Amyotrophic Lateral Sclerosis (ALS)……...…….7

1.4 Experimental Protocols……...…....9

1.4.1 Visual Oddball Task…….……9

1.4.2 Resting-State…….……..……10

1.5 This Dissertation ……..….10

1.6 Overall Discussion…….……...……14

2. MULTIMODAL EXPLORATION OF NON-MOTOR NEURAL FUNCTIONS IN ALS PATIENTS USING SIMULTANEOUS EEG-FNIRS RECORDING……..18

2.1 Background…….…….20

2.2 Methods……23

2.2.1 Subjects…….….23

2.2.2 Experimental Protocol……...……24

2.2.3 Data Acquisition…….…….25

2.2.4. Data Analysis……..…….26

2.3 Results…….29

2.3.1 EEG Results…….….29

2.3.2 fNIRS Results…….……...…31

2.3.3 Correlation Results…….……..….33

2.4 Discussion…….……..36

3. ELECTRICAL AND VASCULAR NEURAL FUNCTIONS IN PEOPLE WITH ALS: AN EEG-FNIRS RESTING-STATE STUDY….43

3.1 Background…….45

3.2 Methods……..……49

3.2.1 Subjects……49

3.2.2 Experimental Protocol…….50

3.2.3 Data Acquisition……...……...……50

3.2.4 EEG Signal Processin.……...……..52

3.2.5. fNIRS Signal Processing…….53

3.2.5.1 Hemodynamic Resting-State Directional Functional Connectivity…….....54

3.2.6 Statistical Analy…….…..55

3.3 Results…….56

3.3.1 EEG Power ……..56

3.3.2 fNIRS Power ……...…….58

3.3.3 Electrical Resting-State Functional Connectivity (RSFC) …59

3.3.4 Hemodynamic Resting-State Functional Connectivity (RSFC)……..……61

3.3.5 Hemodynamic Resting-State Directional Functional Connectivity (RSDFC)…….. 63

3.4 Discussion…….....65

Appendix…….……...……...…..74

4. MULTIMODAL FUSION OF EEG-FNIRS: A MUTUAL INFORMATION-BASED HYBRID CLASSIFICATION FRAMEWORK……..…..83

4.1 Background……..85

4.2 Methods……...….93

4.2.1 Subjects…….……..……..93

4.2.2 Experimental Protocol ……..……93

4.2.3 Data Acquisition …….....……94

4.2.4 Data Analysis ……94

4.3 Results…….….101

4.4 Discussion……..…….……...…..105

Appendix……..…….……...…..110

5. DEEP LEARNING BASED MULTIMODAL EEG-FNIRS CLASSIFICATION: AN APPLICATION TO MOTOR IMAGERY….117

4.1 Background…….……..118

4.2 Methods…….……...….123

4.3 Results…….…….….131

4.4 Discussion……..…….…….……...…..135

VITA……...……..……..….143

LIST OF FIGURES

page

Figure 1.1. International 10-20 system electrode placement on a 3-D head from two views of top (top-left) and side (top-right). The bottom figure shows 10-20 system (red electrodes) and the extended system (white electrodes) on a 2-D plot……..4

Figure 1.2. The waveform of ERP components ……..…….5

Figure 1.3. Emitter-detector pairs showing the banana-shaped paths of light ……..……7

Figure 2.1. A schematic montage of the EEG sensors-fNIRS optodes……...……27

Figure 2.2. Boxplots showing changes (mean±SD) in average P300 amplitude (top left), P600 (top right), N200 (bottom left), and N400 amplitude (bottom right) for ALS participants (red) and healthy controls (blue). For each plot, the maximum *p*-value among channels is shown at……...30

Figure 2.3. Average time-frequency decomposition across all healthy controls (left) and ALS participants (right) for channel Fz. The significant differences between each group (healthy vs. ALS) for each frequency band are illustrated by a black dashed rectangle……...….……31

Figure 2.4. Average target HbO responses evolving from 2 sec pre-stimulus to 6 sec post-stimulus for both ALS (red) and control (blue) groups. The vertical dashed line and the shaded yellow area denote the target stimulus onset and post-stimulus respectively……32

Figure 2.5. Spearman correlation (rho) between obtained significant EEG features in the delta, theta, and beta frequency bands and windowed fNIRS peak HbO in the healthy control (left) and patient (right) groups. Significant corrected *p*-values ($p<0.05$ before

rounding to the nearest 100th) are shown in white, and all other values are displayed in black. Only correlation maps with significant *p*-values and their counterparts in the patient group are displayed……...…….34

Figure 3.1. Schematic head model of the fNIRS-EEG sensors' placement…….……49

Figure 3.2. Channel map of averaged EEG power within the delta, theta, alpha and beta frequency bands for healthy controls and ALS patients…….……54

Figure 3.3. Channel map of averaged HbO2 power for very low frequency oscillations (VLFO) and low frequency oscillations (LFO) for healthy controls and ALS patients..56

Figure 3.4. Head plots of RSFC activation index (negative logarithm of the p-values) obtained from the statistical comparison of averaged magnitude squared EEG coherence between ALS patients and healthy controls in four frequency bands (delta, theta, alpha, and beta) and for three channels as seed channels (Fz, Cz, Pz). The significant p-values after multiple comparisons correction are illustrated with dashed lines between the seed channel (highlighted in blue) and the significant region at the other end (highlighted in red based on the connection's activation index)…….58

Figure 3.5. Frontal head plots illustrating activation indices (negative logarithm of the *p*-values) calculated from the statistical comparison of averaged HbO2 correlation between ALS patients and healthy controls for 8 seed channels. The significant *p*-values after multiple comparisons are illustrated by dashed lines between the seed channel (highlighted in blue) and the significant region at the other end (highlighted in red based on the connection's activation index). The numbers in the figure indicate channel numbers…….59

Figure 3.6. Directional functional connectivity matrix for Healthy controls (top), ALS patients (middle) and significantly altered connections in ALS patients (bottom). Channel numbers are illustrated at the left and bottom side of each matrix……..…..61

Figure S3.1. Channel map of averaged HbR power for very low frequency oscillations (VLFO) and low frequency oscillations (LFO) in healthy controls and ALS patients...72

Figure S3.2. Frontal head plots illustrating activation indices (negative logarithm of the *p*-values) calculated from the statistical comparison of averaged HbR correlations between ALS patients and healthy controls for eight seed channels (highlighted in blue)……...73

Figure 4.1. Sequential feature selection pseudo-code.……..…….94

Figure 4.2. Classification accuracy of single and hybrid modalities for variable sizes of the selected optimal feature subset (averaged across sub-folds of the validation dataset for fold 1 (top) and fold 2 (bottom)).……..97

Figure 4.3. Relative portions of included features from each feature category/subcategory averaged over optimal selected feature sets from all sub-folds....98

Figure 4.4. Classification performance characteristics for single and hybrid modalities……..99

Figure 4.5 Classification performance characteristics for the selected optimal feature subset and the original set of features without any feature selection procedure..…….100

Figure S4.1. The oddball-based visuo-mental dual-task paradigm and an example of the arithmetic operation the participant performed..……....…….105

Figure 5.1. Overview of task blocks and timing. At each imagination block, only one of the pictures of the right- or left-hand was depicted for subjects……...…….117

Figure 5.2. Block diagram of dual CNN for EEG and FNIRS. Automatically extracted features are merged at the output layer of CNN and then fed to a FCN.……..…….122
Figure 5.3. Classification results for MI versus rest classification obtained from LDA, FCN, and CNN+FCN for each subject using only EEG data. Error bars show the standard deviation of test accuracy across five folds.…….....…….123
Figure 5.4. Classification results for MI versus rest classification obtained from LDA, FCN, and CNN+FCN for each subject using only fNIRS data. Error bars show the standard deviation of test accuracy across five folds.……...…...…….124
Figure 5.5. Classification results for MI versus rest classification obtained from LDA, FCN, and CNN+FCN for each subject using hybrid EEG-fNIRS data. Error bars show the standard deviation of test accuracy across five folds.…….……...…….124
Figure 5.6. Classification results for left versus right MI classification obtained from LDA, FCN, and CNN+FCN for each subject using only EEG data. Error bars show the standard deviation of test accuracy across five folds.……...……...…….125
Figure 5.7. Classification results for left versus right MI classification obtained from LDA, FCN, and CNN+FCN for each subject using only fNIRS data. Error bars show the standard deviation of test accuracy across five folds.…….……...…….125
Figure 5.8. Classification results for left versus right MI classification obtained from LDA, FCN, and CNN+FCN for each subject using hybrid EEG-fNIRS data. Error bars show the standard deviation of test accuracy across five folds.……...…….126

LIST OF TABLES

page

Table 2.1. ALS Subjects Demographic Information…….24

Table 3.1. ALS Subjects Demographic Information……47

Table S3.1. Healthy control's demographic information ……...……71

Table 5.1. Classification performance metrics for MI-state versus resting-state classification and for left MI versus right MI classification obtained from LDA, FCN, and CNN+FCN methods using single and hybrid modalities.……..……127

CHAPTER 1: INTRODUCTION AND OVERVIEW

1.1 MOTIVATION

Any type of structural, chemical, or electrical dysfunction in neural cells can alter human brain functions. The human brain is a highly organized functional network with numerous neurons and connections between them serving various functions including cognition, thought, emotions, sensory functions, motor functions, memory, and language. This highly organized functional network is served and supported by a dense network of intercommunicating blood vessels and capillaries to deliver nutrients such as oxygen and glucose to the neurons for metabolism. Up to 1 billion people around the world currently suffer from neurological disorders due to injury, disease or inheritance (alsa.org). These neurological disorders, including amyotrophic lateral sclerosis (ALS), multiple sclerosis, Alzheimer's disease (AD), Parkinson's disease (PD), epilepsy, and stroke, can affect different aspects of normal brain functions and cause various symptoms including partial or complete paralysis, communication difficulties, seizures, poor cognitive abilities, attention deficits, decreased alertness, numbness, and pain, all of which can affect activities of daily living for these patients.

Much effort and many studies have sought to characterize the biomarkers of neural disorders for clinical applications, including early diagnosis and the engineering of assistive equipment. A category of assistive tools known as brain computer interfaces (BCI) have been designed and developed for patients who have lost their normal neuromuscular pathways to support their interactions with their environment. A BCI is a communication pathway between a brain under recording equipment and an external computer such that the computer takes commands directly from the brain, bypassing the

normal pathway of central and peripheral nerves (Wolpaw 2007). Specifically, the signals that are recorded from the brain are the input to the BCI system, which are then processed with various signal processing techniques to be translated into an output that delivers the user's intentions for communication or control (e.g. word spelling). Users receive visual, auditory, or tactile feedback on this output, which affects their brain activity and consequently their subsequent outputs. Despite great advances in the enhancement of BCIs for neuromuscular diseases, these systems are not sufficiently robust for consistently assisting patients due to variations in day-to-day and subject-to-subject performance, along with inefficient performance in long-term use (Kellmeyer et al., 2018). One reason for this instability is that most of these systems neglect the involvement of essential neural biomarkers and patient signatures such as cognitive markers (Kuruvilla et al., 2013). Thus, understanding the different neural characteristics of these disorders with respect to the task and paradigm will be pivotal for practical BCI use. This can lead to quantifying different neural functions essential in optimizing BCI-relevant parameters, and thus, maximizing BCI efficacy.

To characterize neural functions and control BCIs, a variety of neuroimaging techniques can be used. This became more practical with the development of non-invasive neuroimaging techniques which can detect and measure brain activities through electrical changes using electroencephalography (EEG), magnetic field changes using magnetoencephalography (MEG), and also through hemodynamic changes with functional magnetic resonance imaging (fMRI), functional near-infrared spectroscopy (fNIRS), and positron emission tomography (PET), though use remains somewhat limited. Due to their complex technical requirements, expense and real time capabilities,

MEG, fMRI and PET are not currently suitable for constant use. However, EEG and fNIRS are likely to have practical value for clinical use in the near future.

Human brain studies quantifying neural functions using neuroimaging have made a path towards many applications related to neurological disorders including diagnosis, symptom characterization, associative factor discovery, and BCI system enhancement. In this research, the primary objective is to use EEG, fNIRS, and the integration of these modalities to explore the neural signatures of pathological conditions including ALS compared to healthy controls during both task and resting-state paradigms. These efforts can eventually support a better understanding of the disease and enhance diagnostic approaches. Moreover, characterizing neural alterations can be used to design more specific, personalized BCI systems based on the most distinguishing neural signatures to improve the performance of such systems for these patients. Specifically, this work will spectrally and temporally quantify brain functions with a focus on new analytical techniques and analyses to add significant knowledge to the current findings. In this chapter, the different modalities that are used in this study will first be briefly introduced. Then ALS will be introduced, and finally the two experimental protocols for data recording will be explained.

1.2 RECORDING MODALITIES

1.2.1 Electroencephalography (EEG)

EEG measures the electrical activity recorded from the scalp which is generated by neurons in the cerebral cortex (Niedermeyer and da Silva 2005). The recorded waveforms are thought to reflect electrical activity from the surface of the brain. EEG is

becoming increasingly important in the diagnosis and treatment of neuro-degenerative diseases and abnormalities (Wolpaw 2007).

For EEG recording, a cap with small metal discs (i.e., Electrodes/channels) is placed on the scalp with the discs in certain positions. These positions are specified using the most commonly International 10/20 standard system or expanded versions (shown in

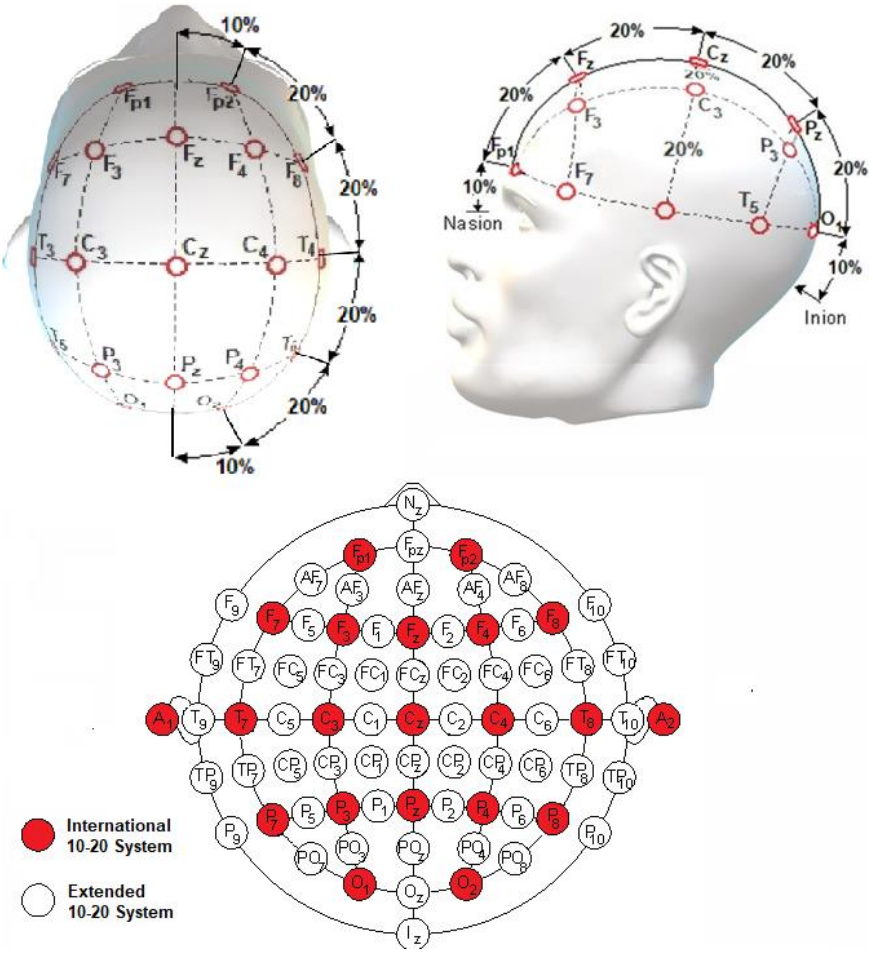

Figure 1.1. International 10-20 system electrode placement on a 3-D head from two views of top (top-left) and side (top-right). The bottom figure shows 10-20 system (red electrodes) and the extended system (white electrodes) on a 2-D plot (Shahriari et al. 2020).

figure 1.1). Each electrode site is labeled with a letter and a number. The letter refers to the area of brain underlying the electrode (e.g. F- Frontal lobe). Even numbers denote the right side of the head and odd numbers the left side of the head. After the electrodes are

placed, the electrode gel is injected to guarantee the conductance between the metal electrode discs and the scalp. The impedance should be kept below 5 $K\Omega$. Finally, the electrical signals of the brain are amplified through a low-noise amplifier device in preparation for later processing.

Most commonly, EEGs are analyzed in the temporal (transient) and spectral (oscillatory) domains. In the temporal domain, the most common analysis is event related potential (ERP) analysis. An ERP is the measured brain response to a specific stimulus which could be visual, auditory, or tactile. It has different components, which are positive and negative local spikes over the time after the onset of stimulus, including the P100, N100, P200, N200 and P300 (also referred to as P1, N1, P2, N2 and P3). The most positive peak between 40 and 75 ms after the onset of stimulus is the P1 which can be

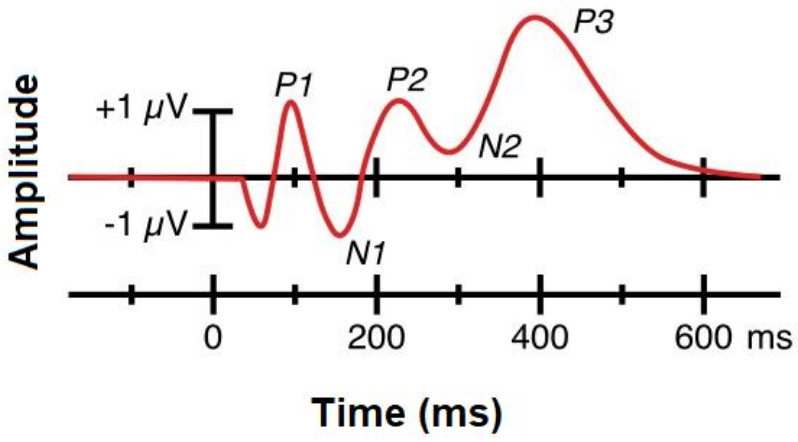

Figure 1.2. The waveform of event related potential (ERP) components ("ERP Info" n.d. Accessed May 20, 2020).

elicited by a paired click paradigm to measure the inhibitory attenuation in the neural response to the second of the two identical stimuli. The N1 is a negative spike between 90 and 200 ms after the onset of a stimulus observed when an unexpected stimulus is presented. The P2 is a positive deflection peaking around 100-250 ms after the stimulus

which is reported to reflect the sensation-seeking behavior of an individual. The N2 is a negative spike about 200 ms after presentation of stimulus which can be strongly elicited in auditory paradigms, and finally, the P3, which can be elicited between 250-400 ms in oddball paradigms, is a major response of interest in the ERP field (Sur et al., 2009). Figure 1.2 shows a schematic visualization of these ERP components.

In the spectral domain, oscillatory activities are used to identify brain-wave characteristics by frequency range. These ranges have traditionally been labeled as delta waves (less than 4 Hz), normally associated with adult slow-wave sleep; theta waves (4-8 Hz) associated with drowsiness, arousal and mental workload; alpha waves (8-12 Hz) largely observed in relaxation with closed eyes and suppressed during mental tasks; beta waves (14-30 Hz) normally associated with motor tasks; and gamma waves (more than 30 Hz) associated with a wide range of cognitive and motor functions (Shahriari et al., 2020). In some applications, frequency ranges may be delineated further with alpha frequencies divided into low alpha (8-10 Hz) and high alpha (11-13 Hz), and beta frequencies into beta 1 (13-16 Hz), beta 2 (16-20 Hz), and beta 3 (20-30 Hz) (Carlson and Birkett 2016).

1.2.2 Functional Near-Infrared Spectroscopy (fNIRS)

fNIRS measures hemodynamic changes in the brain. The dynamics of blood flow inside capillaries are called hemodynamics. This technique is non-invasive, and it can be combined with other neuroimaging modalities. The fNIRS system captures hemodynamic responses in the brain and has been shown to be less prone to motion artifacts. The drawbacks of this system are its low temporal resolution, its indirect

measuring of neural activity, the short distance penetration strength (~3 cm), and the delay in hemodynamic response.

As shown in figure 1.3, in fNIRS, near infrared light is emitted from device sources (emitters) that propagates through the scalp, skull and the grey matter surface underneath in a banana shaped path and interacts with the hemodynamics of the cortex. Then a detector, that is placed 3~4 cm far away from the emitter, receives the attenuated light that reaches the skin. The amount of attenuation of the received light is based on the absorption of original light by hemoglobin (Gratton et al., 1994). The average changes in oxygenated hemoglobin (HbO) and deoxygenated hemoglobin (HbR) concentration inside brain capillaries can then be calculated based on the attenuation and the Beer-Lambert law.

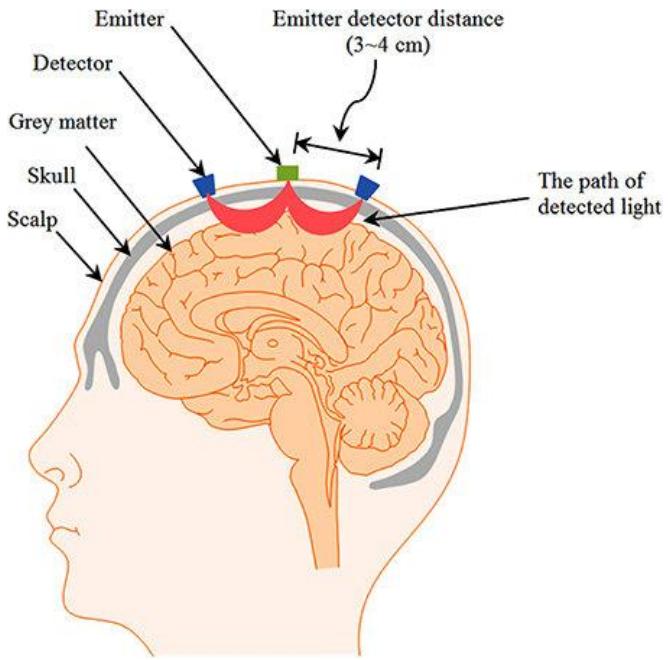

Figure 1.3. Emitter-detector pairs showing the banana-shaped paths of light (Naseer and Hong 2015).

1.3 Amyotrophic Lateral Sclerosis (ALS)

Amyotrophic lateral sclerosis, also known as Lou Gehrig's disease in the United States, was first described by Jean-Martin Charcot in the late nineteenth century (Rowland 2001). Based on U.S. population studies, approximately 5,000 people in the U.S. are diagnosed with ALS annually. It is estimated that at least 16,000 people in the U.S. have the disease at any given time, and every 90 minutes, someone is diagnosed with the disease and someone else passes away from it. People who develop ALS are typically between the ages of 40 and 70, with an average age of 55 at the time of diagnosis. However, in some cases ALS can occur in persons in their third or fourth decade of life. ALS is 20 percent more common in men than in women. However, with increasing age, the incidence of ALS is more equal between men and women (alsa.org).

ALS is a progressive debilitating disease affecting the upper and lower motor neurons. Typically, upper motor neuron degeneration contributes to muscle spasticity and hyperreflexia, whereas lower motor neuron degeneration leads to muscle atrophy and cramping (Fang et al., 2015). Prognostic impairments associated with worse survival are characterized by the locked-in and completely locked-in states (LIS and CLIS). Particularly in these late stages of disease, patients lose all residual motor control, including eye gaze, and they also lose vital autonomous movements such as respiratory and bulbar functions. Despite total paralysis and complete lack of motor control, some brain functions are preserved, and this neural function can be used to run assistive BCI tools (Borgheai et al., 2020). Encouraging results have been seen with BCIs as a communication tool for these patients. As ALS patients progressively lose the ability to move, these devices aid them by giving them some ability to interact with their environment and thereby improve their quality of life (Kübler et al., 2005).

Although ALS was originally known as a motor neurodegenerative disease, within the past several years it has been recognized as a multi-system disorder affecting not only the motor system degenerates but non-motor systems (i.e., behavior and cognition) as well (Beeldman et al., 2016). Up to 50% of patients with ALS develop cognitive impairments, with estimates of frontotemporal dementia (FTD) in these patients ranging from 15% to 41% (Lomen-Hoerth et al., 2003). In a study by Montuschi et. al (Montuschi et al., 2015) involving 207 ALS patients, they found that 13% of the patients showed symptoms of dementia, while 37% presented with non-demented executive impairments. Generally, frontal impairments in ALS are associated with executive dysfunctions (Beeldman et al., 2016). Several studies have shown that ALS patients have considerable executive dysfunction, including poor working memory (WM), poor sustained attention, poor response inhibition, and the loss of visual attention (Ringholz et al., 2005; Silvoni 2009; Zaehle et al., 2013). Additionally, there is evidence of non-motor dysfunctions beyond the behavioral and executive domains, including language and social cognition which are extremely heterogeneous in these patient cohorts (Consonni et al., 2016). Notably, it has been reported that ALS patients' cognitive impairments are correlated negatively with their survival (Montuschi et al., 2015).

1.4 EXPERIMENTAL PROTOCOLS

The explorations of neural alterations to find clinically established disease markers require data recording with experimental protocols including cognitive tasks, motor tasks, and the resting-state. Two experimental protocols which were used in this study will be introduced in this section.

1.4.1 Visual Oddball Task

The oddball paradigm is a commonly used experiment that triggers various ERP components including the N1, N2, N4, P2, and P3. In particular, in a visual oddball task, one of the components, the P3 will be elicited in the brain after a visual stimulus. The visual oddball task and its property to produce a P3 was exploited by Farwell and Donchin to design a BCI for spelling words through the sequential selection of characters on a screen (Farwell and Donchin 1988). In this paradigm, a matrix consisting of characters is shown on the screen. The user is instructed to focus on the target letter for spelling while each row and column of the matrix flashes pseudorandomly, with each row and column flashing once per trial. After averaging the of several trials to improve the signal to noise ratio the elicited electrical activity associated with the onset of target letter flashes can then be detected.

1.4.2 Resting-State

Resting-state studies may be central to understanding information processing as they provide insight into alterations in spontaneous cognition associated with ALS (Buckner and Vincent 2007). In the resting-state protocol, the subjects are instructed to relax, try not to think about any particular matter, and remain awake while data is recorded. The subjects are either asked to keep their eyes open and typically focus on a constant circle which is shown on a screen in front of them or to close their eyes, depending on the type of study. Although resting-state studies do not exclusively reflect conscious mental activity, they may reflect more intrinsic properties of functional brain organization (Vincent et al., 2008) after filtering out the effect of autonomic nervous system. These studies may also represent spontaneous coherent fluctuations in

functionally connected brain regions (Mohammadi et al., 2009). Resting-state recordings therefore have substantial roles in many studies investigating altered functional brain networks.

1.5 THIS DISSERTATION

The major goal of this study is to quantify the neural functions of ALS patients using EEG, fNIRS, and the integration of these modalities with state-of-the-art techniques including time-frequency based decompositions and functional and directional connectivity methods, and to use the quantified neural functions to classify different brain states through state-of-the-art techniques including information theory based fused feature optimization and deep learning based automatic feature extraction. This study contains four major goals as follows:

Research Aim 1: Multimodal exploration of non-motor neural functions in ALS patients during a visual-arithmetic task by spectro-temporal based methods using simultaneous EEG-fNIRS recording.

Despite the high prevalence of non-motor impairments reported in ALS patients, little is known about the functional neural markers underlying these dysfunctions. In this research, a new dual-task multimodal framework relying on simultaneous EEG and fNIRS recordings is developed to characterize integrative non-motor neural functions in this cohort.

This work has been published in the Journal of neural engineering (2019), under the title "Multimodal exploration of non-motor neural functions in ALS patients using simultaneous EEG-fNIRS recording". Our findings demonstrated that ALS subjects have smaller increases in EEG delta and theta power, decreases in beta power, reductions in

HbO responses, and distortions overall, in both early and later EEG event-related potentials, compared to healthy controls. Moreover, significant correlations between EEG features and HbO responses were observed in healthy controls but were absent in ALS patients. These outcomes highlight the important role non-motor dysfunctions in electrical and hemodynamic neural dynamics as well as their interrelationships in ALS.

Research Aim 2: Investigation of electrical and vascular resting-state neural functions in ALS patients by spectro-temporal based methods of network analysis using simultaneous EEG-fNIRS recording.

Recent studies have reported conflicting results on alterations in resting-state functional brain networks in ALS. No study to date has explored simultaneous electrophysiological and hemodynamic changes of the resting-state brain in ALS. Using complementary multimodal EEG and fNIRS recordings and analysis techniques, we explored the underlying multidimensional neural and vascular contributions to altered oscillations and functional connectivity in people with ALS.

This work has been published in the Journal of IEEE Transactions on Neural Systems and Rehabilitation Engineering (2020), under the title "Electrical and hemodynamic neural functions in people with ALS: an EEG-fNIRS resting-state study". Our findings showed increased fronto-parietal EEG connectivity in the alpha and beta bands and increased interhemispheric and right intra-hemispheric fNIRS connectivity in the frontal and prefrontal regions in people with ALS. Frontal, central, and temporal theta and alpha EEG power were reduced in people with ALS, as were parietal and occipital alpha EEG power, while frontal and parietal hemodynamic spectral power were increased in people with ALS. These results suggest that electro-vascular disruption in neuronal networks extends to the extra-motor regions in ALS patients, which can ultimately

introduce novel neural markers of ALS that can be further exploited as diagnostic and prognostic tools.

Research Aim 3: Enhancing the performance of classification between pathological conditions and healthy controls using optimized subset of features extracted from spectral and temporal decompositions of integrated EEG-fNIRS simultaneous recording during a visual-arithmetic task.

EEG-fNIRS multimodal approaches have considerable potential to improve classification performance by measuring two different brain functions. However, they suffer from a lack of computational methods to optimally integrate the features reflecting these two different brain functions. Using an information-theory based approach, we consider the complementarity between the two modalities to enhance classification performance.

This work has been published in the Journal of Biomedical Optics Express (2020), under the title "Multimodal fusion of EEG-fNIRS: a mutual information-based hybrid classification framework". We found considerably improved hybrid classification performance using our mutual information-based feature selection algorithm as compared to the individual modalities and as compared to conventional classification without feature selection.

Research Aim 4: Proposing a deep learning based approach for automatic feature extraction from multimodal EEG-fNIRS data to enhance motor imagery classification, which can be used in future BCI applications for people with neurological disorders including ALS patients.

Since deep learning approaches can be designed to not require manual feature extraction despite the prior knowledge requirements in conventional classification

algorithms to find appropriate features for the classification task, the conventional quantification methods of neural functions are being replaced by deep learning approaches strong capabilities in automatically quantifying various neural functions.

This work is in preparation for submission to the Journal of Neurocomputing, under the title "Deep learning based multimodal EEG-fNIRS classification: an application to motor imagery". The results demonstrated that our deep learning based classification approaches outperformed conventional classification methods. Moreover, the automatic feature extraction strategy implemented using a dual convolutional neural network for multimodal EEG-fNIRS improved classification accuracy compared to other approaches based on manual feature extraction.

1.6 OVERALL DISCUSSION

In this dissertation, we explored the non-motor neural alterations of ALS patients reflected by simultaneously recorded EEG-fNIRS data both during task performance and in the resting-state using state-of-the-art spectro-temporal based quantification techniques including wavelet-based decompositions and functional and directional connectivity methods. Our results revealed significant neural alterations in ALS patients compared to healthy controls in specific frequency bands of EEG power, specific frequency bands of EEG connectivity, temporal characteristics of EEG event-related potentials, specific frequency bands of fNIRS responses, temporal characteristics of fNIRS responses, correlations between EEG power features and fNIRS temporal features, and correlations between EEG and fNIRS power. The insights obtained through this work can enhance our understanding of the underlying non-motor neural processes in ALS and enrich diagnostic and prognostic techniques by using ALS neural signatures

to classify them from healthy controls. In the next step we, then used our previously obtained markers as distinguishing features for classifying ALS patients from healthy controls. For this purpose, we used mutual information-based fused feature optimization for EEG-fNIRS to select the best features among all extracted neural markers, which considerably improved classification performance in when classifying data from people with ALS versus healthy controls based on mental workload. These results support the idea of using complementary features from fused EEG-fNIRS in neuro-clinical studies in the optimized decoding of neural information, and thus, improving the performance of relevant applications, including BCI and neuro-pathological diagnosis. Moreover, we examined our findings in motor imagery classification, which is a fundamental processing step in BCIs with applications for people with neurological disorders including ALS patients. To do this, we proposed a convolutional neural network-based classification architecture for automatic feature extraction from EEG-fNIRS data, which outperformed conventional classification methods using manually extracted features. These outcomes suggest promising improvements in BCI performance using multimodal EEG-fNIRS and deep learning classifiers with automatic feature extraction, which can be utilized in clinical applications for people with neurological disorders including ALS patients. These findings can be further developed to optimally automate the quantification of neural functions in neurological disorders with less dependence on prior knowledge and thereby facilitate BCIs and other clinical applications for patients with neurological disorders.

REFERENCES

Beeldman, Emma, Joost Raaphorst, Michelle Klein Twennaar, Marianne de Visser, Ben A. Schmand, and Rob J. de Haan. 2016. "The Cognitive Profile of ALS: A Systematic Review and Meta-Analysis Update." *Journal of Neurology, Neurosurgery & Psychiatry*.

Borgheai, Seyyed Bahram, John McLinden, Alyssa Hillary Zisk, Sarah Ismail Hosni, Roohollah Jafari Deligani, Mohammadreza Abtahi, Kunal Mankodiya, and Yalda Shahriari. 2020. "Enhancing Communication for People in Late-Stage ALS Using an fNIRS-Based BCI System." *IEEE Transactions on Neural Systems and Rehabilitation Engineering: A Publication of the IEEE Engineering in Medicine and Biology Society* 28 (5): 1198–1207.

Buckner, Randy L., and Justin L. Vincent. 2007. "Unrest at Rest: Default Activity and Spontaneous Network Correlations." *NeuroImage* 37 (4): 1091–96; discussion 1097–99.

Carlson, Neil R., and Melissa A. Birkett. 2016. *Physiology of Behavior*. Pearson.

Consonni, Monica, Eleonora Catricalà, Eleonora Dalla Bella, Valentina C. Gessa, Giuseppe Lauria, and Stefano F. Cappa. 2016. "Beyond the Consensus Criteria: Multiple Cognitive Profiles in Amyotrophic Lateral Sclerosis?" *Cortex; a Journal Devoted to the Study of the Nervous System and Behavior* 81 (August): 162–67.

"ERP Info." n.d. Accessed May 20, 2020. https://erpinfo.org/the-erp-boot-camp.

"Facts You Should Know." n.d. ALSA.org. Accessed May 20, 2020. http://www.alsa.org/about-als/facts-you-should-know.html.

Fang, Fang Fang, Caroline Ingre, Per Roos, Freya Kamel, and Fredrik Piehl. 2015. "Risk Factors for Amyotrophic Lateral Sclerosis." *Clinical Epidemiology*. https://doi.org/10.2147/clep.s37505.

Farwell, L. A., and E. Donchin. 1988. "Talking off the Top of Your Head: Toward a Mental Prosthesis Utilizing Event-Related Brain Potentials." *Electroencephalography and Clinical Neurophysiology*. https://doi.org/10.1016/0013-4694(88)90149-6.

Gratton, G., J. S. Maier, M. Fabiani, W. W. Mantulin, and E. Gratton. 1994. "Feasibility of Intracranial near-Infrared Optical Scanning." *Psychophysiology* 31 (2): 211–15.

Kellmeyer, Philipp, Moritz Grosse-Wentrup, Andreas Schulze-Bonhage, Ulf Ziemann, and Tonio Ball. 2018. "Electrophysiological Correlates of Neurodegeneration in Motor and Non-Motor Brain Regions in Amyotrophic Lateral Sclerosis-Implications for Brain-Computer Interfacing." *Journal of Neural Engineering* 15 (4): 041003.

Kübler, A., F. Nijboer, J. Mellinger, T. M. Vaughan, H. Pawelzik, G. Schalk, D. J. McFarland, N. Birbaumer, and J. R. Wolpaw. 2005. "Patients with ALS Can Use Sensorimotor Rhythms to Operate a Brain-Computer Interface." *Neurology* 64 (10): 1775–77.

Kuruvilla, Mili S., Jordan R. Green, Hasan Ayaz, and Daniel L. Murman. 2013. "Neural Correlates of Cognitive Decline in ALS: An fNIRS Study of the Prefrontal Cortex." *Cognitive Neuroscience* 4 (2): 115–21.

Lomen-Hoerth, C., J. Murphy, S. Langmore, J. H. Kramer, R. K. Olney, and B. Miller. 2003. "Are Amyotrophic Lateral Sclerosis Patients Cognitively Normal?" *Neurology*.

Mohammadi, Bahram, Katja Kollewe, Amir Samii, Klaus Krampfl, Reinhard Dengler, and Thomas F. Münte. 2009. "Changes of Resting State Brain Networks in Amyotrophic Lateral Sclerosis." *Experimental Neurology* 217 (1): 147–53.

Montuschi, Anna, Barbara Iazzolino, Andrea Calvo, Cristina Moglia, Leonardo Lopiano, Gabriella Restagno, Maura Brunetti, et al., 2015. "Cognitive Correlates in Amyotrophic Lateral Sclerosis: A Population-Based Study in Italy." *Journal of Neurology, Neurosurgery, and Psychiatry* 86 (2): 168–73.

Naseer, Noman, and Keum-Shik Hong. 2015. "Corrigendum "fNIRS-Based Brain-Computer Interfaces: A Review"." *Frontiers in Human Neuroscience*.

Niedermeyer, Ernst, and F. H. Lopes da Silva. 2005. *Electroencephalography: Basic Principles, Clinical Applications, and Related Fields*. Lippincott Williams & Wilkins.

Ringholz, G. M., S. H. Appel, M. Bradshaw, N. A. Cooke, D. M. Mosnik, and P. E. Schulz. 2005. "Prevalence and Patterns of Cognitive Impairment in Sporadic ALS." *Neurology* 65 (4): 586–90.

Rowland, L. P. 2001. "How Amyotrophic Lateral Sclerosis Got Its Name: The Clinical-Pathologic Genius of Jean-Martin Charcot." *Archives of Neurology* 58 (3): 512–15.

Shahriari, Yalda, Walter Besio, Sarah Ismail Hosni, Alyssa Hillary Zisk, Seyyed Bahram Borgheai, Roohollah Jafari Deligani, and John McLinden. 2020. "Electroencephalography." *Neural Interface Engineering*. https://doi.org/10.1007/978-3-030-41854-0_1.

Silvoni, Stefano. 2009. "300-Based Brain-Computer Interface Communication: Evaluation and Follow-up in Amyotrophic Lateral Sclerosis." *Frontiers in Neuroscience*.

Vincent, Justin L., Itamar Kahn, Abraham Z. Snyder, Marcus E. Raichle, and Randy L. Buckner. 2008. "Evidence for a Frontoparietal Control System Revealed by Intrinsic Functional Connectivity." *Journal of Neurophysiology* 100 (6): 3328–42.

Wolpaw, Jonathan R. 2007. "Brain-Computer Interfaces (BCIs) for Communication and Control." *Proceedings of the 9th International ACM SIGACCESS Conference on Computers and Accessibility - Assets '07*. https://doi.org/10.1145/1296843.1296845.

Zaehle, Tino, Andreas Becke, Nicole Naue, Judith Machts, Susanne Abdulla, Susanne Petri, Katja Kollewe, et al., 2013. "Working Memory in ALS Patients: Preserved Performance but Marked Changes in Underlying Neuronal Networks." *PloS One* 8 (8): e71973.

CHAPTER 2: MULTIMODAL EXPLORATION OF NON-MOTOR NEURAL FUNCTIONS IN ALS PATIENTS USING SIMULTANEOUS EEG-FNIRS RECORDING

Published in the Journal of Neural Eng. doi:10.1088/1741-2552/ab456c.

S B Borgheai[1,3], R J Deligani[1,3], J McLinden[1], A Zisk[2], S I Hosni[1], M Abtahi[1], K Mankodiya[1], Y Shahriari[1,4]

[1]Department of Electrical, Computer, and Biomedical Engineering, University of Rhode Island, Kingston, RI, United States of America

[2] Interdisciplinary Neuroscience Program, University of Rhode Island, Kingston, RI, United States of America

[3]These authors contributed equally to this work.

[4]Author to whom any correspondence should be addressed.

Email: yalda_shahriari@uri.edu

ABSTRACT

Objective: Despite the high prevalence of non-motor impairments reported in patients with amyotrophic lateral sclerosis (ALS), little is known about the functional neural markers underlying such dysfunctions. In this study, a new dual-task multimodal framework relying on simultaneous electroencephalogram (EEG) and functional near-infrared spectroscopy (fNIRS) recordings was developed to characterize integrative non-motor neural functions in people with ALS.

Approach: Simultaneous EEG-fNIRS data were recorded from six subjects with ALS and twelve healthy controls. Through a proposed visuo-mental paradigm, subjects performed a set of visuo-mental arithmetic operations. The data recorded were analyzed with respect to event-related changes both in the time and frequency domains for EEG and de/oxygen-hemoglobin level (HbR/HbO) changes for fNIRS. The correlation of EEG spectral features with fNIRS HbO/HbR features were then evaluated to assess the mechanisms of ALS on the electrical (EEG)-vascular (fNIRS) interrelationships.

Main results: We observed overall smaller increases in EEG delta and theta power, decreases in beta power, reductions in HbO responses, and distortions both in early and later EEG event-related potentials in ALS subjects compared to healthy controls. While significant correlations between EEG features and HbO responses were observed in healthy controls, these patterns were absent in ALS patients.

Significance: Our results highlight the important role of ALS non-motor dysfunctions in electrical and hemodynamic neural dynamics as well as their interrelationships. The

insights obtained through this study can enhance our understanding of the underlying non-motor neural processes in ALS and enrich future diagnostic and prognostic techniques.

Keywords amyotrophic lateral sclerosis (ALS); non-motor dysfunction; electroencephalogram (EEG); functional near-infrared spectroscopy (fNIRS); multimodal frameworks

2.1 BACKGROUND

Despite the high prevalence of non-motor dysfunctions in ALS, little is known about their underlying functional neural variations (Kellmeyer et al., 2018). Burke et al. (2017) (Burke et al., 2017) suggested that distinct cognitive-behavioral phenotypes may relate to differential disruption of extramotor cortical networks, but the connections between neural and cognitive findings require further investigation for neural characterization, specifically in ALS. Thus, there is an enormous need for more research to elucidate neural markers of non-motor dysfunction in ALS. Such explorations can advance our understanding of neural abnormalities in the disease. This may provide complementary objective signatures of disease progression and enrich current diagnostic and prognostic techniques.

To investigate the characteristics of neural signatures in ALS, most studies have relied on electroencephalography (EEG) because of its high temporal resolution, cost-effectiveness, and portability (Abiri et al., 2019). These studies either used resting-state or activation paradigms in which subjects were asked to perform an active task. In the former case, power spectral bands (Santhosh et al., 2005) or functional connectivity (Iyer et al., 2015) are features reported commonly to address differences between participants with ALS and controls. In activation paradigms that can reflect cognitive dysfunctions

directly, event-related potentials (ERPs) are the commonly evaluated temporal responses (responses in the time domain). For example, abnormalities in the P300 response, together with early components, such as P100 or N200, elicited during an oddball paradigm, are the temporal features most frequently reported to be impaired in ALS patients (Kellmeyer et al., 2018; Raggi et al., 2010; Abiri et al., 2019).

However, because of EEG's low spatial resolution and signal-to-noise ratio (SNR), ERP analysis depends on the number of trials (for averaging). This is an issue in typical ERP-based visual paradigms, particularly, in the later stages of ALS, when ocular problems develop and lack of fine eye-gaze control can affect visual paradigms' efficiency (Murguialday et al., 2011). Hence, there is a need for compensatory methods to overcome these shortcomings (Kellmeyer et al., 2018). Two complementary paths may address these issues. The first is to look for other distinctive EEG features (rather than temporal features), such as power spectral activities in new types of activation paradigms. Few studies on ALS patients have characterized EEG spectral power responses (Kübler et al., 2001; Kübler et al., 1999), in which the slow cortical potential (SCP) is most commonly used in the learned self-regulation process or motor-related paradigms, rather than cognitive activation designs. However, given that executive dysfunction is a major impairment reported in ALS patients, more studies are needed to explore neural oscillatory characteristics of executive dysfunction through cognitive paradigms in ALS patients. The second path is to incorporate other neuroimaging modalities with EEG simultaneously to capture complementary neural dynamical features, such as hemodynamic activities in addition to EEG electrical responses. To do so, functional near-infrared spectroscopy (fNIRS) is the only neuroimaging technique that can be used plausibly for ALS patients, considering their disease's progression and their immobility

(Raggi et al., 2010), as fNIRS measures the brain's hemodynamic activities, is portable and can be used longitudinally at patients' bedsides (Schudlo and Chau 2014; Naseer and Hong 2015; Lloyd-Fox et al., 2015).

In this chapter, we introduced a novel compensatory method to explore non-motor neural degeneration in ALS patients. We developed an innovative visuo-mental dual-task that combined a visuo-spatial oddball paradigm with a set of arithmetic operations to induce and record both hemodynamic and electrical responses simultaneously using EEG-fNIRS. Studies have shown that while fNIRS signals are effective in mirroring cerebral oxygenation changes in response to various cognitive functions (Schudlo and Chau 2014; Naseer and Hong 2015; Lloyd-Fox et al., 2015; Shin et al., 2016; Shin et al., 2017), including mental arithmetic tasks, they also can reflect distinctive patterns between patients with ALS and healthy controls (Kuruvilla et al., 2013; Chaudhary et al., 2017). The proposed paradigm allows us to obtain the following advantages over the methods used previously. First, our paradigm's dual-task nature is speculated to be particularly effective in capturing cognitive dysfunctions in ALS that single-task paradigms do not fully reflect (Putze et al., 2014; Pettit et al., 2013). Second, the complementary electrical and hemodynamic information gained through EEG and fNIRS recordings can compensate for the single modality shortcomings, such as the patient's inability to perform fine visual tasks particularly in the later stages of their disease—this complementary information can offer unique opportunities for future neuroimaging studies of ALS. Third, the associations between EEG and fNIRS can be further explored to investigate how ALS affects the interrelations between electrical (EEG) and vascular (fNIRS) dynamics. The insights obtained through this study can advance our understanding of integrative non-motor markers in ALS, aid in identifying relations

between electrical and vascular responses in ALS and can ultimately introduce novel neural markers of ALS that can be exploited as diagnostic and prognostic predictors.

2.2 METHODS

2.2.1 Subjects

A total of 18 subjects were recruited and assigned to two groups: 6 individuals with ALS (5 males) and 12 age-matched healthy controls (5 males). All the protocols in this study were approved by the Institutional Review Board (IRB) of the University of Rhode Island (URI) and written informed consents were provided directly by each subject or patient's caregiver. The average age of the patient group was 57.0±15.7 years old and the average age of the control group was 56.4±15.4 years old. Specifically, in our patient group we have one young (No. 1) subject, whom we matched with two young healthy controls. Excluding the young participants, the average of the elder patients' age was 62.6±8.4 years old compared to 62.7±4.8 years old for the elder healthy participants. Half of the patients required mechanical ventilation, the youngest one of whom, was in a completely locked-in state (CLIS). Age-matched control subjects had no reported history of visual, mental, or substance-related issues. All participants in both groups had at least some level of post-secondary education. Two healthy controls were excluded from fNIRS data analysis because of their poor signal quality in fNIRS calibration settings. All subjects provided informed consent (or assent) for the study and were reimbursed financially. Because of communication and/or ocular impairments in three of our ALS patients, two used eye-tracking systems (Tobii EyeX). Table 2.1 shows the ALS subjects' demographics, including age, gender, disease duration and ALSFRS-R.

2.2.2 Experimental Protocol

Subjects participated in several sessions (4.7±3.8), with 2 runs per session. To familiarize the subjects with our BCI set up, including the recording protocol and the task, they all participated in training sessions before the main experimental recordings. In addition, in each session, there were a few quick test runs to make sure that the subjects understood the task, which were evaluated by discussing their results. We continued performing test runs until we were sure the subjects were comfortable with the task. Following the conventional oddball P300 paradigm, a 2×2 matrix of digits was displayed over the intensified letter in our visuo-mental dual-task paradigm. Each subject was instructed to focus on a target character (14 targets per run), while each row and column was intensified once per trial to cause two target intensifications per character. Upon each target intensification, subjects were instructed to perform predefined mental arithmetic tasks, i.e., add pairs of numbers in the matrix either diagonally (first target flash) or vertically (second target flash), and then double the larger result from their addition. The stimulation intensification time was set to 300 ms, followed by a 6 sec inter-stimulus interval (ISI). The relatively long ISI adopted compared to conventional EEG-based oddball tasks allowed the fNIRS recordings to reflect evoked hemodynamic activities.

Table 2.1. ALS Subjects Demographic Information.

Participant No.	Age	Gender	Disease Duration (years)	ALSFRS-R (max 48)	Educational Level
1	29	M	4	0	College Degree
2	55	M	11	4	Graduate Degree
3	70	M	8	14	Some Postsecondary
4	67	M	2	7	College Degree
5	69	F	11	23	College Degree
6	52	M	3	22	Some Postsecondary
Mean ± SD	57.0±15.7	-	6.5 ±4.0	11.6±9.5	-

Although fNIRS paradigms use longer stimulus and resting periods, normally ranging from 8 to 12 sec (Naseer and Hong 2015), these times were reduced in our paradigm because of the potential to extend our work in future communication studies of ALS. Generally, longer pauses increase the amount of time required to select each character in communication systems—this can make the communication system slow and impractical in real-life scenarios. The inherent dual nature of our visuo-mental paradigm is hypothesized to provoke both electrical and hemodynamic responses associated with visual oddball stimulations and mental arithmetic operations.

2.2.3 Data Acquisition

Both signals were recorded simultaneously using a single cap mounted both with EEG electrodes and fNIRS optodes. fNIRS data were recorded using NIRScout (NIRx Inc.) with two NIR lights (760 nm and 850 nm wavelengths) and digitized at 7.81 Hz. EEG data were recorded simultaneously using the g.USBamp amplifier (g.tec Medical Tech.) and digitized at 256 Hz. Figure 2.1 shows a schematic head model of the fNIRS-EEG sensors' placement. As depicted in this figure, five emitters and two detectors acquired seven fNIRS channels covering the frontal areas responsible for higher cognitive functions associated with mathematical operations paradigms (Pettit et al., 2013). Following the Modified Combinatorial Nomenclature (MCN) montage, emitters were placed at Fz, F3, F4, AF3, and AF4, and detectors at F1 and F2. EEG was recorded from eight channels: Fz*, Cz, P3, Pz, P4, PO7, PO8, and Oz covering all frontal, central, parietal, and occipital areas used commonly in conventional P300 paradigms (FAF2, denoted, Fz* was the nearest electrode placement to fNIRS occupied Fz according to 128-channel montage) (Krusienski et al., 2008). This montage was intended to capture

one aspect of the dual-task, i.e., the visuospatial task, with conventional EEG montages (Krusienski et al., 2008), and the arithmetic operations with frontal fNIRS and EEG channels reported previously (Bauernfeind et al., 2011). This montage follows standards closely and is convenient to mount, making it an appropriate candidate for future applications. All experimental protocols, data acquisition, and stimulus presentation labels were controlled using BCI2000 and NIRStar software (Schalk and Mellinger 2010; Simis et al., 2018).

2.2.4. Data Analysis

EEG data were bandpass filtered at 0.5-30 Hz and detrended. fNIRS data were also band-pass filtered at 0.01-0.2 Hz. Then, both datasets were checked for extreme values and outliers which led to the removal of a total of three runs from two ALS participants. EEG data were segmented to 800 ms windows starting from the onset of each target stimulus and averaged across all runs for each subject. ERP features were then extracted from EEG as follows: Peaks and latencies of the P200, P300, and P600 components were defined as the maximum peaks between 100-250, 250-400, and 650-800 ms post-stimulus, respectively, while N200 and N400 components were defined as the minimum peaks between 150-280 and 360-560 ms post-stimulus, respectively. For fNIRS, Oxy-hemoglobin (HbO) and deoxy-hemoglobin (HbR) concentration changes were extracted from raw optical intensity data using the modified Beer-Lambert Law (Kocsis et al., 2006). After baseline correction using the 2 to -1 sec pre-stimulus window, the peaks of both HbO and HbR were then extracted within each post-stimulus interval with three different time window lengths (0-2, 2-4, 4-6 sec) to account for fNIRS features.

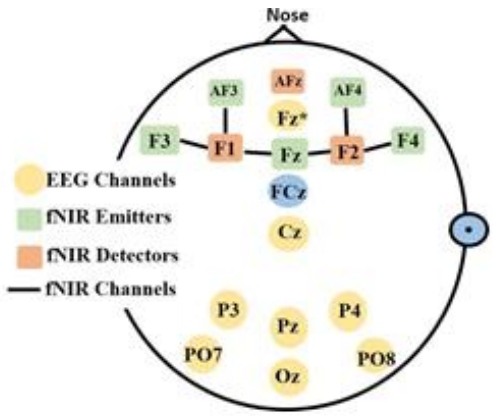

Figure 2.1. A schematic montage of the EEG sensors-fNIRS optodes.

For time-frequency analysis, EEG data were normalized and segmented into 9 sec epochs, beginning from 4 sec pre-stimulus to 5 sec post-stimulus. A set of 30 complex Morlet wavelets ranging from 1-30 Hz and 3-10 cycles was used for time-frequency decomposition based on the equation 2.1.

$$w = e^{2j\pi ft} e^{\frac{-t^2}{2\sigma^2}} \tag{2.1}$$

In this equation, w is the complex Morlet wavelet defined as the product of a complex sine wave and a Gaussian window, j is the imaginary operator, f is the frequency in Hz, and t is the time in seconds, centered at $t = 0$, σ is the width of the Gaussian defined as $\sigma = \frac{n}{2\pi f}$ and n is number of cycles. The baseline-corrected spectrograms were obtained by dividing each frequency bin and time point by the baseline -2 to -1 sec average and log-transforming. The spectrograms from the first 5 sec post-stimulus were then averaged across four traditional frequency bands: delta (1-3 Hz), theta (4-7 Hz), alpha (8-12 Hz), and beta (13-30 Hz). In each frequency band, features were the averages of band power over sliding 500 ms windows from 0-5 sec post-stimulus with 50% overlap.

To statistically compare the results between groups, a nonparametric bootstrapping procedure was used. This method is useful for small or unequal sample sizes (Oruç et al., 2011) and has greater statistical power and makes fewer assumptions about the data's distribution compared to canonical methods (Vizioli et al., 2010). For this purpose, all of each subject's runs were averaged, and then the aforementioned features were extracted for each type of modality and analysis. Then, through the bootstrapping procedure, resamples were generated for each feature. Each resample was obtained by randomly selecting six healthy control subjects (equal to the number of ALS subjects), averaging each feature across all six randomly selected subjects, and finally, subtracting the group means to generate the histogram (probability distribution) of group differences. This procedure was iterated 1000 times to create a distribution. The proportion of resamples less than zero (or greater than zero depending on which tail of the histogram hits the zero point) to all resamples yielded p-values (Oruç et al., 2011). The difference in the means was determined to be statistically significant if the p-value was less than 0.05. To account for multiple comparisons in both the fNIRS and EEG statistical analyses, the false discovery rate (FDR) method was used to compute adjusted p-values ($p<0.05$) (Hochberg and Benjamini 1990).

Finally, Spearman correlation analysis was conducted to explore the relations between significant EEG and fNIRS features over time. To do so, correlations were calculated between a set of windowed EEG spectral features (i.e., delta, theta, and beta power) and windowed peak HbO/HbR values for the frontal EEG-fNIRS channels. EEG features used 1-sec sliding windows with a 0.5 sec overlap in the time range of 0-4 sec post-stimulus, while fNIRS used 2-sec windows with a 1-sec overlap in the time range of 0-6 sec post-stimulus.

2.3 RESULTS

2.3.1 EEG Results

We observed attenuated ERP features overall in ALS patients compared to healthy controls. In particular, frontal (Fz), parietal (P3, Pz, P4), parieto-occipital (PO7, PO8), and occipital (Oz) P200 amplitudes were attenuated significantly in ALS patients ($p<0.05$), and averaged 0.19±0.06 in the frontal channel (Fz) compared to healthy controls, averaging 0.31±0.16 in the same channel. P300 amplitudes were attenuated significantly in all channels in patients ($p<0.001$), and averaged 0.21±0.07 in the frontal channel compared to healthy controls, with an average of 0.38±0.14 in the same channel (Figure 2.2, top left). P600 amplitudes also were attenuated significantly in all channels ($p<0.001$), and averaged 0.11±0.04 for patients in the frontal channel compared to healthy controls, with an average of 0.43±0.19 (Figure 2.2, top right). N200 amplitudes were attenuated significantly in all channels ($p<0.001$), and averaged -0.0.10±0.0.05 in the frontal channel for patients compared to healthy controls, who averaged -0.25±0.16 (Figure 2.2, bottom left). Similarly, N400 amplitudes were attenuated significantly in all channels ($p<0.03$), and averaged -0.30±0.11 in the frontal channel for patients compared to healthy controls, who averaged -0.41±0.13 (Figure 2.2, bottom right). The P300 and N200 features were observed to have significantly shorter latencies in patients compared to the healthy controls. Patients' P300 latencies, which averaged 263±12, 267±13, and 275±9 ms, preceded those of healthy controls significantly at 291±25, 307±22, and 303±15 ms in the frontal (Fz), central (Cz), and parietal (Pz) channels, respectively ($p<0.001$). Parieto-occipital (PO8) and occipital (Oz) N200 latencies were significantly

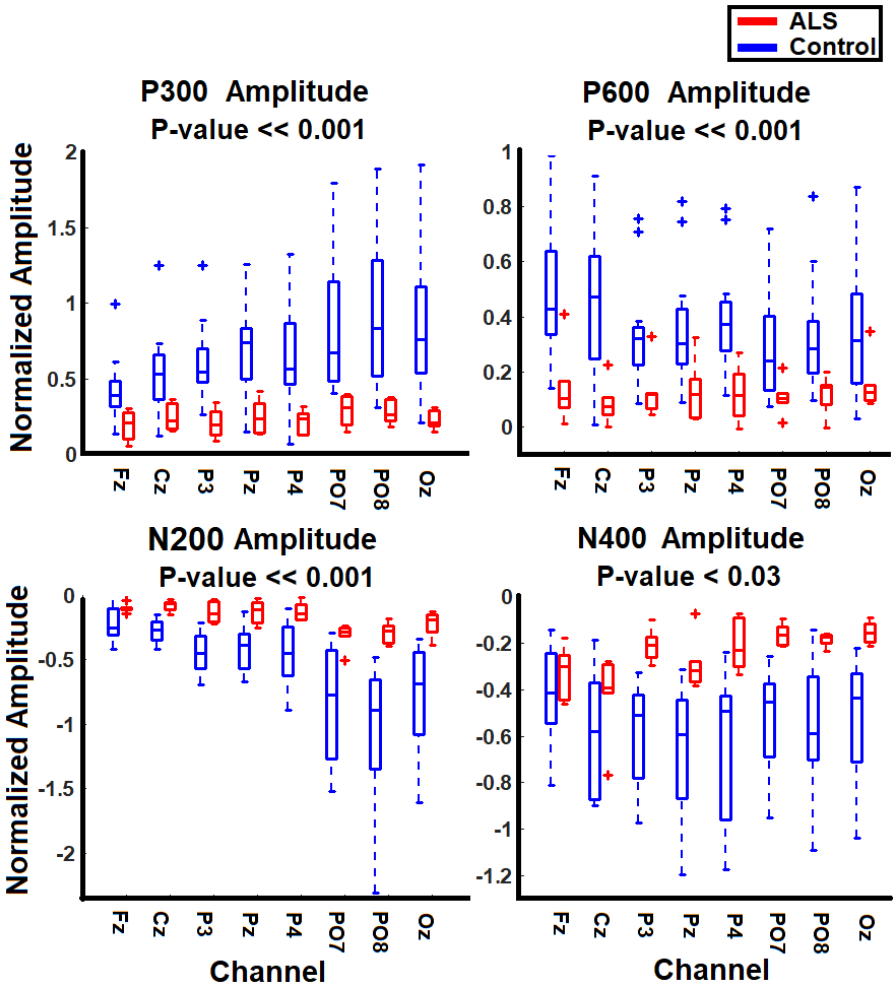

Figure 2.2. Boxplots showing changes (mean±SD) in average P300 amplitude (top left), P600 (top right), N200 (bottom left), and N400 amplitude (bottom right) for ALS participants (red) and healthy controls (blue). For each plot, the maximum *p*-value among channels is shown at the top.

shorter in patients ($p<0.05$) and averaged 238±19 and 222±5 ms compared to healthy controls, whose latencies averaged 269±14 and 258±16 ms in channels PO8 and Oz, respectively.

Figure 2.3 illustrates the average time-frequency decomposition across all healthy controls (left) and all ALS participants (right) for the frontal EEG channel (Fz). We observed that delta power was significantly lower in participants with ALS than in healthy controls within the 1-2.5 sec (ALS: 1.7±1.9 dB, Control: 3.8±2.1 dB) and 2.75-

4.75 sec post-stimulus windows (ALS: 1.1±1.5 dB, Control: 3.0±2.3 dB) ($p<0.01$). Similarly, in the theta band, we observed that power in participants with ALS was significantly lower than in healthy controls within the 0.75-2.25 sec (ALS: 1.1±3.4 dB, Control: 3.6±2.2 dB) and 2.5-4.75 sec post-stimulus windows (ALS: 0.5±1.6 dB, Control: 3.5±4.3 dB) ($p<0.001$). In the beta band, we observed a significantly lower power in healthy controls than in participants with ALS within the 0.5-4 sec post-stimulus window (ALS: -0.3±1.4 dB, Control: -1.2±1.9 dB) ($p<0.02$). No significant changes

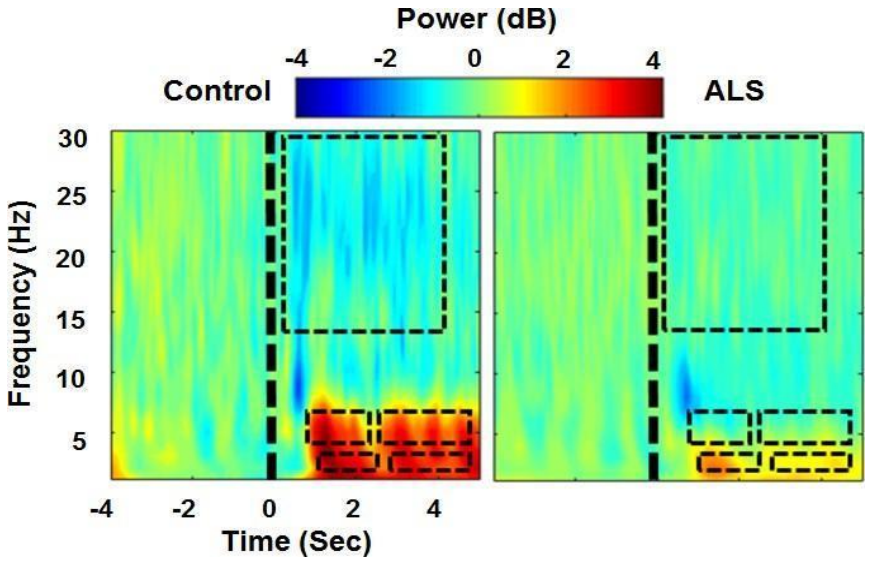

Figure 2.3. Average time-frequency decomposition across all healthy controls (left) and ALS participants (right) for channel Fz. The significant differences between each group (healthy vs. ALS) for each frequency band are illustrated by a black dashed rectangle.

between the two groups were observed in the alpha band.

2.3.2 fNIRS Results

Event-related HbO and HbR activities were calculated, epoched, and grand-averaged across all runs and subjects in both groups. Figure 2.4 illustrates the grand-average HbO responses from 2 sec target pre-stimulus to 6 sec target post-stimulus for both groups. We observed that our designed task-evoked hemodynamic responses in the

ISI following target stimulus presentation in both the patient and control groups. Most channels showed an initial dip in HbO responses in both groups, followed by a rise. Between-group differences were particularly clear in the channels located on the left frontal and prefrontal lobes (primarily F3-F1 and F1-Fz). In channel F3-F1, the peak value of the average HbO occurred 4.23 sec post-stimulus with $(1.1\pm1.3)\times10^{-4}$ mM for the ALS group compared to 5.71 sec post-stimulus with $(2.3\pm13.2)\times10^{-5}$ mM for controls. The average initial dip in this channel reached its minimum of $(-3.2\pm5.1)\times10^{-5}$ mM 0.06 sec post-stimulus in the ALS group compared with the minimum of $(-3.5\pm4.8)\times10^{-5}$ mM at 1.89 sec post-stimulus for the healthy group. In channel F1-Fz, the peak value of average HbO occurred 5.5 sec post-stimulus with $(9.4\pm13.2)\times10^{-5}$ mM for the ALS group compared to 6.0 sec post-stimulus with $(6.5\pm13.4)\times10^{-5}$ mM for the controls. This channel's initial dip was greater in the ALS group with a minimum of $(-4.85\pm14.5)\times10^{-5}$ mM at 1.72 sec post-stimulus compared to $(-1.8\pm3.9)\times10^{-5}$ mM at 1.88 sec post-stimulus for the healthy controls.

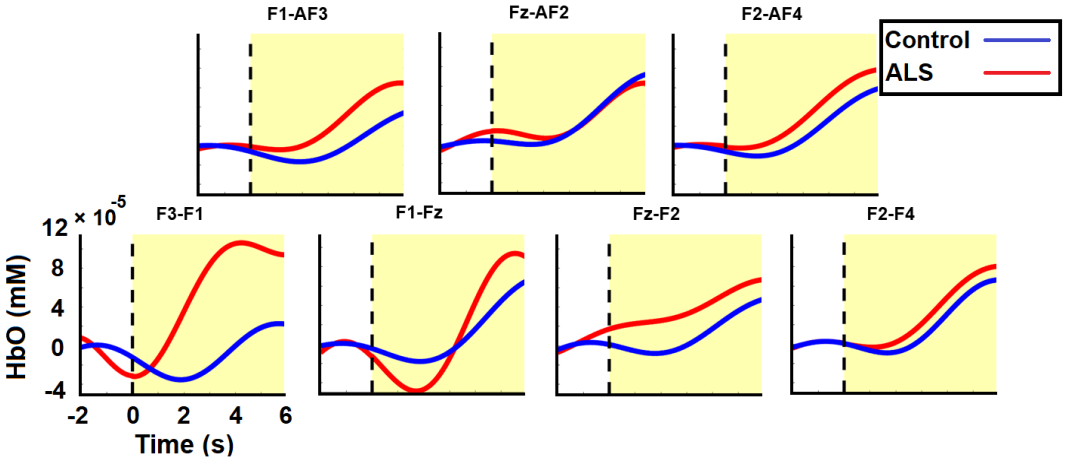

Figure 2.4. Average target HbO responses evolving from 2 sec pre-stimulus to 6 sec post-stimulus for both ALS (red) and control (blue) groups. The vertical dashed line and the shaded yellow area denote the target stimulus onset and post-stimulus respectively.

2.3.3 Correlation Results

As shown in figure 2.5, generally significant ($p \leq 0.02$) positive correlation was observed between windowed peak HbO 2-6 sec post-stimulus and windowed EEG-delta features 1.5-3 sec post-stimulus in healthy subjects. Additionally, delta band features in the 1-3 sec windows were significantly ($p \leq 0.02$) correlated with peak HbO in the 2-4 sec windows in healthy controls. Significant ($p \leq 0.03$) positive correlation was also generally observed between EEG-theta features in the 1.5-3 sec windows and peak HbO in the 1-6 sec windows in healthy controls. Significance in correlation remains between both delta and theta band features in the 1.5-3 sec windows and peak HbO in the 2-6 sec windows after FDR correction in healthy subjects. However, no significant correlation was observed between patient group peak HbO and delta or theta band features in any of the time windows. In the control group, significant positive correlation ($p<0.05$) was observed between beta band features in the 1.5-3 sec windows and peak HbO features in

the 0-3 sec windows, as well as between the 1.5-2.5 sec beta band window and 2-4 sec post-stimulus peak HbO window ($p \leq 0.03$). In contrast, significant ($p \leq 0.04$) negative correlation was observed between later beta band features and earlier peak HbO windows in the patient group. However, the significance in the beta band in both healthy and patient groups was not present after FDR-correction. No significant correlation between peak HbR features and EEG features in any frequency band or time window was observed. Some sporadic significant ($p < 0.05$) negative correlation was observed between peak HbR and EEG features in the delta and theta bands for the patient group, but they did not remain significant after FDR correction.

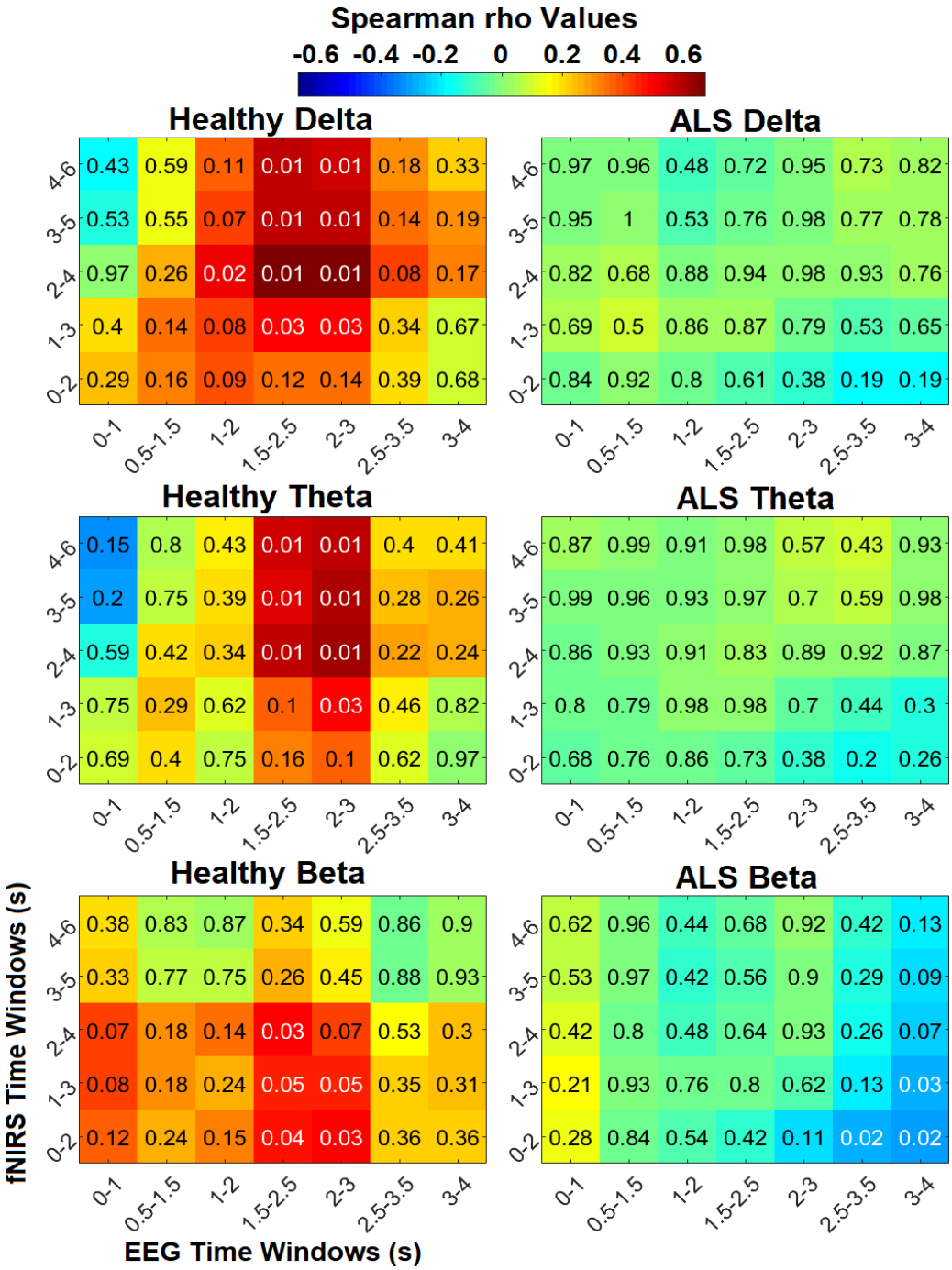

Figure 2.5. Spearman correlation (rho) between obtained significant EEG features in the delta, theta, and beta frequency bands and windowed fNIRS peak HbO in the healthy control (left) and patient (right) groups. Significant corrected *p*-values ($p<0.05$ before rounding to the nearest 100^{th}) are shown in white, and all other values are displayed in black. Only correlation maps with significant *p*-values and their counterparts in the patient group are displayed.

2.4 DISCUSSION

In general, the task developed in this study can be divided into two major and cognitively different segments that represent our paradigm's dual nature. Segment-1 (SG1), 0-300 ms after stimulus onset, is associated with general early attentional components involving arousal or visuospatial selective attention, followed by segment-2 (SG2), >300 ms after stimulus onset, which reveals task-specific processes, including mathematical operations as well as working memory.

Overall, we observed a significantly greater increase in frontal delta power in healthy controls than in patients. Delta power increases in mental calculation tasks are interpreted typically as relevant to "internal concentration" blocking interference during task performance (Fernández et al., 1995). As in our proposed visuo-mental dual-task paradigm, subjects attempt to concentrate on performing a set of internal arithmetic tasks independent of external visual stimuli, thus, we expected to observe increased delta during math operations. Interestingly, the increase in the delta was observed largely after ~1-sec delay (Figure 2.3) in both groups, showing that the delta deviations refer to later cognitive/calculation components (SG2). The suppressed delta increase in the ALS group is speculated to be related to a degraded internal concentration during calculations (Fernández et al., 1995).

In the theta frequency band, healthy participants showed a profound power increase, while this pattern was attenuated significantly in the patient group. Generally, theta oscillations are associated with several cognitive components, including attention to stimuli and working memory processes (Deligani et al., 2019; Borgheai et al., 2019; Deiber et al., 2007). Therefore, it is plausible to associate increased theta power in our mental task with an inherent increased workload and the task's attentional demand. Thus,

the mental dimension (i.e., the arithmetic task) we added to the conventional visual oddball paradigm would engage more working memory and attentional components.

While we did not observe any significant difference in the alpha frequency band between participants with ALS and controls, a significant decrease in the beta was seen in the healthy group compared to the patients. Frontal beta activity is associated with top-down control processes (Bastos et al., 2015; Siegel et al., 2012), particularly in general task-related processing. Beta power is reported to be enhanced during the intended maintenance of mental status, or status quo (Engel and Fries 2010). Thus, the initial beta suppression observed after target presentation (in the SG1 period) might be attributable to the changing mental state after stimulus onset. Later beta suppression (in the SG2 period) can be attributed to content-specific frontal beta modulation parallel with working memory processing and decision making which confirms the results of recent studies (Spitzer and Haegens 2017; Wimmer et al., 2016). Therefore, ALS patients' lack of beta power modulation while performing the mental task can be interpreted as dysfunctions in the top-down control process related to general workload processing.

The healthy group's hemodynamic responses confirmed that our relatively short ISI can evoke sufficient hemodynamic activity to generate a reliable comparative framework between the groups. In ALS group, weak correlations were observed between hemodynamic levels and EEG-theta, and no significant correlation between HbO levels and delta powers was observed in these patients. However, we observed a significant positive correlation between EEG-delta and HbO level in healthy controls. Notably, while EEG-fNIRS correlation maps largely were positive for healthy controls, they were mainly negative in ALS and revealed a desynchronization pattern of electrical (EEG)-vascular (fNIRS) responses during mental tasks. Interestingly, as figure 5 illustrates, later

time windows in fNIRS showed a more significant correlation between frontal HbO elevation and EEG-spectral features in healthy controls confirming the intrinsic slowness of hemodynamic responses relative to electrical activities (Plichta et al., 2007). Overall, the lack of hemodynamic signatures in ALS patients combined with the absence of correlative patterns with EEG-features can potentially introduce new spatial candidates for disease-specific cognitive markers.

Small number of ALS patients recruited in this study due to relative difficulty of recruiting and/or recording from this population was a major limitation which can be addressed by considering larger samples of ALS patients in future studies to further explore the generalizability of the obtained neuro-markers to the neurogenesis of ALS. More specific clinical information such as emotional impairments which appear to affect neural features such as ERP characteristics (Campanella et al., 2004) is another potential direction to further expand our study. For example, apathy is a common issue in ALS (Unglik et al., 2018), and motivation is known to affect BCI performance (Kleih et al., 2010), which can be critical for ALS patients as one of the main BCI end-users. Future studies to further expand the cognitive and behavioral tests which consider more specific clinical information particular to ALS will no doubt provide valuable insights into existing ALS research.

Overall, this chapter's findings demonstrated the integrative characteristics of non-motor neural signatures in patients with severe motor deficits that are reflected in both electrical and hemodynamic neural features and suggest future exploitation of these signatures as potential diagnostic and prognostic markers. The results could improve our integrative understanding of mental workload in healthy brain functions while elucidating the potential mechanisms of ALS's effect on non-motor functions.

REFERENCES

Abiri, Reza, Soheil Borhani, Eric W. Sellers, Yang Jiang, and Xiaopeng Zhao. 2019. "A Comprehensive Review of EEG-Based Brain-Computer Interface Paradigms." *Journal of Neural Engineering* 16 (1): 011001.

Bastos, André Moraes, Julien Vezoli, Conrado Arturo Bosman, Jan-Mathijs Schoffelen, Robert Oostenveld, Jarrod Robert Dowdall, Peter De Weerd, Henry Kennedy, and Pascal Fries. 2015. "Visual Areas Exert Feedforward and Feedback Influences through Distinct Frequency Channels." *Neuron*. https://doi.org/10.1016/j.neuron.2014.12.018.

Bauernfeind, Günther, Reinhold Scherer, Gert Pfurtscheller, and Christa Neuper. 2011. "Single-Trial Classification of Antagonistic Oxyhemoglobin Responses during Mental Arithmetic." *Medical & Biological Engineering & Computing*. https://doi.org/10.1007/s11517-011-0792-5.

Borgheai, S. B., R. J. Deligani, J. McLinden, M. Abtahi, S. Ostadabbas, K. Mankodiya, and Y. Shahriari. 2019. "Multimodal Evaluation of Mental Workload Using a Hybrid EEGfNIRS Brain-Computer Interface System*." *2019 9th International IEEE/EMBS Conference on Neural Engineering (NER)*.

Burke, Tom, Marta Pinto-Grau, Katie Lonergan, Peter Bede, Meabhdh O'Sullivan, Mark Heverin, Alice Vajda, Russell L. McLaughlin, Niall Pender, and Orla Hardiman. 2017. "A Cross-Sectional Population-Based Investigation into Behavioral Change in Amyotrophic Lateral Sclerosis: Subphenotypes, Staging, Cognitive Predictors, and Survival." *Annals of Clinical and Translational Neurology* 4 (5): 305–17.

Campanella, S., M. E. Vanhoolandt, and P. Philippot. 2004. "Emotional Deficit in Subjects with Psychopathic Tendencies as Assessed by the Minnesota Multiphasic Personality Inventory-2: An Event-Related Potentials Study." *Neuroscience Letters*. https://doi.org/10.1016/j.neulet.2004.09.061.

Chaudhary, Ujwal, Bin Xia, Stefano Silvoni, Leonardo G. Cohen, and Niels Birbaumer. 2017. "Brain–Computer Interface–Based Communication in the Completely Locked-In State." *PLOS Biology*. https://doi.org/10.1371/journal.pbio.1002593.

Deiber, Marie-Pierre, Pascal Missonnier, Olivier Bertrand, Gabriel Gold, Lara Fazio-Costa, Vicente Ibañez, and Panteleimon Giannakopoulos. 2007. "Distinction between Perceptual and Attentional Processing in Working Memory Tasks: A Study of Phase-Locked and Induced Oscillatory Brain Dynamics." *Journal of Cognitive Neuroscience*. https://doi.org/10.1162/jocn.2007.19.1.158.

Deligani, R. J., S. I. Hosni, T. M. Vaughan, L. M. McCane, D. J. Zeitlin, D. J. McFarland, D. J. Krusienski, and Y. Shahriari. 2019. "Neural Alterations During Use of a P300-Based BCI by Individuals with Amyotrophic Lateral Sclerosis*." *2019 9th International IEEE/EMBS Conference on Neural Engineering (NER)*. https://doi.org/10.1109/ner.2019.8717044.

Engel, Andreas K., and Pascal Fries. 2010. “Beta-Band Oscillations—signalling the Status Quo?” *Current Opinion in Neurobiology*. https://doi.org/10.1016/j.conb.2010.02.015.

Fernández, Thalía, Thalía Harmony, Mario Rodríguez, Jorge Bernal, Juan Silva, Alfonso Reyes, and Erzsébet Marosi. 1995. “EEG Activation Patterns during the Performance of Tasks Involving Different Components of Mental Calculation.” *Electroencephalography and Clinical Neurophysiology*.

Hochberg, Yosef, and Yoav Benjamini. 1990. “More Powerful Procedures for Multiple Significance Testing.” *Statistics in Medicine*. https://doi.org/10.1002/sim.4780090710.

Iyer, Parameswaran Mahadeva, Catriona Egan, Marta Pinto-Grau, Tom Burke, Marwa Elamin, Bahman Nasseroleslami, Niall Pender, Edmund C. Lalor, and Orla Hardiman. 2015. “Functional Connectivity Changes in Resting-State EEG as Potential Biomarker for Amyotrophic Lateral Sclerosis.” *PloS One* 10 (6): e0128682.

Kellmeyer, Philipp, Moritz Grosse-Wentrup, Andreas Schulze-Bonhage, Ulf Ziemann, and Tonio Ball. 2018. “Electrophysiological Correlates of Neurodegeneration in Motor and Non-Motor Brain Regions in Amyotrophic Lateral Sclerosis-Implications for Brain-Computer Interfacing.” *Journal of Neural Engineering* 15 (4): 041003.

Kleih, S. C., F. Nijboer, S. Halder, and A. Kübler. 2010. “Motivation Modulates the P300 Amplitude during Brain–computer Interface Use.” *Clinical Neurophysiology*.

Kocsis, L., P. Herman, and A. Eke. 2006. “The Modified Beer–Lambert Law Revisited.” *Physics in Medicine and Biology*. https://doi.org/10.1088/0031-9155/51/5/n02.

Krusienski, D. J., E. W. Sellers, D. J. McFarland, T. M. Vaughan, and J. R. Wolpaw. 2008. “Toward Enhanced P300 Speller Performance.” *Journal of Neuroscience Methods*.

Kübler, Andrea, Boris Kotchoubey, Thilo Hinterberger, Nimr Ghanayim, Juri Perelmouter, Margarete Schauer, Christoph Fritsch, Edward Taub, and N. Birbaumer. 1999. “The Thought Translation Device: A Neurophysiological Approach to Communication in Total Motor Paralysis.” *Experimental Brain Research*. https://doi.org/10.1007/s002210050617.

Kübler, Andrea, Nicola Neumann, Jochen Kaiser, Boris Kotchoubey, Thilo Hinterberger, and Niels P. Birbaumer. 2001. “Brain-Computer Communication: Self-Regulation of Slow Cortical Potentials for Verbal Communication.” *Archives of Physical Medicine and Rehabilitation*.

Kuruvilla, Mili S., Jordan R. Green, Hasan Ayaz, and Daniel L. Murman. 2013. “Neural Correlates of Cognitive Decline in ALS: An fNIRS Study of the Prefrontal Cortex.” *Cognitive Neuroscience*. https://doi.org/10.1080/17588928.2013.797889.

Lloyd-Fox, Sarah, M. Papademetriou, M. K. Darboe, N. L. Everdell, R. Wegmuller, A. M. Prentice, S. E. Moore, and C. E. Elwell. 2015. “Functional near Infrared Spectroscopy

(fNIRS) to Assess Cognitive Function in Infants in Rural Africa." *Scientific Reports*. https://doi.org/10.1038/srep04740.

Murguialday, A. Ramos, A. Ramos Murguialday, J. Hill, M. Bensch, S. Martens, S. Halder, F. Nijboer, B. Schoelkopf, N. Birbaumer, and A. Gharabaghi. 2011. "Transition from the Locked in to the Completely Locked-in State: A Physiological Analysis." *Clinical Neurophysiology*.

Naseer, Noman, and Keum-Shik Hong. 2015. "fNIRS-Based Brain-Computer Interfaces: A Review." *Frontiers in Human Neuroscience*. https://doi.org/10.3389/fnhum.2015.00003.

Oruç, Ipek, Olav Krigolson, Kirsten Dalrymple, Lindsay S. Nagamatsu, Todd C. Handy, and Jason J. S. Barton. 2011. "Bootstrap Analysis of the Single Subject with Event Related Potentials." *Cognitive Neuropsychology*. https://doi.org/10.1080/02643294.2011.648176.

Pettit, Lewis D., Mark E. Bastin, Colin Smith, Thomas H. Bak, Thomas H. Gillingwater, and Sharon Abrahams. 2013. "Executive Deficits, Not Processing Speed Relates to Abnormalities in Distinct Prefrontal Tracts in Amyotrophic Lateral Sclerosis." *Brain*. https://doi.org/10.1093/brain/awt243.

Plichta, M. M., S. Heinzel, A-C Ehlis, P. Pauli, and A. J. Fallgatter. 2007. "Model-Based Analysis of Rapid Event-Related Functional near-Infrared Spectroscopy (NIRS) Data: A Parametric Validation Study." *NeuroImage*. https://doi.org/10.1016/j.neuroimage.2006.11.028.

Putze, Felix, Sebastian Hesslinger, Chun-Yu Tse, Yunying Huang, Christian Herff, Cuntai Guan, and Tanja Schultz. 2014. "Hybrid fNIRS-EEG Based Classification of Auditory and Visual Perception Processes." *Frontiers in Neuroscience*. https://doi.org/10.3389/fnins.2014.00373.

Raggi, Alberto, Sandro Iannaccone, and Stefano F. Cappa. 2010. "Event-Related Brain Potentials in Amyotrophic Lateral Sclerosis: A Review of the International Literature." *Amyotrophic Lateral Sclerosis*. https://doi.org/10.3109/17482960902912399.

Santhosh, Jayashree, Manvir Bhatia, Shweta Sahu, and Sneh Anand. 2005. "Decreased Electroencephalogram Alpha Band [8-13 Hz] Power in Amyotrophic Lateral Sclerosis Patients: A Study of Alpha Activity in an Awake Relaxed State." *Neurology India*. https://doi.org/10.4103/0028-3886.15071.

Schalk, Gerwin, and Jürgen Mellinger. 2010. *A Practical Guide to Brain–Computer Interfacing with BCI2000: General-Purpose Software for Brain-Computer Interface Research, Data Acquisition, Stimulus Presentation, and Brain Monitoring*. Springer Science & Business Media.

Schudlo, Larissa C., and Tom Chau. 2014. "Dynamic Topographical Pattern Classification of Multichannel Prefrontal NIRS Signals: II. Online Differentiation of

Mental Arithmetic and Rest." *Journal of Neural Engineering*. https://doi.org/10.1088/1741-2560/11/1/016003.

Shin, Jaeyoung, Klaus-R Müller, and Han-Jeong Hwang. 2016. "Near-Infrared Spectroscopy (NIRS)-Based Eyes-Closed Brain-Computer Interface (BCI) Using Prefrontal Cortex Activation due to Mental Arithmetic." *Scientific Reports*. https://doi.org/10.1038/srep36203.

Shin, Jaeyoung, Klaus-Robert Muller, and Han-Jeong Hwang. 2017. "Hybrid EEG-NIRS Brain-Computer Interface under Eyes-Closed Condition." *2017 Asia-Pacific Signal and Information Processing Association Annual Summit and Conference (APSIPA ASC)*.

Siegel, Markus, Tobias H. Donner, and Andreas K. Engel. 2012. "Spectral Fingerprints of Large-Scale Neuronal Interactions." *Nature Reviews Neuroscience*. https://doi.org/10.1038/nrn3137.

Simis, Marcel, Karin Santos, João Sato, Felipe Fregni, and Linamara Battistella. 2018. "T107. Using Functional near Infrared Spectroscopy (fNIRS) to Assess Brain Activity of Spinal Cord Injury Patient, during Robot-Assisted Gait." *Clinical Neurophysiology*. https://doi.org/10.1016/j.clinph.2018.04.108.

Spitzer, Bernhard, and Saskia Haegens. 2017. "Beyond the Status Quo: A Role for Beta Oscillations in Endogenous Content (Re)Activation." *Eneuro*. https://doi.org/10.1523/eneuro.0170-17.2017.

Unglik, Johanna, Catherine Bungener, Daniel Delgadillo, François Salachas, Pierre François Pradat, Gaëlle Bruneteau, Timothée Lenglet, et al., 2018. "Emotional Feeling in Patients Suffering from Amyotrophic Lateral Sclerosis." *Gériatrie et Psychologie Neuropsychiatrie Du Viellissement*.

Vizioli, Luca, Kay Foreman, Guillaume A. Rousselet, and Roberto Caldara. 2010. "Inverting Faces Elicits Sensitivity to Race on the N170 Component: A Cross-Cultural Study." *Journal of Vision* 10 (1): 15.1–23.

Wimmer, K., M. Ramon, T. Pasternak, and A. Compte. 2016. "Transitions between Multiband Oscillatory Patterns Characterize Memory-Guided Perceptual Decisions in Prefrontal Circuits." *Journal of Neuroscience*. https://doi.org/10.1523/jneurosci.3678-15.2016.

CHAPTER 3: ELECTRICAL AND VASCULAR NEURAL FUNCTIONS IN PEOPLE WITH ALS: AN EEG-FNIRS RESTING-STATE STUDY

Published in IEEE Transactions on Neural Systems and Rehabilitation Engineering. doi:10.1109/TNSRE.2020.3031495

Roohollah Jafari Deligani[1], Sarah Ismail Hosni[1], Seyyed Bahram Borgheai[1], John McLinden[1], Alyssa Hillary Zisk[2], Kunal Mankodiya[1], and Yalda Shahriari[1]

[1]Department of Electrical, Computer and Biomedical Engineering; University of Rhode Island, Kingston, RI 02881, USA

[2]Interdisciplinary Neuroscience Program; University of Rhode Island, Kingston, RI 02881, USA

Email: yalda_shahriari@uri.edu

ABSTRACT

Objective: Amyotrophic lateral sclerosis (ALS) is a complex neurodegenerative disease that causes the progressive loss of voluntary muscle control. Recent studies have reported conflicting results on alterations in resting-state functional brain networks in ALS by adopting unimodal techniques that measure either electrophysiological or vascular-hemodynamic neural functions. However, no study to date has explored simultaneous electrical and vascular-hemodynamic changes in the resting-state brain in ALS. Using complementary multimodal electroencephalography (EEG) and functional near-infrared spectroscopy (fNIRS) recording and analysis techniques, we explored the underlying multidimensional neural contributions to altered oscillations and functional connectivity in people with ALS. *Methods:* 10 ALS patients and 9 age-matched controls underwent multimodal EEGfNIRS recording in the resting state. Resting-statefunctional connectivity (RSFC) and power spectra of both modalities in both groups were analyzed and compared statistically. *Results:* Increased fronto-parietal EEG connectivity in the alpha and beta bands and increased interhemispheric and right intra-hemispheric fNIRS connectivity in the frontal and prefrontal regions were observed in ALS. Frontal, central, and temporal theta and alpha EEG power decreased in ALS, as did parietal and occipital alpha EEG power, while frontal and parietal hemodynamic spectral power increased in ALS. *Significance:* These results suggest that electro-vascular disruption in neuronal networks extends to the extra-motor regions in ALS patients, which can ultimately introduce novel neural markers of ALS that can be exploited further as diagnostic and prognostic tools.

Index Terms—Amyotrophic lateral sclerosis (ALS), electroencephalography (EEG), functional near-infrared spectroscopy (fNIRS), resting-state functional connectivity (RSFC).

3.1 BACKGROUND

Amyotrophic lateral sclerosis (ALS) is a complex neurodegenerative disease fundamentally characterized by the progressive loss of voluntary muscle control attributable to motor neuron degeneration. Neuroimaging studies have consistently provided growing evidence of extra-motor involvement in addition to the motor neural involvement known well in ALS pathophysiology (Christidi et al., 2018; Fraschini et al., 2018; Kopitzki et al., 2016; Mohammadi et al., 2009; Iyer et al., 2015). Exploration of potential perturbations in underlying interconnected motor and extra-motor neural networks during cognitive tasks, motor functions, and the resting-state represents an important tool to ALS' effect on functional cortical networks and clarify further pathophysiology and clinically established disease markers for a large group of patients. Resting-state studies may be central to information processing as they provide insight into alterations in spontaneous cognition associated with the disease (Buckner and Vincent 2007). Although these resting-state studies do not reflect conscious mental activity exclusively, they may reflect more intrinsic properties of functional brain organization (Vincent et al., 2008) and represent the spontaneous coherent fluctuations in functionally connected brain regions (Mohammadi et al., 2009).

Resting-state functional connectivity (RSFC) has been investigated widely to identify potential ALS biomarkers, as performance confounds attributable to potential

ALS patients' motor or cognitive impairments do not affect the resting-state (Luo et al., 2012). However, conflicting RSFC findings have led to a lack of consistent functional connectivity markers for ALS patients (Pievani et al., 2014), and the way functional cortical networks are altered in ALS patients is not yet understood clearly (Kopitzki et al., 2016; Fraschini et al., 2016). One study reported decreased RSFC in both the right and left prefrontal cortex (Agosta et al., 2013), while others have reported increased RSFC in prefrontal regions in ALS patients (Douaud et al., 2011; Luo et al., 2012; Iyer et al., 2015). Fraschini et al. (Fraschini et al., 2018) reported overall decreased RSFC in ALS patients using electroencephalography (EEG) recordings, while Kopitzki et al. (Kopitzki et al., 2016) reported overall preserved RSFC using functional near-infrared spectroscopy (fNIRS). Using functional magnetic resonance imaging (fMRI), Verstraete et al. (Verstraete et al., 2010) reported overall preserved RSFC in the motor and sensorimotor network, while other groups also have reported increased RSFC in the motor (Luo et al., 2012; Pievani et al., 2014), premotor (Iyer et al., 2015), and sensorimotor (Luo et al., 2012; Iyer et al., 2015) networks. Further, these studies have different views on the way their findings are related to the underlying neural dynamics of the disease. For example, increased functional connectivity in ALS patients has been interpreted both as a reflection of impairment in the neurons' inhibitory functions and as a physiological compensation for reduced structural integrity (Iyer et al., 2015). These divergent findings might be attributable to differences in methodological approaches and/or neuroimaging techniques that may affect RSFC estimation (Fraschini et al., 2016; Pievani et al., 2014), which corroborates the essential need to utilize complementary multimodal approaches to explore underlying neural alterations comprehensively.

Despite the widely explored RSFC in ALS patients, little investigation has been conducted to gain further insight about how ALS alters the causal organization of brain regions. To date, only a few studies have explored the direction of information flow between different regions (Shahriari et al., 2015; Blain-Moraes et al., 2013) and little is known about disrupted resting-state directional functional connectivity (RSDFC) in ALS patients (Fang et al., 2016).

Several neuroimaging modalities have been used to measure the neural and hemodynamic alterations of functional cortical networks in ALS, but there are methodological issues that may affect these findings' reliability (Fraschini et al., 2016). fMRI is an established method used widely to investigate vascular activities in ALS, but it is costly and many patients with ALS have body positioning constraints that affect scanning (Fraschini et al., 2016). Alternatively, fNIRS measures vascular dynamics and is quite portable and simple to set up for clinical application even in patients with severe motor impairment, for whom fMRI is contraindicated (Kopitzki et al., 2016). Moreover, fNIRS is less sensitive to potential motion artifacts, which eliminates motion-induced spurious functional relations between cortical regions and does not influence measurement differences in patient studies. More recently, fNIRS has been used in ALS neural investigation studies (Kopitzki et al., 2016; Borgheai et al., 2019), and as an input to brain-computer (BCI) systems to help patients with severe motor disabilities, including those with ALS, communicate (Naseer and Hong 2015). However, fNIRS use has its own limitations. The individual channel-wise functional connection fNIRS measures has raised reliability issues, and thus, cluster-wise measurements are recommended instead for reliable interpretations (Zhang et al., 2011), which requires a large number of fNIRS

optodes to analyze different functional clusters. This causes a decay in temporal resolution attributable to the one-by-one light emission queue of the optodes (Kamran et al., 2016), which affects fNIRS' suitability as a method to study larger numbers of clusters. EEG is another alternative neuroimaging method with high temporal resolution that allows analysis of functional connections in different specific frequency bands, each of which has characteristic biological and pathophysiological significance. EEG can measure the neurons' direct electrical activities, while fNIRS and fMRI both measure the vascular dynamics that serve only as an indirect measure of neural activity. As neurons' functional states affect both their electrical and vascular-hemodynamic properties, many studies have explored the fundamental electrical and vascular activities of neurological functions using multimodal techniques (Anwar et al., 2016; Nguyen et al., 2012; Al-Shargie et al., 2016). Accordingly, our recent studies and others have suggested multimodal measures' (electrical-EEG and vascular-fNIRS) important role in discovering cognitive neural markers, including those for attention and memory (Borgheai et al., 2019), mental distress (Al-Shargie et al., 2016), language perception (Schneider et al., 2015), and emotion (Balconi et al., 2018). However, to our knowledge, no study has characterized alterations in resting-state electrical and vascular functional neural networks in patients with ALS. Such a study is of particular interest in functional network investigations of ALS, as there is no fundamental understanding of this disease's pathological effects on patients' heterogeneous brain network connectivity.

The first goal of this chapter is to explore power spectra and RSFC alterations in ALS using complementary multimodal EEG-fNIRS recording and analysis techniques. While fNIRS allows the examination of correlated low oscillatory hemodynamic

fluctuations on the metabolic level, EEG allows investigation of the temporal dynamics of precise band-specific electrical activity affected directly by underlying neural interactions. Therefore, band-specific vascular and electrical power analyses were conducted. Using coherence and correlation analysis, RSFC network analysis across different cortical regions including prefrontal, frontal, parietal, and occipital were further performed. In addition to that, to gain further insight into how ALS alters exchange of information between two brain regions, the RSDFC alterations in ALS will also be explored using Granger causality analysis for fNIRS data.

3.2 METHODS

3.2.1 Subjects

Ten participants with ALS (age 58.2±11.6 years, two females, see Table 3.1) and nine healthy controls (age 61±3.8 years, six females) were recruited for this study. ALS patients had functional rating scale-revised (ALSFRS-R) scores of 23.2±13.7 (Mean±SD) on a 48-point scale, on which 48 represents normal function in activities of daily living (ADL) and 0 represents a complete loss of function (Cedarbaum et al., 1999). Age-matched control subjects had no reported history of visual, mental, or substance-related issues.

3.2.2 Experimental Protocol

Subjects participated in two sessions with one run per session. All subjects were instructed to close their eyes and remain awake during the resting state recording. The subjects were also asked to relax and try not to think about any particular matter. In each run, five minutes of resting state EEG-fNIRS data were acquired, which is the optimum recording duration to obtain robust functional connectivity in brain networks (Geng et al., 2017).

Table 3.1. ALS Subjects Demographic Information.

Participant No.	**Age**	**Gender**	**ALSFRS-R (max 48)**
ALS-1	55	M	4
ALS-2	67	M	7
ALS-3	69	F	23
ALS-4	52	M	22
ALS-5	72	M	36
ALS-6	61	M	39
ALS-7	33	M	10
ALS-8	52	M	-
ALS-9	54	F	39
ALS-10	67	M	29
Mean ± SD	58.2±11.6	-	23.2±13.7

3.2.3 Data Acquisition

Both signals were recorded simultaneously using a single cap mounted with both EEG electrodes and fNIRS optodes. fNIRS data were recorded using NIRScout (NIRx Inc.) with two NIR lights (760 nm and 850 nm wavelengths) and digitized at 7.81 Hz. EEG data were recorded using the g.USBamp amplifier (g.tec Medical Tech.) and digitized at 256 Hz. Figure 1 shows a schematic head model of the fNIRS-EEG sensors' placement. EEG was recorded from fourteen channels: F1*, Fz*, F2*, Cz, P3, P7, Pz, P4, P8, PO7, PO8, T7, T8, and Oz covering all of the frontal, central, parietal, temporal

and occipital areas, which are investigated commonly in whole head surface ALS studies (Fraschini et al., 2018; Kopitzki et al., 2016; Iyer et al., 2015) (note: F1*, Fz* and F2* respectively, were the nearest electrode placements to fNIRS-occupied F1, Fz, and F2 according to the 128-channel montage). As depicted in figure 3.1, most of the fNIRS channels were mounted on the frontal and prefrontal areas that cover the regions in which the extra-motor ALS alterations and cognitive impairments are reported most often (Christidi et al., 2018). Moreover, as prefrontal eyeblink artifacts are reported to be one of the greatest sources of distortion of EEG in the prefrontal and frontal regions (Chang et al., 2016), fNIRS was employed as an outperforming modality for those regions. To achieve this purpose, six emitters and five detectors acquired fourteen fNIRS channels that covered the frontal and prefrontal regions primarily, together with two emitters and two detectors that formed two channels in the parietal lobe. Following the modified combinatorial nomenclature (MCN) montage, emitters were placed at FPZ, AF3, AF4, Fz, F3, F4, CP5, and CP6, and detectors at FP1, FP2, AFZ, F1, F2, P5 and P6. Each fNIRS channel used an emitter-detector pair with the optimal 3-cm separation recommended by Yamamoto et al. (Yamamoto et al., 2002). This multimodal montage follows standards closely and is convenient to mount, making it an appropriate candidate for future multimodal applications. All experimental protocols, data acquisition, and stimulus presentation labels were controlled using BCI2000 and NIRStar software.

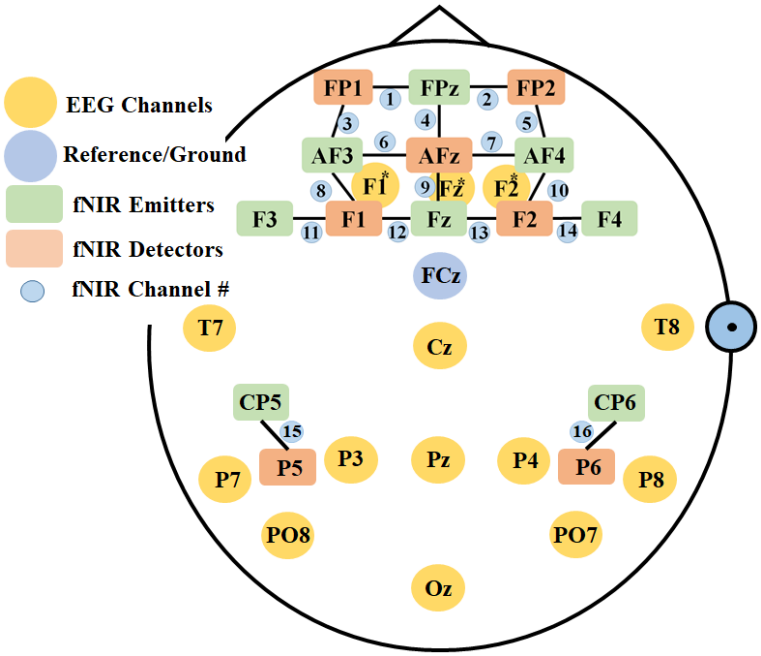

Figure 3.1. Schematic head model of the fNIRS-EEG sensors' placement.

3.2.4 EEG Signal Processing

EEG data were bandpass filtered at 0.5–30 Hz and detrended. Then, the data were checked for extreme values and outliers. The power spectra were computed for the delta (0.5-3.5 Hz), theta (3.5–8.5 Hz), alpha (8.5–12.5 Hz), and beta (12.5–30 Hz) frequency bands (Adler et al., 2003; Zeitlhofer et al., 1993) by applying a Hanning window 1.5 seconds long with a 50% overlap to reduce spectral leakage and then using a Fast Fourier Transform (FFT). Coherence was used to measure EEG RSFC between two regions. Coherence represents the linear relation between two signals at a specific frequency and is one of the methods used most commonly to analyze functionally cooperative cortical neuronal networks. First, for each signal, a set of Hanning windows 1.5 seconds long with a 50% overlap was used to obtain spectral density. Then, the coherence was computed through the modulus of the cross-spectrum of the signals normalized to the

product of their auto-spectra, after which the mean coherence was obtained for each specific frequency band across all of the frequency bands aforementioned. All of the measures obtained were averaged further over all runs.

3.2.5 fNIRS Signal Processing

fNIRS data were bandpass-filtered at 0.009–0.1 Hz as is done commonly in resting-state fNIRS studies to remove higher frequency physiological artifacts such as respiratory and cardiac signals, and long-term baseline drift (Sasai et al., 2011). Oxygenated hemoglobin (HbO) and deoxygenated hemoglobin (HbR) concentration changes were extracted from raw optical intensity data using the modified Beer–Lambert law (Kocsis et al., 2006). All time series were checked for outliers, including poorly-connected channels detected during the initial recording calibration and time series with sudden sharp peaks. After the data were preprocessed, the power spectra were computed for two frequency bands: very low frequency oscillations (VLFO) (0.009-0.04 Hz) and low frequency oscillations (LFO) (0.04-0.1 Hz) to investigate possible frequency-specific hemodynamic organizations across different regions of the resting-state brain (Fernandez Rojas et al., 2017).

For the fNIRS functional connectivity analysis, we calculated the Pearson's correlation coefficient for all pairs of channels to obtain RSFC measures. According to figure 1, channel numbers 1 to 5 were considered as prefrontal channels, channel numbers 6 to 14 as frontal and channel numbers 15 to 16 as parietal channels. Finally, all the connectivity measures were averaged over runs and across all subjects within each group for the between group comparison. Given that the HbO signal has shown more

implications in characterizing resting-state blood flow dynamics than has the HbR signal, and significant connectivity results in similar studies (Kopitzki et al., 2016; Sasai et al., 2011) are related primarily to HbO, our results focused largely on HbO, while the HbR results are shown in the supplementary section.

3.2.5.1 Hemodynamic Resting-State Directional Functional Connectivity (RSDFC)

RSDFC was also computed for preprocessed fNIRS signals through Granger causality (GC) analysis to measure the strength and directions of causal relationships between channels. Granger causality analysis utilizes univariate and bivariate autoregressive estimated models of two variables (channels X and Y) to investigate the potential contribution of using one variable in terms of improving the estimation of the other variable's autoregressive model. For this purpose, the univariate autoregressive models of X and Y are expressed in equations 3.1 and 3.2.

$$X(t) = \sum_{n=1}^{k} a_n X(t-n) + e_X \tag{3.1}$$

$$Y(t) = \sum_{n=1}^{k} b_n Y(t-n) + e_Y \tag{3.2}$$

In these equations X and Y are the variables for which current values are predicted, t is time point, k is the model order, a is the vector of the autoregression coefficients and e is the estimation error. In a similar way, the bivariate autoregressive models of X and Y are expressed in equations 3.3 and 3.4.

$$X(t) = \sum_{n=1}^{k} a_n X(t-n) + \sum_{n=1}^{k} b_n Y(t-n) + e_{XY} \tag{3.3}$$

$$Y(t) = \sum_{n=1}^{k} c_n Y(t-n) + \sum_{n=1}^{k} d_n X(t-n) + e_{YX} \quad (3.4)$$

The error terms in these equations are e_{XY} and e_{YX} which indicate that the error terms are from a bivariate model in which previous values of X are predicted from previous values of X and from previous values of Y and also previous values of Y are predicted from previous values of Y and from previous values of X. Finally, the Granger causality strength of Y on X can be measured using equation 3.5 which is the natural logarithm of the ratio of error variances generated by univariate autoregressive estimation and bivariate autoregressive estimation.

$$GC = \ln\left(\frac{var(e_X)}{var(e_{XY})}\right) \quad (3.5)$$

All the signals were segmented into smaller parts using a sliding windows of 10 seconds length with 50% overlap between windows. The Granger causality strength was calculated within each window and then averaged over all windows and runs. This process was repeated for all pairs of channels to generate the directional connectivity matrix. The optimal model order ($k = 11$) was obtained using Bayes information criterion (BIC).

3.2.6 Statistical Analysis

To statistically compare the results between groups, a nonparametric permutation testing procedure was used for power spectral, RSFC and RSDFC measures. To do so, all of the data points from healthy control and ALS patients (19 points) for each measure in each related frequency band separately were combined and nine data points (equal to the size of the smaller group) were selected randomly. Then, the mean of this group was

subtracted from the mean of the remainder of the data points to generate a surrogate difference between two groups selected randomly. This procedure was iterated 1000 times to create a null histogram (probability distribution) of the group differences. The proportion of the histogram points less or greater than the difference observed between the ALS and healthy group, depending on which tail of the histogram met the observation point, determined the *p*-values. The difference in the means was statistically significant if $p<0.05$. Finally, to account for multiple comparisons, all channels (or connections between channels in RSFC and RSDFC analysis) were considered a family of comparisons and all of the results were corrected by comparing them to the distribution of the maximum values among all family members of comparison obtained at each iteration of the permutation testing. The threshold *p*-value for correction was set to 0.05.

3.3 RESULTS

3.3.1 EEG Power

Figure 3.2 shows the channel map of the mean EEG power within the four aforementioned frequency bands for the healthy controls and ALS patients. We observed an overall power decrease in the ALS cohort relative to the control group. Permutation testing together with multiple comparisons revealed specifically a significant decrease in patients' theta power in channels F2 (Healthy 2.91±0.43 μV^2, ALS 2.16±0.38 μV^2, p=0.004), FCz (Healthy 2.93±0.38 μV^2, ALS 2.37±0.34 μV^2, p=0.02), T7 (Healthy 2.23±0.85 μV^2, ALS 1.61±0.6 μV^2, p=0.007), T8 (Healthy 2.01±0.91 μV^2, ALS 1.13±0.84 μV^2, p=0.006) and Cz (Healthy 2.71±0.56 μV^2, ALS 2.25±0.36 μV^2, p=0.03). Alpha power was also found to be significantly decreased in patients in channels FCz

(Healthy 4.13±0.37 μV^2, ALS 2.67±0.72 μV^2, p=0.01), T7 (Healthy 3.42±0.73 μV^2, ALS 1.81±0.52 μV^2, p<0.001), T8 (Healthy 3.21±0.77 μV^2, ALS 1.42±0.83 μV^2, p=0.005), Cz (Healthy 4.44±0.82 μV^2, ALS 3.18±0.72 μV^2, p=0.008), P7 (Healthy 4.56±0.82 μV^2, ALS 2.53±0.58 μV^2, p=0.03), P3 (Healthy 5.63±0.84 μV^2, ALS 3.37±0.42 μV^2, p=0.004), Pz (Healthy 6.23±1.12 μV^2, ALS 3.84±0.52 μV^2, p=0.005), P4 (Healthy 5.71±1.12 μV^2, ALS 3.36±0.81 μV^2, p=0.02), P8 (Healthy 5.4±0.94 μV^2, ALS 2.92±0.57 μV^2, p=0.01), PO7 (Healthy 5.61±0.72 μV^2, ALS 2.94±0.75 μV^2, p=0.006), PO8 (Healthy 5.84±0.91 μV^2, ALS 3.02±0.75 μV^2, p=0.005), and Oz (Healthy

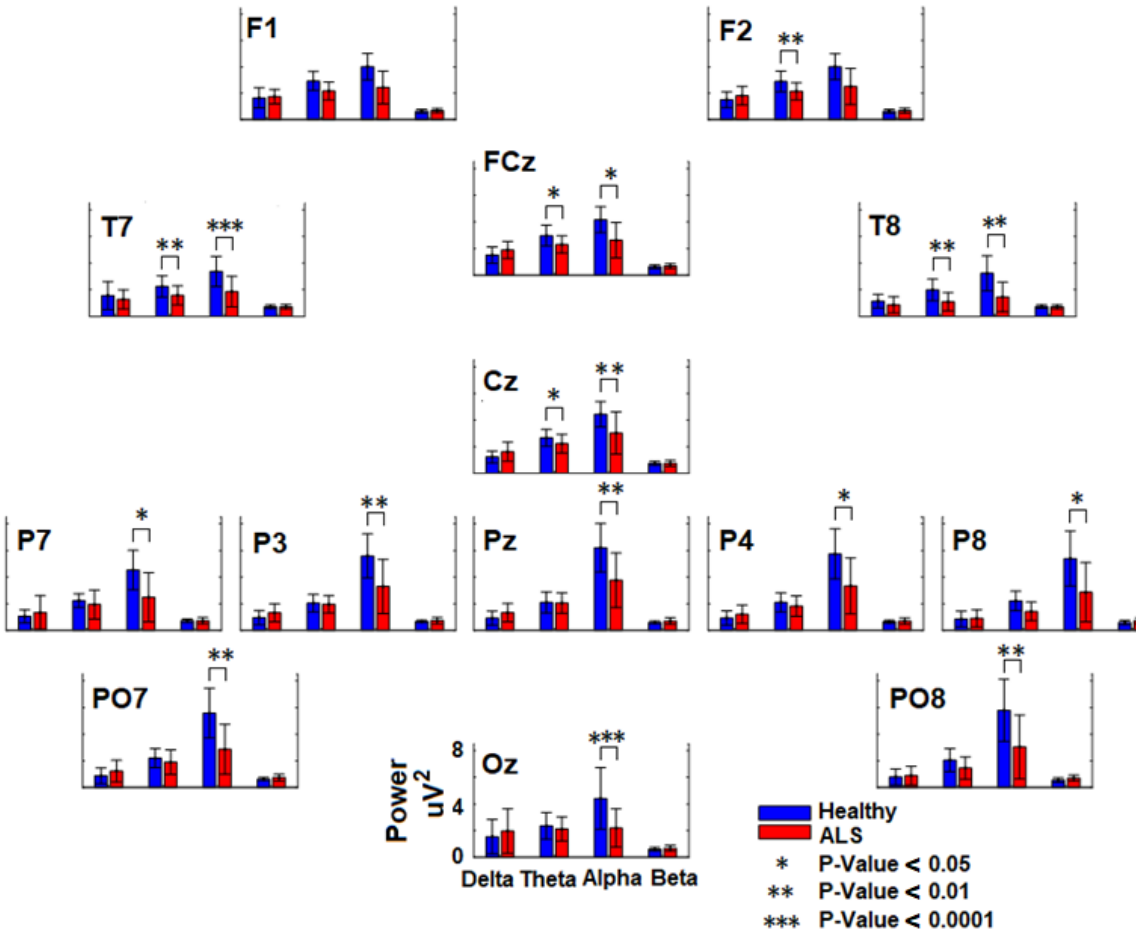

Figure 3.2. Channel map of averaged EEG power within the delta, theta, alpha and beta frequency bands for healthy controls and ALS patients.

4.43±0.76 μV^2, ALS 2.23±0.72 μV^2, p<0.001). No significant EEG power difference was observed in the delta and beta frequency bands.

3.3.2 fNIRS Power

Figure 3.3 shows the channel map of the mean HbO power within the VLFO and LFO ranges for healthy controls and ALS patients. Despite an overall EEG power decrease in patients, a general HbO power increase in patients was observed. Our statistical analysis revealed specifically a significant power increase in LFO in ALS patients in both the left parietal (CH15: Healthy 0.41±0.08 μmol^2, ALS 0.48±0.08 μmol^2, p=0.03) and right parietal (CH16: Healthy 0.40±0.12 μmol^2, ALS 0.49±0.1 μmol^2, p=0.03) channels. Compared to LFO power, more significant increases were found in the VLFO power in patients across all frontal channels, including: AF3-F1 (CH8: Healthy 0.79±0.45 μmol^2, ALS 1.02±0.52 μmol^2, p=0.02), Fz-AFz (CH9: Healthy 0.72±0.57 μmol^2, ALS 0.95±0.52 μmol^2, p=0.02), AF4-F2 (CH10: Healthy 0.78±0.49 μmol^2, ALS 0.98±0.61 μmol^2, p=0.02), F3-F1 (CH11: Healthy 0.64±0.54 μmol^2, ALS 0.88±0.53 μmol^2, p=0.01), Fz-F1 (CH12: Healthy 0.59±0.45 μmol^2, ALS 0.95±0.51 μmol^2, p=0.005), Fz-F2 (CH13: Healthy 0.59±0.57 μmol^2, ALS 0.93±0.50 μmol^2, p=0.005), F4-F2 (CH14: Healthy 0.66±0.43 μmol^2, ALS 0.93±0.63 μmol^2, p=0.006), and in left parietal (CH15: Healthy 0.59±0.40 μmol^2, ALS 0.89±0.62 μmol^2, p=0.002) and right parietal (CH16: Healthy 0.56±0.43 μmol^2, ALS 0.98±0.61 μmol^2, p<0.001) channels.

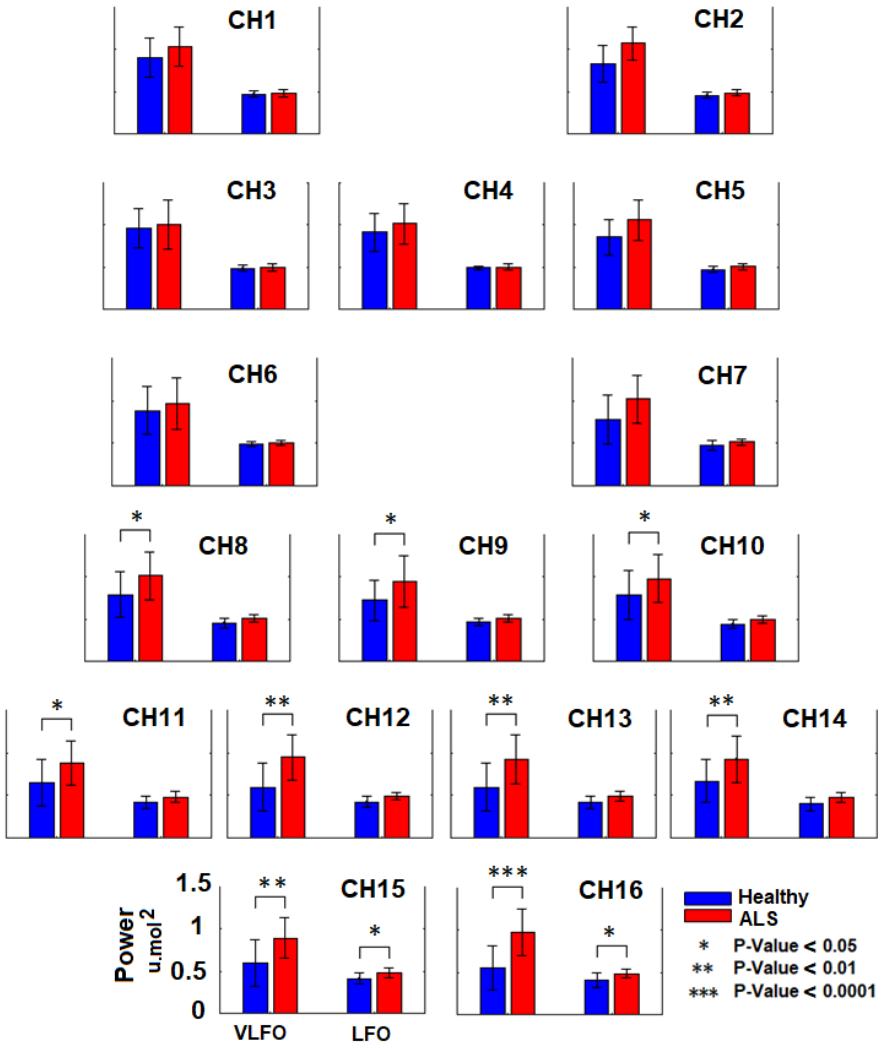

Figure 3.3. Channel map of averaged HbO power for very low frequency oscillations (VLFO) and low frequency oscillations (LFO) for healthy controls and ALS patients.

3.3.3 Electrical Resting-State Functional Connectivity (RSFC)

Figure 3.4 illustrates the negative logarithm of the *p*-values, or "activation index" as used in previous studies (Liu et al., 2015). These *p*-values were obtained from the statistical comparison of the mean magnitude squared EEG coherence between ALS patients and healthy controls in four frequency bands (delta, theta, alpha and beta) and

for three channels (Fz, Cz, Pz) as seed channels (note: results from other seed channels are reported here but not shown in the figure). The significant *p*-values after correction for multiple comparisons are illustrated by dashed lines between the corresponding connections. The statistical analysis revealed a significant alpha band RSFC increase in patients in fronto-parietal connections, including: F1-P3 (Healthy 0.24±0.01, ALS 0.41±0.03, p=0.009), F2-P4 (Healthy 0.20±0.03, ALS 0.36±0.06, p=0.007), Cz-P3 (Healthy 0.22±0.03, ALS 0.38±0.08, p=0.02). More importantly, a significant RSFC increase in the beta band was found in patients in the fronto-parietal connections including: F1-P3 (Healthy 0.21±0.04, ALS 0.44±0.04, p=0.002), F1-Pz (Healthy 0.21±0.06, ALS 0.42±0.04, p=0.002), F1-P4 (Healthy 0.16±0.02, ALS 0.33±0.02, p=0.004), Fz-P3 (Healthy 0.19±0.08, ALS 0.42±0.05, p<0.001), Fz-Pz (Healthy 0.21±0.03, ALS 0.44±0.04, p<0.001), Fz-P4 (Healthy 0.18±0.03, ALS 0.37±0.06, p<0.001), F2-P3 (Healthy 0.16±0.03, ALS 0.374±0.033, p<0.001), F2-Pz (Healthy 0.2±0.04, ALS 0.4±0.04, p<0.001), and F2-P4 (Healthy 0.18±0.07, ALS 0.36±0.04, p<0.001). Finally, P3-P4, an inter-hemispheric parietal connection, showed increased RSFC in ALS (Healthy 0.38±0.05, ALS 0.58±0.07, p=0.01).

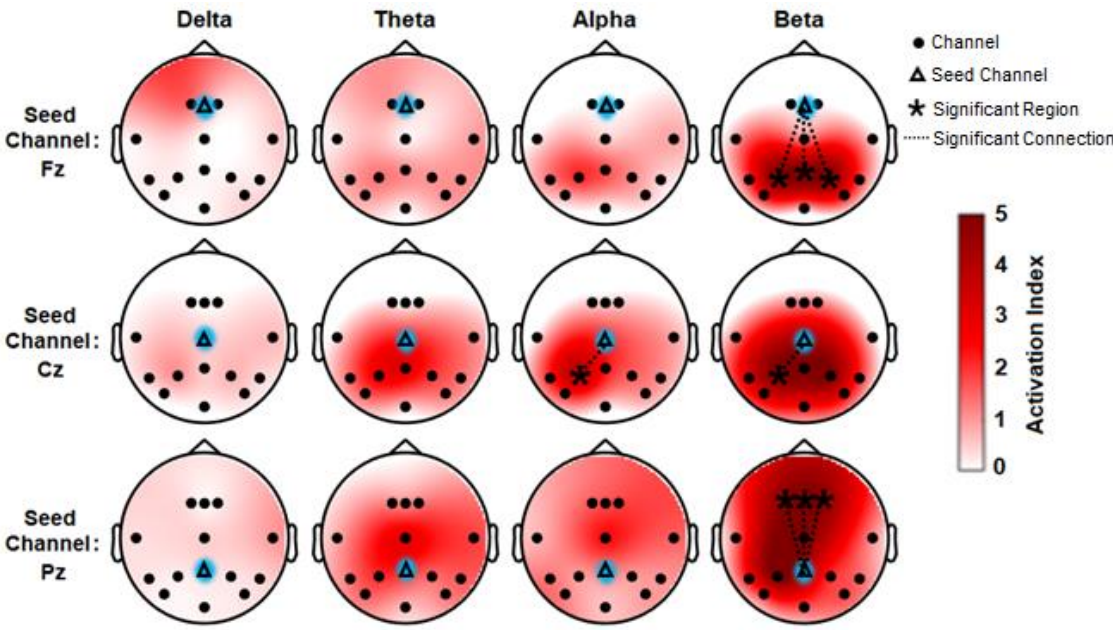

Figure 3.4. Head plots of RSFC activation index (negative logarithm of the p-values) obtained from the statistical comparison of averaged magnitude squared EEG coherence between ALS patients and healthy controls in four frequency bands (delta, theta, alpha, and beta) and for three channels as seed channels (Fz, Cz, Pz). The significant p-values after multiple comparisons correction are illustrated with dashed lines between the seed channel (highlighted in blue) and the significant region at the other end (highlighted in red based on the connection's activation index).

3.3.4 Hemodynamic Resting-State Functional Connectivity (RSFC)

Figure 3.5 illustrates the activation index based on obtained *p*-values for different regions calculated from the statistical comparison of the averaged HbO correlation between ALS patients and healthy controls for eight seed channels that had significantly altered connections with other channels. The significant *p*-values after multiple comparisons are illustrated with dashed lines between the corresponding regions. The magnitude squared correlation of HbO revealed a significant RSFC increase in patients within the right prefrontal region (CH2-CH4, Healthy 0.56±0.09, ALS 0.81±0.10, p=0.02), and within the right frontal region (CH13-CH4, Healthy 0.56±0.09, ALS

0.81±0.1, p=0.02; CH13-CH7, Healthy 0.61±0.08, ALS 0.73±0.05, p=0.03). Investigating interhemispheric RSFC also revealed a significant increase in patients in various within-frontal connections including: (CH6-CH7, Healthy 0.74±0.05, ALS 0.89±0.07, p=0.04; CH6-CH10, Healthy 0.61±0.07, ALS 0.79±0.09, p=0.02; CH6-CH13, Healthy 0.47±0.06, ALS 0.79±0.07, p=0.01; CH11-CH14, Healthy 0.48±0.08,

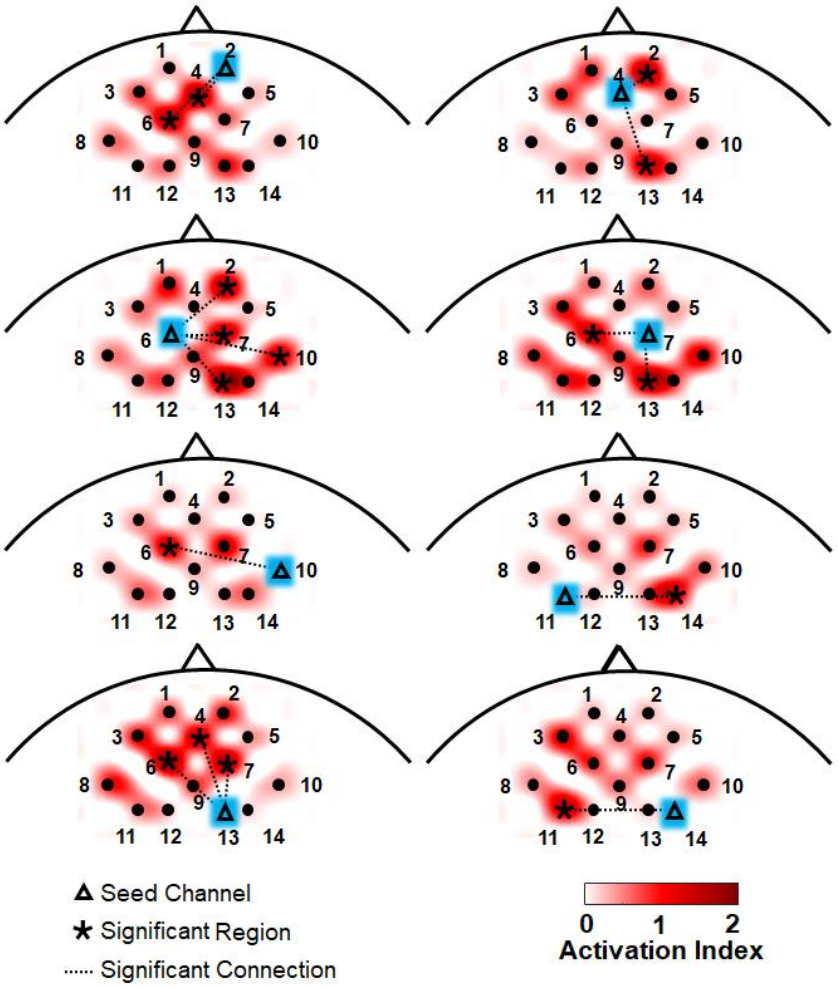

Figure 3.5. Frontal head plots illustrating activation indices (negative logarithm of the p-values) calculated from the statistical comparison of averaged HbO correlation between ALS patients and healthy controls for 8 seed channels. The significant p-values after multiple comparisons are illustrated by dashed lines between the seed channel (highlighted in blue) and the significant region at the other end (highlighted in red based on the connection's activation index). The numbers in the figure indicate channel numbers.

ALS 0.74±0.11, p=0.02) and also between the frontal and prefrontal regions (CH6-CH2, Healthy 0.71±0.05, ALS 0.83±0.06, p=0.02).

3.3.5 Hemodynamic Resting-State Directional Functional Connectivity (RSDFC)

Figure 3.6 illustrates the connectivity matrix for Healthy controls (top), ALS patients (middle) and significantly altered connections in ALS patients (bottom). Channel numbers are illustrated at the left and bottom side of each matrix (Channel locations are shown in figure 3.1). Inside the matrix, each block shows the averaged strength of RSDFC by a relative color from bottom labeled channels as sources towards left labeled channels as sinks. In this way, the upper triangular matrix accounts for feedforward connections (mostly from posterior towards anterior regions) and the lower triangular matrix accounts for feedback connections (mostly from anterior towards posterior regions). Individual connections between channels that had significant strength change are bordered by black rectangles and also shown in the bottom matrix. We observed a RSDFC increase in the ALS cohort relative to the control group in one single feedback connection within prefrontal region (CH2 to CH4, Healthy 0.89±0.13, ALS 1.13±0.27, p=0.01;) and overall RSDFC increase in feedforward connections from frontal channels towards prefrontal channels (CH13 to CH1, Healthy 0.73±0.15, ALS 1.07±0.21, p=0.005; CH8 to CH4, Healthy 0.80±0.09, ALS 1.11±0.15, p=0.004; CH11 to CH4, Healthy 0.72±0.17, ALS 1.17±0.33, p=0.005; CH12 to CH4, Healthy 0.84±0.20, ALS 1.16±0.19, p=0.005; CH13 to CH4, Healthy 0.71±0.11, ALS 1.10±0.14, p=0.007; CH14 to CH4, Healthy 0.91±0.26, ALS 1.23±0.16, p=0.005) and from parietal channels towards prefrontal channels (CH15 to CH1, Healthy 0.69±0.14, ALS 1.08±0.19,

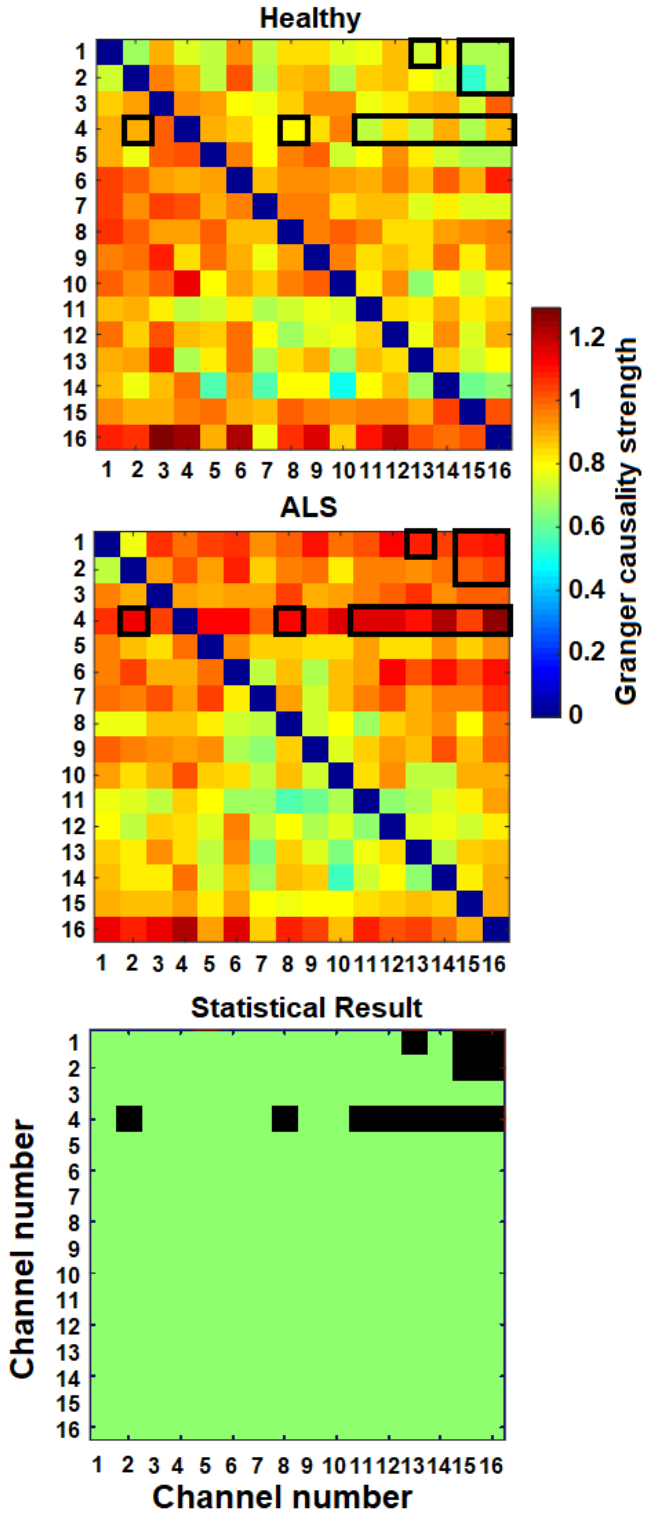

Figure 3.6. Directional functional connectivity matrix for Healthy controls (top), ALS patients (middle) and significantly altered connections in ALS patients (bottom). Channel numbers are illustrated at the left and bottom side of each matrix (Channel locations are shown in figure 3.1)

Healthy 0.54±0.18, ALS 0.99±0.19, p=0.006; CH16 to CH2, Healthy 0.69±0.15, ALS 1.05±0.17, p=0.005; CH15 to CH4, Healthy 0.70±0.15, ALS 1.04±0.23, p=0.004; CH16 to CH4, Healthy 0.87±0.19, ALS 1.25±0.22, p=0.004).

3.4 DISCUSSION

In this chapter, the electrical and vascular functional neural alterations of ALS were characterized by integrating EEG and fNIRS in a multimodal framework of recording and analyses. Functional network organizational impairments specific to ALS were characterized using frequency-band specific RSFC measures and spectral power in both hemodynamic and electrical activities during the resting-state. The causal network organizational impairments were also characterized using RSDFC measures in hemodynamic activities. Our comparative group analysis demonstrated significantly increased fronto-parietal EEG connectivity in the alpha and beta bands and significantly increased prefronto-parietal and prefronto-frontal fNIRS feedforward connectivity, along with increased interhemispheric and intra-right hemisphere fNIRS connectivity in the frontal and prefrontal regions in the ALS group. Furthermore, we observed an overall reduction in alpha and theta EEG spectral power in the frontal, central, and temporal regions, and alpha power reduction in the parietal and occipital regions of the brain, as well as increased hemodynamic spectral power in the frontal (VLFO) and parietal regions (VLFO and LFO) in ALS patients.

Our findings of increased functional connectivity in ALS are consistent with various hemodynamic and electrophysiological resting-state functional connectivity studies, across various cortical networks in ALS patients, including the Default Mode

network (DMN), the Fronto-Parietal network (FPN), Dorsal Attention network (DAN), and the salience network. For example, increased functional connectivity in ALS has been consistently reported in resting-state fMRI studies (Verstraete et al., 2010b); (Agosta et al., 2013b); (Douaud et al., 2011b); (Luo et al., 2012b); (Zhu et al., 2015); (Menke et al., 2016); (Ma et al., 2015a) primarily in the DMN and FPN which involve the prefrontal, frontal, and parietal regions. This increased functional connectivity has been shown to be associated with clinical and cognitive deficits in ALS patients (Agosta et al., 2013c), disease progression rates, and regions of decreased structural connectivity(Douaud et al., 2011c); (Luo et al., 2012c). Functional connectivity increases have been suggested to reflect primarily the extensive involvement of extra-motor networks in ALS rather than simply a physiological compensation mechanism for the reduced structural integrity or a reflection of a progressive loss of inhibitory cortical influence as an element of ALS' pathophysiology.

Although functional connectivity analysis reveals useful information about functionally synchronized brain regions, it does not imply the information transfer or causal influence between them. Using fNIRS modality, we found increased feedforward RSDFC from parietal towards frontal and prefrontal and from frontal towards prefrontal regions. Our fNIRS reports of increased directional connectivity is consistent with EEG findings of (Blain-Moraes et al., 2013). They have used an information theory based metric known as normalized symbolic transfer entropy and found increased fronto-parietal feedforward connectivity in ALS while doing cognitive task using a P300-based speller. They have interpreted these findings as a compensation for ALS-related loss of input into the global workspace such that sensory stimuli are represented with sufficient

strength for conscious processing. Another similar study (Blain-Moraes et al., 2013; Shahriari et al., 2015a) the authors have used directed transfer function analysis and reported increased feedforward and feedback connectivity in fronto-parietal and centro-parietal in the beta band. Patterns of fronto-parietal information flow have been reported to be associated with the ability to process external stimuli (Dehaene 2001) and therefore alterations in these patterns may reflect an underlying source of the changes in executive function and behavior in ALS patients (Blain-Moraes et al., 2013).

Incongruently, other resting-state fMRI studies have reported contradictory findings of reduced functional connectivity in ALS and in networks involved in cognitive and behavioral functions (Tedeschi et al., 2012a); (Mohammadi et al., 2009b); (Li et al., 2017). Thus, the characteristic signatures of RSFC impairments in ALS remain incongruent in the literature, as there is no clear agreement whether ALS-specific functional connectivity impairments represent an increased or decreased synchronization. Variations in the underlying structural degeneration, as well as methodological differences, including instability of independent component analysis (ICA)-based resting state analysis compared to other methods such as structural imaging-derived network-guided component analysis used in the functional connectivity analysis and seed region-based functional connectivity analysis (Zhou et al., 2013), may greatly contribute to variations in these observed signatures. Despite these incongruent results, alterations in the functional organization of the extra-motor networks have been interpreted generally as correlates of cognitive dysfunctions in ALS.

Resting-state electrophysiological studies have provided additional evidence that points to extra-motor networks' extensive involvement in ALS based on functional

connectivity findings. However, the precise neuroelectric signatures of the altered cortical communication mechanisms have not been characterized fully to date (Dukic et al., 2019a). Increased functional connectivity over the alpha and beta bands in areas corresponding to the DMN and FPN in ALS have been identified in (Iyer et al., 2015b) using nodal connectivity measures among localized sources of EEG recordings, which is consistent with our results. Although there was no clear association between frequency band-specific findings and ALS pathological changes, the authors linked patients' overall increased functional connectivity to enhanced cortical network recruitment as compensation for structural neuronal loss or alternatively, as a result of loss of inhibitory control over network regions, which suggests a biomarker for early cortical changes in ALS. Fraschini et al. (Matteo Fraschini et al., 2016b) reported significant network topology alterations in the beta band, similar to our finding for ALS patients. They linked their findings of frequency-specific beta band network alterations to reports that beta band connectivity is associated with maintaining the current cognitive state (i.e.,status quo) (Engel and Fries 2010a). In (M. Fraschini et al., 2018b), reduced bilateral central and temporal alpha band functional connectivity estimated at the source level was reported in ALS patients compared with healthy controls, suggesting the hypothesis of widespread alterations in synchronization to extra-motor connections. In a high-density longitudinal resting-state EEG study of ALS (Nasseroleslami et al., 2019), characteristic patterns of increased EEG-gamma coherence between frontal-parietal regions and EEG-theta coherence between bilateral regions over motor areas have been also identified. Based on correlations with these same patients' structural MRIs, the authors also

suggested this increased neural communication reflects the extensive involvement of extra-motor pathways.

To date, multimodal investigations of ALS functional neural alterations have not characterized electrical-vascular functions of the underlying neural network alterations in these cohorts. However, a few studies conducted combined structural and functional explorations to investigate multidimensional connectivity in ALS. For example, in a study conducted by Verstraete et al. (Verstraete et al., 2010c) using combined fMRI and diffusion tensor imaging (DTI), the authors reported no significant functional change in ALS patients. Similarly, Kopitzki et al. (Kopitzki et al., 2016c) obtained the same results for functional connectivity using DTI and fNIRS modalities. In this study, the authors placed eight individual fNIRS optodes separately and apart from each other all over the head. Because individual channel-wise RSFC measured by fNIRS has reliability issues (Zhang et al., 2011b) attributable to difficulty matching channel-to-channel for both RSFC strength and location precisely, this may explain the contrast with our fNIRS findings.

Our complementary electrical and vascular functional connectivity results of increased frontal-parietal connectivity using EEG and increased frontal and prefrontal connectivity using fNIRS are consistent with many resting-state studies that employed unimodal neuroimaging techniques including EEG or fMRI. Consistent with these previous studies, the prefrontal, frontal, and parietal brain regions are well-defined functionally coherent areas during the resting-state and overlap with the DMN, FPN, and DAN. The observed alterations in these regions point to the extensive role of cognitive and extra-motor networks in addition to motor pathways identified conventionally in

ALS. The DMN is known widely to provide a baseline state of the brain that represents memory, emotional processing, self-reference, spontaneous cognition, and aspects of consciousness (Raichle 2015). Increased resting state connectivity in the DMN has been consistently reported in ALS and was often significantly associated with greater disability and faster progression rates (Mohammadi et al., 2009c); (Tedeschi et al., 2012b). Moreover, executive functioning impairments in ALS have been reported to be associated with the FPN and DAN networks, which are believed to act as control systems for various cognitive activities including attention and executive processing (Vincent et al., 2008b); (Corbetta and Shulman 2002); (Christidi et al., 2012). Furthermore, we observed increased connectivity in hemodynamic activities in the frontal and right prefrontal regions, which is consistent with the findings of (Ma et al., 2015b). As the left frontal and prefrontal regions including the left lateral and left anterior prefrontal areas, are highly responsible for task and stimulus oriented control processes, such as response planning and stimulus-response relations (Yunusova et al., 2019a), this might explain why these areas did not demonstrate significant activation or connectivity changes in ALS during our resting-state analysis when there was no specific task or stimulus. On the other hand, constant monitoring for upcoming stimuli as a non-task oriented activity is controlled largely by the right frontal and prefrontal regions, including the right lateral frontal and rostral prefrontal areas (Yunusova et al., 2019b). As activity related to constant monitoring for upcoming stimuli has been reported to occur in the resting-state (Francis et al., 2017), the increased connectivity and power of hemodynamic activities in ALS patients is likely a compensatory mechanism for monitoring deficits. This is also consistent with Hammer et al.'s (Hammer et al., 2011) findings on ALS patients in a dual

spatial-working memory processing task, implying altered processing in the right dorsolateral prefrontal cortex. All of these can be associated with the previous ALS findings that have suggested that executive dysfunctions, including issues with information maintenance and monitoring, attentional processing, working memory, language, and social cognition, are present in people with ALS (Raaphorst et al., 2009); (Volpato et al., 2010). The alterations in functional connectivity observed in the extra-motor network provide further evidence that ALS is a multisystem disease that might have special markers in addition to its characteristic motor dysfunctions.

Notably, our results of significant increased fronto-parietal connectivity were found primarily in the EEG-beta frequency band, which supports our previous work (Shahriari et al., 2015b). As beta band neural coupling has been reported to be expressed more strongly if the maintenance of the current status is intended or predicted (Engel and Fries 2010b), the increased fronto-parietal connectivity in this frequency band in the patients can be interpreted as a compensatory mechanism for maintenance and monitoring deficits of the frontal-parietal control system. In (Clark, Blizzard, and Dickson 2015), the increased functional connectivity in ALS has been hypothesized to result from the loss of intracortical inhibitory influence supported by neurophysiological findings of altered cortical beta-desynchronization in motor execution in ALS patients during movement preparation and post-movement beta-rebound (Proudfoot et al., 2017); (Bizovičar et al., 2014).

In this chapter, the alterations in functional communication patterns in ALS were also characterized by spectral power analysis. Our EEG results are consistent with several studies that have reported a decrease in neural spectral power in ALS. For example, a

recent study (Dukic et al., 2019b) observed reductions in EEG spectral power in the prefrontal region in the delta and theta bands, the sensorimotor region in the beta band, and in the occipital and temporal regions in the delta, alpha, and beta bands in ALS patients. Our finding of overall reduced alpha band power also supports the findings in (Mai et al., 1998) and (Santhosh et al., 2005) of which the authors reported that the decrease in alpha power was associated with reduced neural activity correlated with the disease-specific structural degeneration that results from the structural loss of pyramidal neurons in ALS. Decreases in theta band spectral power have also been reported in resting-state studies of ALS (Jayaram et al., 2015), similar to our findings in the central and temporal regions of the brain.

In addition to reduced EEG spectral power, our band-specific hemodynamic results indicated increased VLFO and LFO activities in the frontal, prefrontal, and parietal regions in our ALS patients. Similarly, in (Luo et al., 2012d), increased vascular activity in extra-motor networks was interpreted to reflect compensatory processes for frontal-parietal network dysfunctions, which was supported with negative correlations with disease progression rates in their study. These interpretations are also consistent with (Agosta et al., 2013d), in which the authors suggested increased VLFO and LFO activity relates to cognitive impairment in ALS. However, the hypothesis of the compensatory mechanism and the spatial characteristics of these low-frequency power alterations in ALS needs to be investigated in future studies.

There are several limitations in this study, including its small sample size and ALS patients' heterogeneous characteristics. If a larger number of patients is recruited in future studies, it will be possible to classify them into subgroups based on the onset of

clinical symptoms, involvement level of motor degeneration, and cognitive deficits to discriminate between different patterns rather than considering putative patterns of altered networks for all ALS patients. In addition, quantitative assessment of cognitive profiles and psychometric behavioral screens, along with other biological information, including respiration, peripheral capillary oxygen saturation, and electromyography in ALS patients should be provided in future studies for more precise interpretations of the results. In terms of further analysis, conducting a framework for RSDFC investigation for EEG similar to what we did for fNIRS and comparing causal interactions between different regions obtained through different modalities is promising for future works to find a better understanding of the underlying neural networks. It is worth noting that further investigations should focus as well on the relations between electrical and hemodynamic aspects of altered neural networks, although caution is needed when interpreting the findings from multimodal measures and comparing them to other modalities that measure different properties of the underlying neural networks. Moreover, these techniques differ with respect to their temporal and spatial resolutions and it is not straightforward to compare their findings. Thus, they should be used instead in a complementary way to improve comprehensive understanding of multimodal findings.

Overall, our EEG-fNIRS multimodal resting state recording could capture functional neural and hemodynamic alterations in ALS, supporting the findings in several previous studies that employed unimodal EEG or fNIRS/fMRI techniques. We observed spectral power alterations in the VLFO and LFO ranges of hemodynamic responses primarily in the frontal and prefrontal regions and in the theta and alpha bands of

electrophysiological responses in ALS. These observations were complemented by the identification of additional functional electrophysiological alterations in the fronto-parietal connections in higher frequency bands (primarily beta), functional hemodynamic alterations in the frontal and prefrontal connections and directional feedforward functional hemodynamic alterations from parietal and frontal towards frontal and prefrontal regions in this cohort. Our proposed multimodal recording and analysis framework permits multidimensional investigations of functional network alterations underlying heterogeneous ALS pathologies. The outcomes can potentially be expanded further as a tool for non-invasive diagnosis and prognosis of the disease in clinical environments. Our findings highlight integrative recording and analysis techniques' importance in capturing broader ranges of disease-specific functional alterations that can potentially provide quantitative biomarkers of ALS pathogenesis.

Appendix: Supplementary Material

In this supplementary section, we present the table of healthy control's demographic information. We additionally present the supplementary results for HbR.

Table S3.1. Healthy control's demographic information

Subject No.	Age	Sex
H-1	59	F
H-2	57	M
H-3	70	M
H-4	60	F
H-5	58	F
H-6	63	F
H-7	60	F
H-8	62	M
H-9	60	F
Mean±SD	61.0±3.8	-

Figure S3.1. shows the channel map of averaged HbR VLFO and LFO power for healthy controls and ALS patients. No significant change in HbR power was observed in ALS patients compared to healthy controls. Figure S3.2. illustrates the activation index based on the obtained p-values for different regions calculated from the statistical comparison of averaged HbR correlations between ALS patients and healthy controls. The magnitude squared correlation of HbR revealed no significant RSFC changes in patients compared to healthy controls.

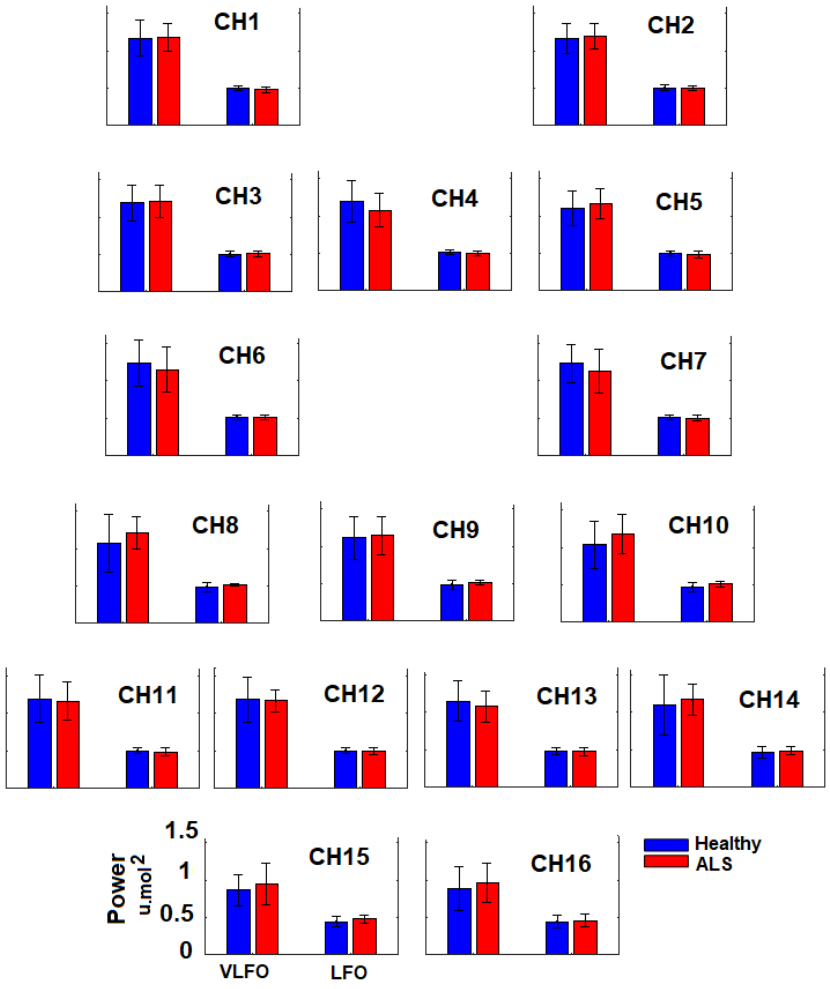

Figure S3.1. Channel map of averaged HbR power for very low frequency oscillations (VLFO) and low frequency oscillations (LFO) in healthy controls and ALS patients.

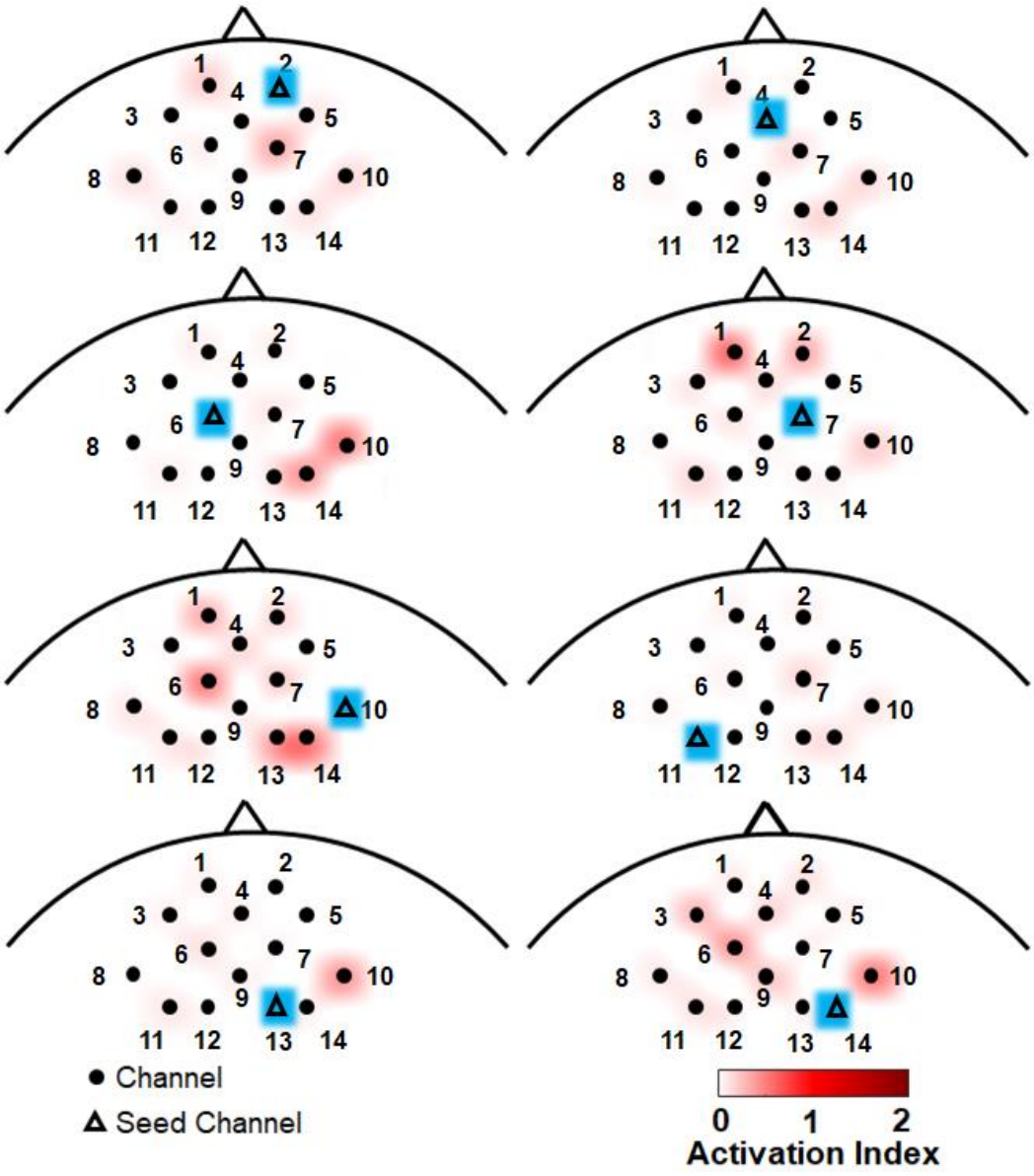

Figure S3.2. Frontal head plots illustrating activation indices (negative logarithm of the *p*-values) calculated from the statistical comparison of averaged HbR correlations between ALS patients and healthy controls for eight seed channels (highlighted in blue).

REFERENCES

Adler, G., S. Brassen, and A. Jajcevic. 2003. "EEG Coherence in Alzheimer?s Dementia." *Journal of Neural Transmission*. https://doi.org/10.1007/s00702-003-0024-8.

Agosta, Federica, Elisa Canu, Paola Valsasina, Nilo Riva, Alessandro Prelle, Giancarlo Comi, and Massimo Filippi. 2013a. "Divergent Brain Network Connectivity in Amyotrophic Lateral Sclerosis." *Neurobiology of Aging*. https://doi.org/10.1016/j.neurobiolaging.2012.04.015.

Al-Shargie, Fares, Masashi Kiguchi, Nasreen Badruddin, Sarat C. Dass, Ahmad Fadzil Mohammad Hani, and Tong Boon Tang. 2016. "Mental Stress Assessment Using Simultaneous Measurement of EEG and fNIRS." *Biomedical Optics Express*. https://doi.org/10.1364/boe.7.003882.

Anwar, A. R., M. Muthalib, S. Perrey, A. Galka, O. Granert, S. Wolff, U. Heute, G. Deuschl, J. Raethjen, and Muthuraman Muthuraman. 2016. "Effective Connectivity of Cortical Sensorimotor Networks During Finger Movement Tasks: A Simultaneous fNIRS, fMRI, EEG Study." *Brain Topography*. https://doi.org/10.1007/s10548-016-0507-1.

Balconi, Michela, Alessandra Frezza, and Maria Elide Vanutelli. 2018. "Emotion Regulation in Schizophrenia: A Pilot Clinical Intervention as Assessed by EEG and Optical Imaging (Functional Near-Infrared Spectroscopy)." *Frontiers in Human Neuroscience*.

Bizovičar, Nataša, Jurij Dreo, Blaž Koritnik, and Janez Zidar. 2014. "Decreased Movement-Related Beta Desynchronization and Impaired Post-Movement Beta Rebound in Amyotrophic Lateral Sclerosis." *Clinical Neurophysiology: Official Journal of the International Federation of Clinical Neurophysiology* 125 (8): 1689–99.

Blain-Moraes, Stefanie, George A. Mashour, Heonsoo Lee, Jane E. Huggins, and Uncheol Lee. 2013. "Altered Cortical Communication in Amyotrophic Lateral Sclerosis." *Neuroscience Letters* 543 (May): 172–76.

Borgheai, S. B., R. J. Deligani, J. McLinden, A. Zisk, S. I. Hosni, M. Abtahi, K. Mankodiya, and Y. Shahriari. 2019. "Multimodal Exploration of Non-Motor Neural Functions in ALS Patients Using Simultaneous EEG-fNIRS Recording." *Journal of Neural Engineering*. https://doi.org/10.1088/1741-2552/ab456c.

Buckner, Randy L., and Justin L. Vincent. 2007. "Unrest at Rest: Default Activity and Spontaneous Network Correlations." *NeuroImage*.

Cedarbaum, Jesse M., Nancy Stambler, Errol Malta, Cynthia Fuller, Dana Hilt, Barbara Thurmond, and Arline Nakanishi. 1999. "The ALSFRS-R: A Revised ALS Functional Rating Scale That Incorporates Assessments of Respiratory Function." *Journal of the Neurological Sciences*.

Chang, Won-Du, Ho-Seung Cha, Kiwoong Kim, and Chang-Hwan Im. 2016. "Detection of Eye Blink Artifacts from Single Prefrontal Channel Electroencephalogram." *Computer Methods and Programs in Biomedicine* 124 (February): 19–30.

Christidi, Foteini, Efstratios Karavasilis, Michail Rentzos, Nikolaos Kelekis, Ioannis Evdokimidis, and Peter Bede. 2018. “Clinical and Radiological Markers of Extra-Motor Deficits in Amyotrophic Lateral Sclerosis.” *Frontiers in Neurology*. https://doi.org/10.3389/fneur.2018.01005.

Christidi, Foteini, Ioannis Zalonis, Nikolaos Smyrnis, and Ioannis Evdokimidis. 2012. “Selective Attention and the Three-Process Memory Model for the Interpretation of Verbal Free Recall in Amyotrophic Lateral Sclerosis.” *Journal of the International Neuropsychological Society: JINS* 18 (5): 809–18.

Clark, Rosemary, Catherine Blizzard, and Tracey Dickson. 2015. “Inhibitory Dysfunction in Amyotrophic Lateral Sclerosis: Future Therapeutic Opportunities.” *Neurodegenerative Disease Management* 5 (6): 511–25.

Corbetta, Maurizio, and Gordon L. Shulman. 2002. “Control of Goal-Directed and Stimulus-Driven Attention in the Brain.” *Nature Reviews Neuroscience*. https://doi.org/10.1038/nrn755.

Dehaene, S. 2001. “Towards a Cognitive Neuroscience of Consciousness: Basic Evidence and a Workspace Framework.” *Cognition*. https://doi.org/10.1016/s0010-0277(00)00123-2.

Douaud, Gwenaëlle, Nicola Filippini, Steven Knight, Kevin Talbot, and Martin R. Turner. 2011a. “Integration of Structural and Functional Magnetic Resonance Imaging in Amyotrophic Lateral Sclerosis.” *Brain*. https://doi.org/10.1093/brain/awr279.

Dukic, Stefan, Roisin McMackin, Teresa Buxo, Antonio Fasano, Rangariroyashe Chipika, Marta Pinto-Grau, Emmet Costello, et al., 2019a. “Patterned Functional Network Disruption in Amyotrophic Lateral Sclerosis.” *Human Brain Mapping* 40 (16): 4827–42.

Fang, Xiaojing, Yuanchao Zhang, Yue Wang, Yuling Zhang, Jun Hu, Jian Wang, Jiuquan Zhang, and Tianzi Jiang. 2016. “Disrupted Effective Connectivity of the Sensorimotor Network in Amyotrophic Lateral Sclerosis.” *Journal of Neurology* 263 (3): 508–16.

Fernandez Rojas, Raul, Xu Huang, Jesus Hernandez-Juarez, and Keng-Liang Ou. 2017. “Physiological Fluctuations Show Frequency-Specific Networks in fNIRS Signals during Resting State.” *Conference Proceedings: ... Annual International Conference of the IEEE Engineering in Medicine and Biology Society. IEEE Engineering in Medicine and Biology Society. Conference* 2017 (July): 2550–53.

Francis, Michael M., Tom A. Hummer, Bethany L. Leonhardt, Jenifer L. Vohs, Matt G. Yung, Nicole F. Mehdiyoun, Paul H. Lysaker, and Alan Breier. 2017. “Association of Medial Prefrontal Resting State Functional Connectivity and Metacognitive Capacity in Early Phase Psychosis.” *Psychiatry Research: Neuroimaging*.

Fraschini, Matteo, Matteo Demuru, Arjan Hillebrand, Lorenza Cuccu, Silvia Porcu, Francesca Di Stefano, Monica Puligheddu, Gianluca Floris, Giuseppe Borghero, and

Francesco Marrosu. 2016a. “EEG Functional Network Topology Is Associated with Disability in Patients with Amyotrophic Lateral Sclerosis.” *Scientific Reports*. https://doi.org/10.1038/srep38653.

Fraschini, M., M. Lai, M. Demuru, M. Puligheddu, G. Floris, G. Borghero, and F. Marrosu. 2018a. “Functional Brain Connectivity Analysis in Amyotrophic Lateral Sclerosis: An EEG Source-Space Study.” *Biomedical Physics & Engineering Express*. https://doi.org/10.1088/2057-1976/aa9c64.

Geng, Shujie, Xiangyu Liu, Bharat B. Biswal, and Haijing Niu. 2017. “Effect of Resting-State fNIRS Scanning Duration on Functional Brain Connectivity and Graph Theory Metrics of Brain Network.” *Frontiers in Neuroscience*.

Hammer, Anke, Stefan Vielhaber, Antoni Rodriguez-Fornells, Bahram Mohammadi, and Thomas F. Münte. 2011. “A Neurophysiological Analysis of Working Memory in Amyotrophic Lateral Sclerosis.” *Brain Research* 1421 (November): 90–99.

Iyer, Parameswaran Mahadeva, Catriona Egan, Marta Pinto-Grau, Tom Burke, Marwa Elamin, Bahman Nasseroleslami, Niall Pender, Edmund C. Lalor, and Orla Hardiman. 2015a. “Functional Connectivity Changes in Resting-State EEG as Potential Biomarker for Amyotrophic Lateral Sclerosis.” *PLOS ONE*.

Jayaram, Vinay, Natalie Widmann, Christian Förster, Tatiana Fomina, Matthias Hohmann, Jennifer Müller Vom Hagen, Matthis Synofzik, Bernhard Schölkopf, Ludger Schöls, and Moritz Grosse-Wentrup. 2015. “Brain-Computer Interfacing in Amyotrophic Lateral Sclerosis: Implications of a Resting-State EEG Analysis.” *Annual International Conference of the IEEE Engineering in Medicine and Biology Society. IEEE Engineering in Medicine and Biology Society. Conference* 2015: 6979–82.

Kamran, Muhammad A., Malik M. Naeem Mannan, and Myung Yung Jeong. 2016. “Cortical Signal Analysis and Advances in Functional Near-Infrared Spectroscopy Signal: A Review.” *Frontiers in Human Neuroscience*.

Kocsis, L., P. Herman, and A. Eke. 2006. “The Modified Beer–Lambert Law Revisited.” *Physics in Medicine and Biology*. https://doi.org/10.1088/0031-9155/51/5/n02.

Kopitzki, Klaus, Andreas Oldag, Catherine M. Sweeney-Reed, Judith Machts, Maria Veit, Jörn Kaufmann, Hermann Hinrichs, et al., 2016a. “Interhemispheric Connectivity in Amyotrophic Lateral Sclerosis: A near-Infrared Spectroscopy and Diffusion Tensor Imaging Study.” *NeuroImage: Clinical*. https://doi.org/10.1016/j.nicl.2016.09.020.

Li, Fangjun, Fuqing Zhou, Muhua Huang, Honghan Gong, and Renshi Xu. 2017. “Frequency-Specific Abnormalities of Intrinsic Functional Connectivity Strength among Patients with Amyotrophic Lateral Sclerosis: A Resting-State fMRI Study.” *Frontiers in Aging Neuroscience* 9 (November): 351.

Liu, Y., W. G. Coon, A. de Pesters, P. Brunner, and G. Schalk. 2015. “The Effects of Spatial Filtering and Artifacts on Electrocorticographic Signals.” *Journal of Neural Engineering* 12 (5): 056008.

Luo, Chunyan, Qin Chen, Rui Huang, Xueping Chen, Ke Chen, Xiaoqi Huang, Hehan Tang, Qiyong Gong, and Hui-Fang Shang. 2012a. “Patterns of Spontaneous Brain Activity in Amyotrophic Lateral Sclerosis: A Resting-State fMRI Study.” *PLoS ONE*. https://doi.org/10.1371/journal.pone.0045470.

Mai, R., D. Facchetti, A. Micheli, and M. Poloni. 1998. “Quantitative Electroencephalography in Amyotrophic Lateral Sclerosis.” *Electroencephalography and Clinical Neurophysiology* 106 (4): 383–86.

Ma, Xujing, Jiuquan Zhang, Youxue Zhang, Heng Chen, Rong Li, Jian Wang, and Huafu Chen. 2015a. “Altered Cortical Hubs in Functional Brain Networks in Amyotrophic Lateral Sclerosis.” *Neurological Sciences: Official Journal of the Italian Neurological Society and of the Italian Society of Clinical Neurophysiology* 36 (11): 2097–2104.

Menke, Ricarda A. L., Malcolm Proudfoot, Joanne Wuu, Peter M. Andersen, Kevin Talbot, Michael Benatar, and Martin R. Turner. 2016. “Increased Functional Connectivity Common to Symptomatic Amyotrophic Lateral Sclerosis and Those at Genetic Risk.” *Journal of Neurology, Neurosurgery, and Psychiatry* 87 (6): 580–88.

Mohammadi, Bahram, Katja Kollewe, Amir Samii, Klaus Krampfl, Reinhard Dengler, and Thomas F. Münte. 2009a. “Changes of Resting State Brain Networks in Amyotrophic Lateral Sclerosis.” *Experimental Neurology*.

Naseer, Noman, and Keum-Shik Hong. 2015. “fNIRS-Based Brain-Computer Interfaces: A Review.” *Frontiers in Human Neuroscience*.

Nasseroleslami, Bahman, Stefan Dukic, Michael Broderick, Kieran Mohr, Christina Schuster, Brighid Gavin, Russell McLaughlin, et al., 2019. “Characteristic Increases in EEG Connectivity Correlate With Changes of Structural MRI in Amyotrophic Lateral Sclerosis.” *Cerebral Cortex* 29 (1): 27–41.

Nguyen, Dang Khoa, Julie Tremblay, Philippe Pouliot, Phetsamone Vannasing, Olivia Florea, Lionel Carmant, Franco Lepore, Mohamad Sawan, Frédéric Lesage, and Maryse Lassonde. 2012. “Non-Invasive Continuous EEG-fNIRS Recording of Temporal Lobe Seizures.” *Epilepsy Research*. https://doi.org/10.1016/j.eplepsyres.2011.10.035.

Pievani, Michela, Nicola Filippini, Martijn P. van den Heuvel, Stefano F. Cappa, and Giovanni B. Frisoni. 2014. “Brain Connectivity in Neurodegenerative Diseases—from Phenotype to Proteinopathy.” *Nature Reviews Neurology*.

Proudfoot, Malcolm, Gustavo Rohenkohl, Andrew Quinn, Giles L. Colclough, Joanne Wuu, Kevin Talbot, Mark W. Woolrich, Michael Benatar, Anna C. Nobre, and Martin R. Turner. 2017. “Altered Cortical Beta-Band Oscillations Reflect Motor System Degeneration in Amyotrophic Lateral Sclerosis.” *Human Brain Mapping* 38 (1): 237–54.

Raaphorst, Joost, Marianne De Visser, Wim Linssen, Rob De Haan, and Ben Schmand. 2009. “The Cognitive Profile of Amyotrophic Lateral Sclerosis: A Meta-Analysis.” *Amyotrophic Lateral Sclerosis*. https://doi.org/10.1080/17482960802645008.

Raichle, Marcus E. 2015. “The Brain’s Default Mode Network.” *Annual Review of Neuroscience* 38 (July): 433–47.

Santhosh, Jayashree, Manvir Bhatia, Shweta Sahu, and Sneh Anand. 2005. “Decreased Electroencephalogram Alpha Band [8-13 Hz] Power in Amyotrophic Lateral Sclerosis Patients: A Study of Alpha Activity in an Awake Relaxed State.” *Neurology India*. https://doi.org/10.4103/0028-3886.15071.

Sasai, Shuntaro, Fumitaka Homae, Hama Watanabe, and Gentaro Taga. 2011a. “Frequency-Specific Functional Connectivity in the Brain during Resting State Revealed by NIRS.” *NeuroImage* 56 (1): 252–57.

Schneider, Sabrina, Lisa Wagels, Florian B. Haeussinger, Andreas J. Fallgatter, Ann-Christine Ehlis, and Alexander M. Rapp. 2015. “Haemodynamic and Electrophysiological Markers of Pragmatic Language Comprehension in Schizophrenia.” *The World Journal of Biological Psychiatry*. https://doi.org/10.3109/15622975.2015.1019359.

Shahriari, Y., E. W. Sellers, L. M. McCane, T. M. Vaughan, and D. J. Krusienski. 2015a. “Directional Brain Functional Interaction Analysis in Patients with Amyotrophic Lateral Sclerosis.” *2015 7th International IEEE/EMBS Conference on Neural Engineering (NER)*.

Tedeschi, Gioacchino, Francesca Trojsi, Alessandro Tessitore, Daniele Corbo, Anna Sagnelli, Antonella Paccone, Alessandro D’Ambrosio, et al., 2012a. “Interaction between Aging and Neurodegeneration in Amyotrophic Lateral Sclerosis.” *Neurobiology of Aging* 33 (5): 886–98.

Verstraete, Esther, Martijn P. van den Heuvel, Jan H. Veldink, Niels Blanken, René C. Mandl, Hilleke E. Hulshoff Pol, and Leonard H. van den Berg. 2010a. “Motor Network Degeneration in Amyotrophic Lateral Sclerosis: A Structural and Functional Connectivity Study.” *PLoS ONE*.

Vincent, Justin L., Itamar Kahn, Abraham Z. Snyder, Marcus E. Raichle, and Randy L. Buckner. 2008a. “Evidence for a Frontoparietal Control System Revealed by Intrinsic Functional Connectivity.” *Journal of Neurophysiology*.

Volpato, Chiara, Francesco Piccione, Stefano Silvoni, Marianna Cavinato, Arianna Palmieri, Francesca Meneghello, and Niels Birbaumer. 2010. “Working Memory in Amyotrophic Lateral Sclerosis: Auditory Event-Related Potentials and Neuropsychological Evidence.” *Journal of Clinical Neurophysiology: Official Publication of the American Electroencephalographic Society* 27 (3): 198–206.

Yamamoto, Tsuyoshi, Atsushi Maki, Takuma Kadoya, Yukari Tanikawa, Yukio Yamada, Eiji Okada, and Hideaki Koizumi. 2002. “Arranging Optical Fibres for the Spatial Resolution Improvement of Topographical Images.” *Physics in Medicine and Biology*.

Yunusova, Yana, Jamal Ansari, Joel Ramirez, Sanjana Shellikeri, Greg J. Stanisz, Sandra E. Black, Susan M. Gillingham, Alex Kiss, Donald T. Stuss, and Lorne Zinman. 2019a. “Frontal Anatomical Correlates of Cognitive and Speech Motor Deficits in Amyotrophic Lateral Sclerosis.” *Behavioural Neurology* 2019 (March): 9518309.

Zeitlhofer, J., P. Anderer, S. Obergottsberger, P. Schimicek, S. Lurger, E. Marschnigg, B. Saletu, and L. Deecke. 1993. “Topographic Mapping of EEG during Sleep.” *Brain Topography*.

Zhang, Han, Yu-Jin Zhang, Lian Duan, Shuang-Ye Ma, Chun-Ming Lu, and Chao-Zhe Zhu. 2011a. “Is Resting-State Functional Connectivity Revealed by Functional near-Infrared Spectroscopy Test-Retest Reliable?” *Journal of Biomedical Optics*. https://doi.org/10.1117/1.3591020.

Zhou, Fuqing, Honghan Gong, Fangjun Li, Ying Zhuang, Yufeng Zang, Renshi Xu, and Ze Wang. 2013. “Altered Motor Network Functional Connectivity in Amyotrophic Lateral Sclerosis: A Resting-State Functional Magnetic Resonance Imaging Study.” *Neuroreport* 24 (12): 657–62.

Zhu, Wenjia, Xiaoling Fu, Fang Cui, Fei Yang, Yuting Ren, Xiaoyun Zhang, Xiaolan Zhang, Zhaohui Chen, Li Ling, and Xusheng Huang. 2015. “ALFF Value in Right Parahippocampal Gyrus Acts as a Potential Marker Monitoring Amyotrophic Lateral Sclerosis Progression: A Neuropsychological, Voxel-Based Morphometry, and Resting-State Functional MRI Study.” *Journal of Molecular Neuroscience: MN* 57 (1): 106–13.

CHAPTER 4: MULTIMODAL FUSION OF EEG-FNIRS: A MUTUAL INFORMATION-BASED HYBRID CLASSIFICATION FRAMEWORK

Published in the Journal of Biomedical Optics Express. doi: 10.1364/BOE.413666

Roohollah Jafari Deligani[1], Seyyed Bahram Borgheai[1], John McLinden[1], and Yalda Shahriari[1,2]

[1]Department of Electrical, Computer and Biomedical Engineering; University of Rhode Island, Kingston, RI 02881, USA

[2]Interdisciplinary Neuroscience Program; University of Rhode Island, Kingston, RI 02881, USA

Email: yalda_shahriari@uri.edu

ABSTRACT

Multimodal data fusion is one of the current primary neuroimaging research directions to overcome the fundamental limitations of individual modalities by exploiting complementary information from different modalities. Electroencephalography (EEG) and functional near-infrared spectroscopy (fNIRS) are especially compelling modalities due to their potentially complementary features reflecting the electro-hemodynamic characteristics of neural responses. However, the current multimodal studies lack a comprehensive systematic approach to properly integrate the complementary features from a multimodal dataset. Identifying a systematic approach to properly fuse EEG-fNIRS data and exploit their complementary potential is crucial in improving performance. This paper proposes a framework for classifying fused EEG-fNIRS data at the feature level, relying on a mutual information-based feature selection approach with respect to the complementarity between features. The goal is to optimize the complementarity, redundancy and relevance between multimodal features with respect to the class labels as belonging to a pathological condition or healthy control. Nine amyotrophic lateral sclerosis (ALS) patients and nine controls underwent multimodal data recording during a visuo-mental task. Multiple spectral and temporal features were extracted and fed to a feature selection algorithm followed by a classifier, which selected the optimized subset of features through a cross-validation process. The results demonstrated considerably improved hybrid classification performance compared to the individual modalities and compared to conventional classification without feature selection, suggesting a potential efficacy of our proposed framework for wider neuro-clinical applications.

4.1 BACKGROUND

Multimodal data fusion is one of the current primary neuroimaging research directions to overcome the fundamental limitations of individual modalities by exploiting complementary information from different modalities. Electroencephalography (EEG) and functional near-infrared spectroscopy (fNIRS) are especially compelling modalities due to their potentially complementary features reflecting the electro-hemodynamic characteristics of neural responses. However, the current multimodal studies lack a comprehensive systematic approach to properly merge the complementary features from their multimodal data. Identifying a systematic approach to properly fuse EEG-fNIRS data and exploit their complementary potential is crucial in improving performance.

Numerous mathematical tools and computational methods have been utilized to combine data from different modalities efficiently and obtain a criterion that optimally selects the best fused features from these different modalities. These fusion methods are especially useful in neuro-clinical studies to support more accurate decoding of neural information, and thus, improve the performance of relevant applications. These algorithms have shown promising applications in various fields, including brain-computer interfaces (BCIs) (M. A. Li et al., 2019; Ma et al., 2016), neuro-pathological diagnosis (Peng et al., 2019; Yang et al., 2017), and neural source localization (K. Liu et al., 2020).

So far, many fusion frameworks have exploited the common and complementary properties of different types of neuroimaging data, including EEG and fNIRS. These modalities are both portable scalp located devices that can be easily employed for data acquisition in multiple populations of patients with neurological impairments.

Considering the first modality, EEG captures macroscopic cortical dynamics with relatively fine temporal resolution (~5 msec). Although EEG classification has been widely investigated to detect and extract underlying pathological neural signatures, outcomes remain poor for multiple reasons, including low signal-to-noise ratio (SNR), poor spatial resolution, and insufficient classifiable measurements which cannot be addressed easily by existing computational algorithms (Ahn et al., 2017). One way to overcome these drawbacks is combining EEG with other modalities in an integrated framework that can provide a complimentary basis for the more accurate and robust detection of neural signatures to improve classification performance. For this purpose, fNIRS has shown promising capacity in improving classification performance (Borgheai et al., 2020; Erdoğan et al., 2019; Hennrich et al., 2015; Hong et al., 2015) as a modality for measuring the underlying hemodynamic properties with higher spatial resolution (~ 1 cm) than EEG. The integration of EEG and fNIRS provides us with two different types of neural data associated with the same regional neural activities, each one reflecting the underlying changes as potentially different sources of information. Exploiting the complementary features of the two data modalities with proper fusion algorithms to achieve a higher classification accuracy for hybrid EEG-fNIRS measures than for single modality approaches can provide a basis for improving performance in many existing neuro-assisted applications ranging from BCI to improving diagnostic methods for neurological impairments.

Fusion frameworks for EEG-fNIRS classification can be broadly classified into two categories based on the level at which the combination takes place. The first category is decision-level, in which the features are separately fed to a classifier, and the outcome

is used in a feedback loop to optimize accuracy. For example, in a motor imagery study conducted by Fazli et al. (Fazli et al., 2012), three groups of features, specifically EEG band-power, oxy-, and deoxy-hemoglobin (HbO and HbR respectively) were separately classified, and then a meta classifier optimally combined the three classifier outputs in a feedback loop based on the global peak cross-validation accuracy of each classifier. Putze et al. (Putze et al., 2014) used a similar framework to classify auditory and visual perception using hybrid EEG-fNIRS spectral and temporal features. Both studies achieved an average of 5% improved classification accuracy over single modality classification. In another study (Al-Shargie et al., 2017b), the authors used decision level fusion to combine the outputs of two local support vector machine (SVM) classifiers, one for EEG signals and the other for fNIRS signals in which each classifier was calibrated based on the optimal operating points of the EEG and fNIRS receiver operating characteristic (ROC) curves. At the end, both outputs were fed to a global classifier, which improved classification accuracy by 7.76% compared to single modal approach. A similar study for classifying mental work achieved 6% improvement compared to single modal data (Y. Liu et al., 2017). Another decision-level hybrid classification criterion is the fuzzy fusion-based approach, as was done in (Ko et al., 2019) to integrate the temporal and spectral features of EEG for motor imagery classification. After employing traditional classification methods, the authors adopted Choquet and Sugeno integrals to consider possible interactions between the obtained outputs from the different classifiers by fusing their posterior probabilities. They achieved ~7% improvement compared to conventional classifiers including linear discriminant analysis (LDA).

The second category is feature-level fusion in which features are concatenated, transformed, or optimally selected before training the classifier. Work on the simple concatenation of EEG-fNIRS features has shown a modest improvement compared to that obtained with a single modality, which is likely caused by the lack of comprehensive computational approaches for a proper feature integration that exploit the complementarity between each modality's unique properties as a preferred alternative over feature concatenation (Ahn et al., 2017). For example, in another study conducted by Buccino et al. (Buccino et al., 2016), EEG-fNIRS features were integrated through concatenation without any feature fusion strategy. In this study, the authors reported that the feature set was small, had no imposed computational load on the classification, and reached a 2% accuracy improvement compared to features from a single modality. In a study by Nguyen et al. (Nguyen et al., 2017), driver drowsiness during long-term simulated driving classified using concatenated EEG-fNIRS features yielded an average 5.5% accuracy improvement using combined classification compared with single modal features. Another modest improvement of 1% using hybrid classification was achieved by concatenating EEG and fNIRS features for distinguishing Parkinson's disease (Abtahi et al., 2020). Feature-level EEG-fNIRS fusion has also been done by projecting the original feature set to a new feature space to provide better separability than the original feature set. These projection methods are known as feature extraction methods, and their main disadvantage is that the newly created feature space is difficult to interpret and may not have a clear physical meaning (Jain et al., 2000). In a study conducted by Saadati et al. (Saadati et al., 2020a), the authors extracted temporal and spectral features from EEG-fNIRS data and then used a convolutional neural network (CNN) to pass the features

through different layers of the network and change the dimensions in a deep learning process for classifying mental workload from EEG-fNIRS data, which improved classification by 7%. Other transformation approaches have used a specific criterion for projecting the feature set into a new space. For example, in a study of mental stress assessment (Al-Shargie et al., 2016), the temporal properties of EEG have been combined with the spatial properties of fNIRS by transforming their signals to a mixed model, respectively using temporal and spatial independent component analysis (ICA), achieving a 3.4% accuracy improvement. In another study (Al-Shargie, Fares, Hasan Al-Nashash, 2019), the authors used a joint sparse canonical correlation analysis (CCA) to jointly estimate multiple pairs of canonical vectors to fuse EEG-fNIRS features and then fed these features to a SVM classifier, which significantly improved the hybrid classification accuracy by 5%. In a similar study on mental stress assessment (Al-Shargie et al., 2017a), a CCA was used, to project two different feature sets into a space with maximum correlation across two sets. The authors reported that by using this criterion, the redundant information has been reduced, and they obtained a 7.9% accuracy improvement. As the last category of feature-level fusion frameworks, feature selection algorithms have been used to optimally select a subset of features from the original combined feature set based on a criterion that maximizes classification performance. Depending on whether the classifier is included in the selection process, feature selection methods can be grouped into wrapper and filter methods (Brown et al., 2012). While wrapper methods generally consider classification performance as the feature selection criterion, filter methods select an optimized feature set independent of the classification algorithm. Thus, in filter methods, the biases of the feature selection procedure do not

interfere with the learning algorithm--this results in improved generalization capability for the classifier. One example of feature selection is the method used by Lin et al. (Lin et al., 2018), who conducted correlation analysis as the selection criterion between EEG and fNIRS channels (features in their study) and selected the most correlated channels, which yielded a 9% sensitivity improvement compared to single modalities. In the use of conventional classification algorithms, fused feature selection is a fundamental difficulty given a large number of possible features and the often small amount of available data. Furthermore, as the number of samples in real-world EEG-fNIRS recordings is relatively small, avoiding underfitting or overfitting is a primary challenge (Saadati et al., 2020a). The existence of redundant information in the original feature space can also hinder classification performance (Yin et al., 2015) since a system that memorizes training data involving redundancy can achieve perfect training performance while completely failing to generalize to new data.

The mutual information criterion is a powerful mathematical tool for feature selection, which can minimize the redundancy between features (i.e. the joint entropy of features subtracted from the individual entropies of the features). Yin et al. (Yin et al., 2015) used this criterion to decode the force and speed of hand clenching. In this study, the authors used band-power, amplitude, phase, and frequency to construct time-phase-frequency EEG features, and the differences between HbO and HbR were extracted as fNIRS features. They used a feature optimization method based on joint mutual information to remove redundant information that may reduce classification accuracy. This combination of EEG-fNIRS features resulted in improved performance (up to a 5% increase). In addition to minimizing redundancy, maximizing the relevance of a feature

set to the discrete output of the classifier can significantly increase classification performance (Meyer et al., 2008). Another important contributing factor to improving classification performance is maximizing the complementarity between features obtained from multimodal data. This property has been defined as a combination of features that can return more information on the output class than the sum of the information returned by each of the features taken individually (Meyer et al., 2008). This advantage has special importance while fusing two different modalities with unique complementary properties, which can be efficiently exploited to improve classification performance. The mutual information criterion has also been adopted for combining other modalities in the literature. The authors in (Baillet et al., 1999) minimized the conditional entropy between EEG and magnetoencephalography (MEG) features to reduce the degree of redundancy or similarity between the two signals for optimal estimation of the parameters to model localized sources. In another study (Akhonda et al., 2018), the authors used EEG and functional magnetic resonance imaging (fMRI) data in a hybrid source activation model by minimizing the mutual information to maximize the independence for joint ICA analysis. In another study (Zhang et al., 2017), the authors used EEG and electrocardiography (ECG) data to classify mental workload. In this study, the authors first extracted features from both modalities and then used a criterion called co-information to maximize the mutual information between the output labels and the integrated feature subset. The authors reported that their proposed fusion method could increase the classification accuracy indicating their multimodal fusion approach is promising to identify mental workload.

To date, EEG-fNIRS multimodal approaches have shown a considerable capacity to improve classification performance by measuring two different brain functions. However, they suffer from a lack of strong computational methods to systematically and optimally integrate the features. Computational integration methods should be developed that consider the differential characteristics of features from multimodal EEG-fNIRS signals. It is anticipated that efforts towards optimizing multimodal integration of EEG and fNIRS can make substantial advancement to the existing brain measurement packages with improved performance compared to EEG or fNIRS modalities alone.

In this chapter, a mutual information-based feature selection algorithm was adopted to propose a classification framework for multimodal EEG-fNIRS data. This study is the first that systematically exploits the complementarity aspect of such multimodal fused features through a feature selection algorithm that quantifies the complementarity between features and selects the optimal fused subset towards improving the classification performance. In this algorithm, the optimal features from a fused set of EEG-fNIRS features were determined with respect to minimized redundancy between features, maximized relevance, and maximized complementarity between features and class labels. EEG and fNIRS data were recorded from healthy participants and participants with ALS during a visuo-mental paradigm and were used to distinguish between the two aforementioned groups as a two-class problem. Features were first extracted from each modality and then the optimized subset of features was selected from the original combined set of EEG and fNIRS features through the aforementioned mutual information-based algorithm. This process was repeated for each modality (i.e., EEG and fNIRS) separately to evaluate the classification performance's improvement due to the

integration of features compared to those obtained from each single modality. Finally, the selected optimal feature sets from each individual modality and from the two modalities combined were fed into a support vector machine (SVM) classifier in which the hyper-parameter was the adequate number of features that was chosen according to the best classification results.

4.2 METHODS

4.2.1 Subjects

A total of 18 subjects were recruited and assigned to two groups: Nine individuals with ALS (ALS: 7 males, average age 56.8 years old) with ALS revised Functional Rating Scale (ALSFRS-R) scores of 0, 4, 4, 23, 22, 39, 41, 33, 26, respectively for subjects 1 to 9 (mean: 21.3±15.5) on a 48-point scale and nine age-matched healthy controls (HC: 4 males, average age 60.7 years old). All the protocols in this study were approved by the Institutional Review Board (IRB) of the University of Rhode Island (URI) and written informed consent was provided directly by each subject or by each patient's caregiver. Age-matched control subjects had no reported history of visual, mental, or substance-related disorders that could potentially affect the results or their performance during data recording.

4.2.2 Experimental Protocol

Subjects participated in two sessions, each consisting of one run with 14 trials. The participants were asked to perform a visuo-mental paradigm based on the conventional visual oddball paradigm followed by a mathematical task, as fully described in section

2.2.2 of chapter 2. The dual nature of our visuo-mental paradigm provokes both electrical and hemodynamic responses associated with visual oddball stimulations and mental arithmetic operations.

4.2.3 Data Acquisition

Both signals were recorded simultaneously using a single cap mounted with both EEG electrodes and fNIRS optodes. More details about data acquisition and cap montage is provided in figure 3.1 of chapter 3.

4.2.3 Data Analysis

EEG data were band-pass filtered at 0.3–35 Hz and detrended to remove baseline drift and out of band artifacts. Then, the data were checked for extreme values and outliers. Participants from both the ALS and HC groups had the same total number of $9 \times 2 \times 14 = 252$ (number of participants × number of runs × number of trials) observation points (i.e., samples) for both modalities (i.e., EEG and fNIRS). For EEG spectral features, the data were decomposed into spectrograms using a set of 30 complex Morlet wavelets ranging from 1-30 Hz and 3-10 cycles. The baseline-corrected spectrograms were obtained by dividing each frequency bin and time point by the baseline (-3 to -1 sec pre-stimulus window) average and calculating the percentage changes. The spectrograms from [0-5 sec] post-stimulus were then averaged across four traditional frequency bands: delta (1-3 Hz), theta (4-7 Hz), alpha (8-12 Hz), and beta (13-30 Hz) to generate four different features. In total, there were $16 \times 4 = 64$ (channels × frequency bands) spectral

features extracted from EEG data. For EEG temporal features, we used event-related potentials (ERPs), the averaged EEG waveforms of time-locked to stimulus or response events, in which the data were segmented to [0-800 ms] post-stimulus and the ERPs were then obtained. Five ERP features corresponding to peak amplitudes of P200, P300, P600, N200, and N400 components were then extracted in which the P200, P300, and P600 components were defined as the maximum peaks between 100-250, 250-400, and 650-800 ms post-stimulus, respectively, while the N200 and N400 components were defined as the minimum peaks between 150-280 and 360-560 ms post-stimulus, respectively. Following our previous work (Borgheai et al., 2019), these features have previously reflected significant differences between ALS patients and healthy controls, and thus have been considered as proper features with high separability for the classification procedure. In total $16 \times 5 = 80$ (channels $\times$ ERP components) temporal features were extracted from the EEG data.

fNIRS data were band-pass filtered at 0.01-0.2 Hz to mitigate physiological noises caused by respiratory and cardiac activities (Scarpa et al., 2010). Then, oxy-hemoglobin (HbO) concentration changes were extracted from the raw optical intensity data as features using the modified Beer-Lambert Law (Kocsis et al., 2006). The average baseline (-2 to -1 sec pre-stimulus window) was then subtracted from the following post-stimulus signal for each epoch, and then, the peak and the area under the curve (AUC) of HbO were extracted using [0-6 sec] post-stimulus window for each of the 16 fNIRS channels, providing a total of $16 \times 2 = 32$ (channels $\times$ feature types) features extracted from fNIRS data.

All features were then normalized by subtracting the mean and dividing by the standard deviation of each feature vector (z-score). Outliers were clipped by setting all the values that were more than three feature standard deviations from the feature mean to only three standard deviations from the mean (Cernadas et al., 2017). This was done to eliminate any degradational effect of the feature value range on the feature selection process. All the EEG and fNIRS vectors of features were then concatenated and the whole dataset was shuffled and partitioned into two main (equal size) folds with five sub-folds in each main fold for cross-validation testing to optimize the features.

To improve the discriminative performance of our classification procedure, we used an optimization framework following that proposed by Meyer et al. (Meyer et al., 2008). This framework consists of three steps: 1) maximizing the relevance of a selected feature set to the class labels, 2) minimizing the redundancy between features within a selected subset of the original features, and 3) maximizing the complementarity between features with respect to the class labels. The optimization formulation in which the features were selected is defined in the equation below.

$$X_S^{Opt} = \arg\max_{X_s \subseteq X} \left\{ \sum_{X_i \in X_S} \sum_{X_j \in X_S} I(X_{i,j}; Y) \right\} \tag{4.1}$$

In this formulation, Y represents the vector of output labels (HC = 1, ALS = -1), X, X_S and $X_{i,j}$ represent the original set of n features (n is the number of features in Equation 4.2), a subset of original features, and a subset of original features consisting of two single features (X_i and X_j) respectively defined in the equations below. The term under optimization inside the objective function represents the mutual information $I(.)$

between $X_{i,j}$ and Y. The term "arg max" states that the objective function is supposed to be maximized by searching for the $X_S \subseteq X$ to find the optimized feature set (i.e., X_S^{Opt}).

$$X = \{X_i : i \in A = \{1,...,n\}\} \tag{4.2}$$

$$X_S = \{X_i : i \in S \subseteq A\} \tag{4.3}$$

$$X_{i,j} = \{X_i, X_j\} \tag{4.4}$$

Equation 4.1 is an optimization formulation for finding a subset of features that can maximize the joint mutual information of class labels with each pair of features inside the selected subset of original features. The joint mutual information of two random variables with another variable can be defined by the equation below.

$$I(X_{i,j};Y) = I(X_i;Y) + I(X_j;Y) - C(X_i;X_j;Y) \tag{4.5}$$

The first two terms in this equation are the mutual information between single features and the class labels. These terms represent the relevance of each feature to the class labels, which means maximizing the term in equation 4.1 will optimize the relevance of each feature alone. The last term, denoted as $C(.)$ represents the interaction among the whole set of both features and the class labels. The lower the interaction term, the less redundant the variables are, and the higher their complementarity is (if the interaction term is negative). The interaction term in equation 4.5 for three variables can be obtained using the entropies and joint entropies of the set of variables according to the equation below.

$$\begin{aligned} C(X_i;X_j;Y) &= H(X_i) + H(X_j) + H(Y) \\ &- H(X_i,X_j) - H(X_i,Y) - H(X_j,Y) + H(X_i,X_j,Y) \end{aligned} \tag{4.6}$$

The entropy of variable(s) is denoted with $H(.)$ in this formulation. If the interaction term becomes negative, it can be inferred from equation 4.5 that $I(X_{i,j};Y) > I(X_i;Y) + I(X_j;Y)$. Therefore, the gain resulting from using the joint mutual information of the two features will be more than the sum of the individual features' information. This property is caused by the existence of complementarity between two features.

As finding the optimized subset of features according to equation 4.1 is a Non-deterministic Polynomial-time hardness (NP-hard) problem (Pisinger, 2006), a semi-optimized strategy based on forward selection search was used to solve this equation (Billionnet et al., 1996). This approach consists of updating a set of selected features X_s with the feature X_i from the set of remaining features that have not been selected yet. This new feature has been paired with all the members of the pre-selected set of features and should maximize the summation of joint mutual information between all paired sets of features and class labels. In other words, instead of attempting to find an optimized solution for equation 4.1, a semi-optimized solution will be substituted based on the equation below using a procedural updating approach.

$$X_S^{Opt} = \arg \max_{\substack{X_s \subseteq X \\ X_i \in X_{-S}}} \left\{ \sum_{X_j \in X_S} I(X_{i,j};Y) \right\} \tag{4.7}$$

In this formulation, X_{-S} represents the whole set of original features with those in X_S removed. This can be defined as the equation below.

$$X_{-S} = \{ X_i : i \in A - S \} \tag{4.8}$$

This strategy starts with an empty set of variables and progressively updates the solution by adding the variable that maximizes the objective function in equation 4.7

until an adequate number of features is reached. The pseudo-code for the sequential feature selection algorithm is shown in figure 4.1.

1. Initialize feature set
$$X_1 = \arg \max_{X_k \in X} [I(X_k; Y)]$$
2. Update original and selected feature set
$$X = X - X_1;\ X_S = X_1$$
3. Select next best feature
$$X^+ = \arg \max_{X_i \in X} [\sum_{X_j \in X_S} I(X_{i,j}; Y)]$$
4. Update original and selected feature set
$$X = X - X_i;\ X_S = X_S + X_i$$
5. While size $(X_S) \leq$ minimum number of features per modality
Go to step 3

Figure 4.1. Sequential feature selection pseudo-code.

A support vector machine (SVM) classifier, which has been widely used for brain signal classification was used to classify data points corresponding to two classes of HC and ALS denoted as $Y \in$ {HC = 1, ALS = -1}. A non-linear polynomial kernel was used for SVM in this study to maximize discrimination between data points, as it allows complex separation surfaces requiring optimization of a reduced number of hyper-parameters. In order to reduce the bias associated with training and test data and to improve the generalizability of the proposed framework, a cross-validation technique was employed in which the generalization error was estimated based on resampling. A 2-fold cross-validation strategy was then used to partition each dataset into separate datasets for feature selection and validation as follows: the dataset was first split into two equal parts. Each half-dataset was separately used as training data to conduct the learning process and optimize the parameters. The results were then applied on the other half (i.e., testing dataset) to produce the classification accuracy for that corresponding fold. The

final accuracy was the average of both folds' accuracies. Within the inner level of the aforementioned cross-validation, each half-dataset was split into five sub-fold to select and validate the best number of features (i.e., our only hyperparameter under optimization at the classification level). In a leave-one-out strategy for the aforementioned 5-fold cross-validation, the feature selection and classifier training was done for each 80% of the half-dataset and was repeated five times to cover all the sub-folds. Each training process was done for a number of optimally selected features ranging from 1 to 32 (32 is the minimum number of features per modality). The classification accuracies of the five validation sets were then averaged for each number of features, and the best number of features was then selected. This whole process was done in a similar way for each single modality and for the multimodal data. To evaluate the classifier, three metrics of accuracy, sensitivity, and specificity were used as follows:

$$Accuracy = \frac{TP + TN}{TP + FN + TN + FP} \tag{4.9}$$

$$Sensitivity = \frac{TP}{TP + FN} \tag{4.10}$$

$$Specificity = \frac{TN}{TN + FP} \tag{4.11}$$

where TP denotes the correct classifications of positive cases, TN denotes the correct classifications of negative cases, FP denotes the incorrect classifications of negative cases into class positive, and FN denotes the incorrect classifications of positive cases into class negative.

4.3 RESULTS

The classification accuracy of the validation dataset for different numbers of selected features using the three modality options (i.e., EEG, fNIRS, EEG+fNIRS) are shown in figure 4.2. The averaged accuracy across the five validation sub-folds of the first main fold (fold 1) is shown in the top plot, and the bottom plot shows the averaged accuracy across the five validation sub-folds of the second main fold (fold 2). In both plots, at first, the curve (classification accuracy) ascends as the size of the optimally selected feature subset increases. It then remains around the range of maximum accuracy after increasing the number of features, reaches its maximum classification accuracy at a certain point, and finally descends. In general, the hybrid EEG-fNIRS modality performs considerably better than other single modalities in terms of the classification accuracy. In the first fold, the optimal number of features with the maximum accuracies for different modalities were: EEG+fNIRS: 87.32% accuracy with 24 features, EEG: 76.71% accuracy with 23 features, and fNIRS: 60.19% accuracy with 26 features. In the second fold, the maximum accuracies for different modalities were: EEG+fNIRS: 87.51% accuracy with 22 features, EEG: 76.39% accuracy with 19 features, and fNIRS: 62.64% accuracy with 25 features.

Figure 4.3 shows the relative portions of included features from each feature category/subcategory when averaged over optimal selected feature sets from all sub-folds. This figure highlights the relative discriminatory importance of each feature in the final classification procedure. As it is seen, EEG spectral features were the most selected features with 49% presence, followed by fNIRS features with 27% and EEG temporal features with 24% presence. The most selected three feature types were beta-band power

with 22% presence, theta-band power with 18% presence, and P300 peak with 16% presence.

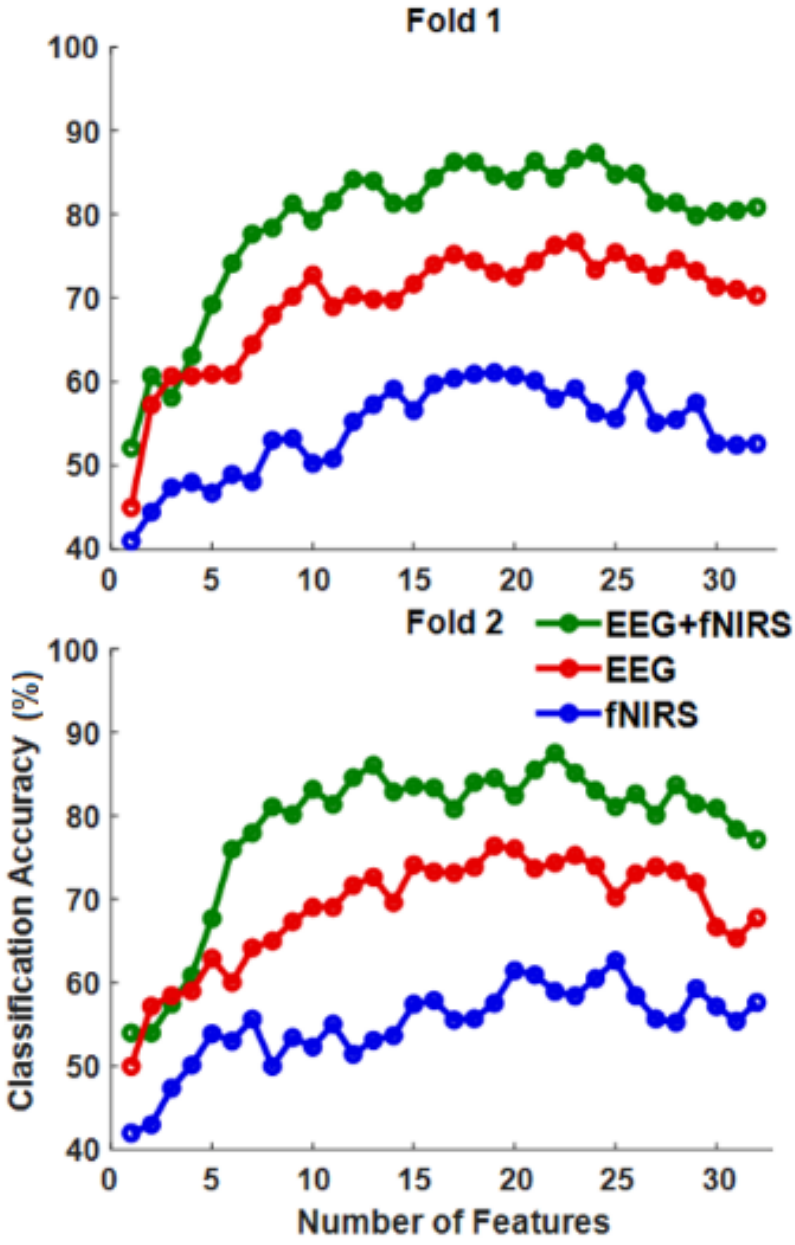

Figure 4.2. Classification accuracy of single and hybrid modalities for variable sizes of the selected optimal feature subset (averaged across sub-folds of the validation dataset for fold 1 (top) and fold 2 (bottom)).

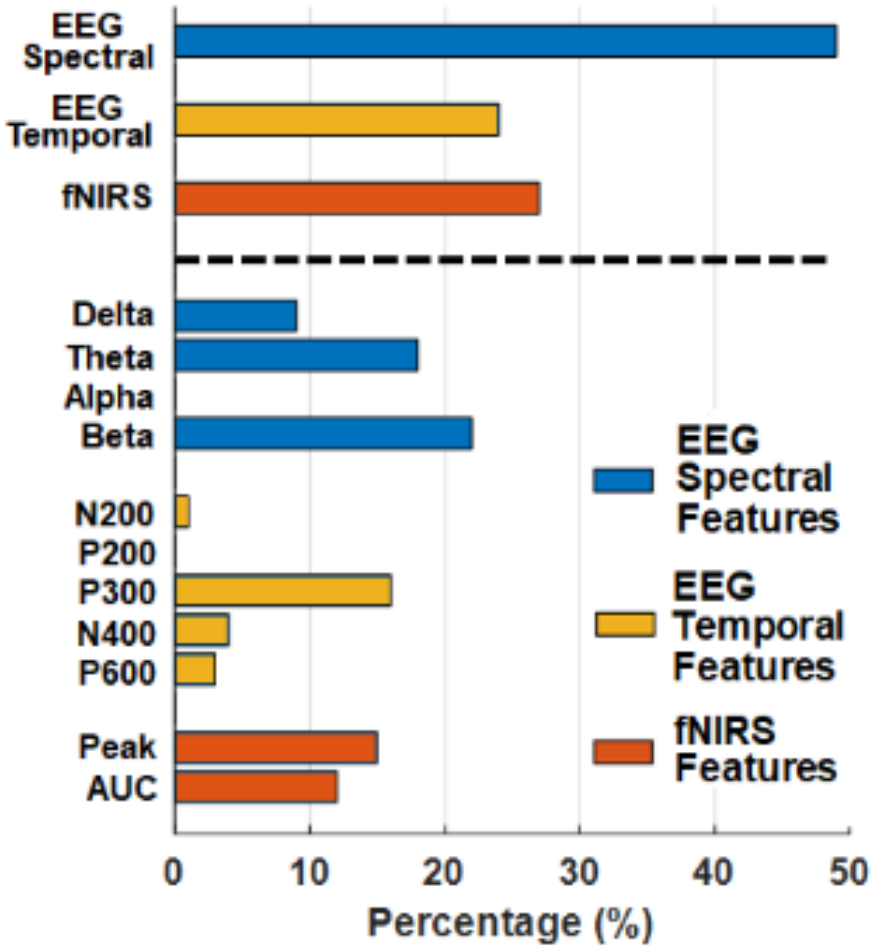

Figure 4.3. Relative portions of included features from each feature category/subcategory averaged over optimal selected feature sets from all sub-folds.

Figure 4.4 shows classification performance characteristics based on the optimal selected subset of features which was obtained from sub-folds for single and hybrid modalities, averaged across both test folds. The hybrid classification achieved the best test accuracy of 85.38%, outperforming EEG with its best accuracy of 73.23%, and fNIRS with its best accuracy of 61.56%.

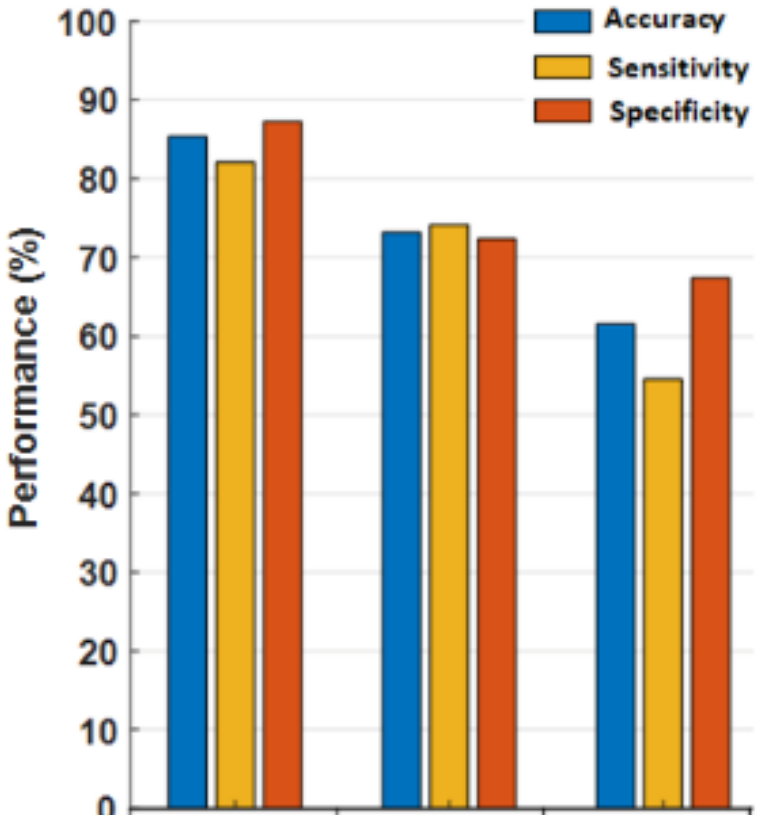

	EEG+fNIRS	EEG	fNIRS
Accuracy	85.38 %	73.23 %	61.56 %
Sensitivity	82.13 %	74.19 %	54.53 %
Specificity	87.26 %	72.38 %	67.42 %

Figure 4.4. Classification performance characteristics for single and hybrid modalities.

Figure 4.5 shows the performance characteristics of the hybrid classification for the optimally selected set of features compared to hybrid classification using all features without any feature selection procedure. The feature selection procedure improved accuracy by 16.67% over the test set.

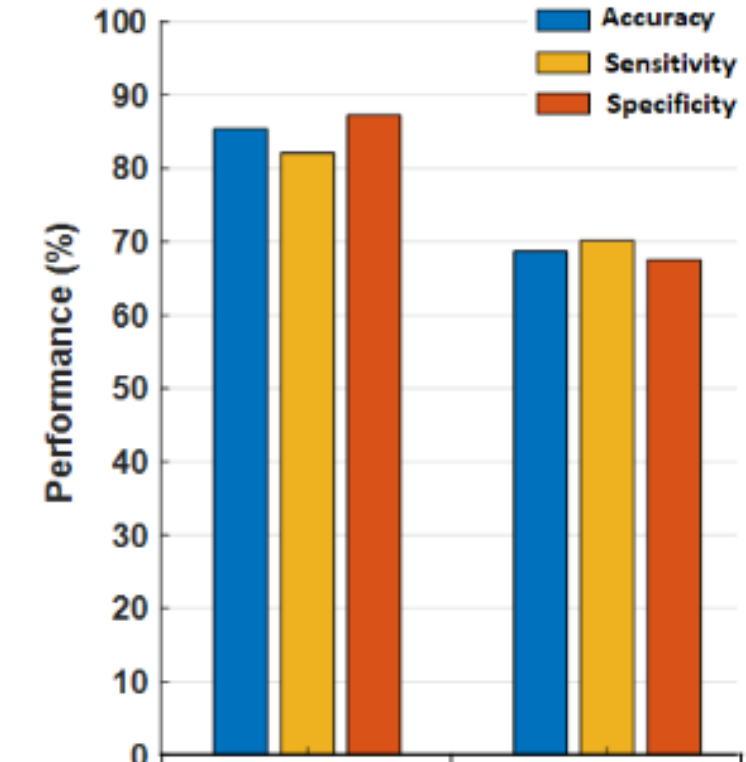

	Selected Features	All Features
Accuracy	85.38 %	68.71 %
Sensitivity	82.13 %	70.14 %
Specificity	87.26 %	67.54 %

Figure 4.5. Classification performance characteristics for the selected optimal feature subset and the original set of features without any feature selection procedure.

4.4 DISCUSSION

In this paper, we used an information theory-based method to optimize feature selection and thereby classify between a healthy group and a pathological one, people with ALS in this case, during a visuo-mental task using multimodal EEG and fNIRS data. The proposed technique takes the first steps to systematically exploit the complementarity aspect of the fused features extracted from electrical and hemodynamic neural activities through a feature selection algorithm that quantifies the complementarity

between features and selects the optimal fused subset to improve classification performance. The feature selection algorithm was adopted from "Meyer et al. [27]" in which the authors used the algorithm for a single-modality dataset and to the best of our knowledge, it has not been applied to any hybrid dual modality dataset in which both modalities have complementary information to make a remarkable increase in the classification performance compared to the simple concatenation of the features if only certain features from each modality that can increase the complementarity function get selected for the classification. Thus, it can be inferred that applying this algorithm to a dual modality dataset can exploit the full potential of such algorithm which was presented in our results. Our results showed that when an integrated set of features from both modalities was used, classification performance was considerably improved compared to when EEG or fNIRS alone was used. Moreover, classification performance was substantially improved for the integrated subset of optimally selected features compared to when no feature selection was done.

Our overall classification results revealed that considerable improvements in all three performance metrics are achievable with the proposed fusion approach. This supports our central hypothesis that the systematic selection of fused complementary EEG and fNIRS features of can improve classification performance. The fused feature selection model enabled us to take advantage of the strengths of both modalities in unified analytics. Although it is impossible to make fair quantitative comparisons with other similar studies as the algorithms were run on different datasets the improvement in hybrid classification accuracy achieved in this study relative to single modality accuracies was competitive with previous EEG and fNIRS fusion studies, including those reported by

Fazli et al. (Fazli et al., 2012) and Putze et al. (Putze et al., 2014). Our improved fusion results may be due to the level of fusion being adopted, as both of their studies applied fusion at the decision level, i.e., using a meta classifier to integrate the outputs from one EEG classifier and one fNIRS classifier. Indeed, the cross-modality inconsistencies which negatively affect the efficiency of modality fusions (Wu et al., 2019) cannot be avoided in decision level fusions, while such inconsistencies between modalities and their features are removed by the feature selection algorithm used in our study. Moreover, it is likely that the outputs from the EEG classifier and fNIRS classifier in these studies are highly correlated with less complementary information, and thus a systematic fusion of the features to properly maximize the complementary benefits from both modalities has been lacking. In contrast to studies done by Fazli et al. (Fazli et al., 2012) and Putze et al. (Putze et al., 2014), Yin et al. (Yin et al., 2015) considered the feature level fusion of bimodal EEG and fNIRS and were able to improve the decoding of motor imagery tasks using a feature selection algorithm based on removing redundancy between the integrated EEG and fNIRS features. However, Yin et al. achieved a modest improvement, which may be due to not systematically exploiting the potential of complementarity and focusing only on removing redundancy between their hybrid modalities in their feature selection method, although the authors mentioned that EEG and fNIRS complement each other in presenting cortex activation.

The technique used for feature selection in our study selects an optimal subset of features that have maximum pairwise mutual information with the specified classes of interest (two classes in our case). Although the most complete method would consider all possible feature subsets, even with a small number of features, this procedure is

computationally impossible and cannot be used in practice (Deriche et al., 2001). Given the fact that most feature sets used to represent EEG and fNIRS signals are sets of different types of features with redundancies and complementarities, this technique considers a trade-off between computational cost and the number of chosen features. This contrasts with other techniques that select features individually without considering interactions between features. The classification accuracy using features obtained by applying our technique outperforms those obtained by applying individual feature selection methods when applied to EEG and fNIRS signals. Moreover, mutual information measures non-linear dependencies between a set of random variables, taking into account higher-order statistical structures existing in the data, as opposed to linear and second-order statistical measures such as correlation and covariance. This makes mutual information-based techniques especially beneficial for a combination of features from different modalities that are likely to have non-linear relationships with each other.

This study considered complementarities between features only up to order two to avoid the additional computational complexity required by higher orders of feature fusion. Future work might consider higher levels of feature fusion with more complexity, requiring greedy search algorithms but potentially providing more advanced solutions. The small sample size and the heterogeneous characteristics of our patient group was another limitation of this study. If a larger number of patients are recruited in future studies, it will be possible to classify them into subgroups based on the onset of clinical symptoms and cognitive deficits to better discriminate between different patterns rather than considering putative patterns of altered brain functions for all ALS patients. In addition, we did not analyze differences in gender and education, which might affect the

obtained neuro-markers measures. Future research with larger patient samples should be conducted to further consider demographic information in smaller sub-groups. Applying the proposed framework in this study to other datasets of integrated EEG and fNIRS in future work will further validate the efficiency of the adopted feature selection algorithm for neuro-clinical studies. Furthermore, in the future, applying other state of the art algorithms that are designed for dual-modality data classification on the same dataset will provide a more robust ground to make fair quantitative comparisons between the proposed framework and other approaches.

Overall, in this study, we adopted a mutual information-based feature selection algorithm to propose a classification framework for hybrid EEG-fNIRS data which was used to classify between a healthy and a pathological group, patients with ALS in this application, during a visuo-mental task. The optimized process of selecting features to increase classification performance was based on exploring three properties of the fused features, including decreasing redundancy, increasing relevance and increasing complementarity. The multimodal results revealed a considerable improvement of classification performance characteristics, including 16% accuracy improvement over hybrid classification with no feature selection, 12% accuracy improvement over single modal classification using EEG, and 23% accuracy improvement over single modal classification using fNIRS. These results support the idea of using complementary features from fused EEG-fNIRS in neuro-clinical studies for optimized decoding of neural information, and thus, improve the performance of relevant applications, including BCI and neuro-pathological diagnosis.

Appendix: Supplementary Material

In this supplementary section, we present the figure and explanation of the experimental paradigm. The participants were asked to perform a visuo-mental paradigm based on the conventional visual oddball paradigm followed by a mathematical task, as fully described in our previous work (Borgheai et al., 2019). Fig. S1 shows the oddball P300 paradigm, but with a 2×2 matrix of digits displayed over the intensified letter in our visuo-mental dual-task paradigm. Each subject was instructed to focus on a target character (14 targets per run), while each row and column was intensified once per trial to cause two target intensifications per character. Upon each target intensification, subjects were instructed to perform predefined mental arithmetic tasks, i.e., add pairs of numbers in the matrix either diagonally (first target flash) or vertically (second target flash), and then double the larger result from their addition. The stimulation intensification time was set to 300 ms, followed by a 6 sec inter-stimulus interval (ISI). The relatively long ISI adopted compared to conventional EEG-based oddball tasks allowed the fNIRS recordings to reflect evoked hemodynamic activities.

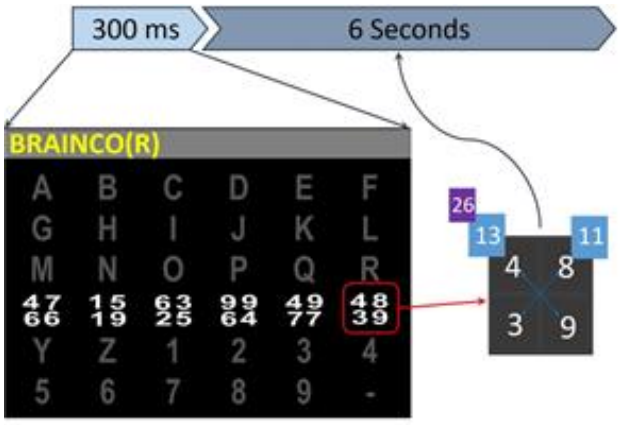

Figure S4.1. The oddball-based visuo-mental dual-task paradigm and an example of the arithmetic operation the participant performed.

REFERENCES

Abdalmalak, A., Milej, D., Diop, M., Shokouhi, M., Naci, L., Owen, A. M., & St. Lawrence, K. (2017). Can time-resolved NIRS provide the sensitivity to detect brain activity during motor imagery consistently? *Biomedical Optics Express*. doi: 10.1364/boe.8.002162

Abtahi, M., Bahram Borgheai, S., Jafari, R., Constant, N., Diouf, R., Shahriari, Y., & Mankodiya, K. (2020). Merging fNIRS-EEG Brain Monitoring and Body Motion Capture to Distinguish Parkinsons Disease. *IEEE Transactions on Neural Systems and Rehabilitation Engineering*. doi: 10.1109/TNSRE.2020.2987888

Ahn, S., & Jun, S. C. (2017). Multi-modal integration of EEG-fNIRS for brain-computer interfaces – Current limitations and future directions. In Frontiers in Human Neuroscience. doi: 10.3389/fnhum.2017.00503

Akhonda, M. A. B. S., Levin-Schwartz, Y., Bhinge, S., Calhoun, V. D., & Adali, T. (2018). Consecutive Independence and Correlation Transform for Multimodal Fusion: Application to EEG and Fmri Data. *ICASSP, IEEE International Conference on Acoustics, Speech and Signal Processing - Proceedings*. doi: 10.1109/ICASSP.2018.8462031

Al-Shargie, Fares, Hasan Al-Nashash, and T. B. T. (2019). Assessment of Mental Stress among Undergraduate Students Using Novel Fusion Method on EEG and fNIRS Features. *Frontiersin*, 1.

Al-Shargie, F., Kiguchi, M., Badruddin, N., Dass, S. C., Hani, A. F. M., & Tang, T. B. (2016). Mental stress assessment using simultaneous measurement of EEG and fNIRS. *Biomedical Optics Express*. doi: 10.1364/boe.7.003882

Al-Shargie, F., Tang, T. B., & Kiguchi, M. (2017a). Assessment of mental stress effects on prefrontal cortical activities using canonical correlation analysis: an fNIRS-EEG study. *Biomedical Optics Express*. doi: 10.1364/boe.8.002583

Al-Shargie, F., Tang, T. B., & Kiguchi, M. (2017b). Stress Assessment Based on Decision Fusion of EEG and fNIRS Signals. *IEEE Access*. doi: 10.1109/ACCESS.2017.2754325

An, X., Kuang, D., Guo, X., Zhao, Y., & He, L. (2014). A deep learning method for classification of eeg data based on motor imagery. *Lecture Notes in Computer Science (Including Subseries Lecture Notes in Artificial Intelligence and Lecture Notes in Bioinformatics)*. doi: 10.1007/978-3-319-09330-7_25

Baillet, S., Garnero, L., Marin, G., & Hugonin, J. P. (1999). Combined MEG and EEG source imaging by minimization of mutual information. *IEEE Transactions on Biomedical Engineering*. doi: 10.1109/10.759053

Bashivan, P., Rish, I., Yeasin, M., & Codella, N. (2016). Learning representations from EEG with deep recurrent-convolutional neural networks. *4th International Conference on Learning Representations, ICLR 2016 - Conference Track Proceedings*.

Besio, W. G., Cao, H., & Zhou, P. (2008). Application of tripolar concentric electrodes and prefeature selection algorithm for brain-computer interface. *IEEE Transactions on Neural Systems and Rehabilitation Engineering*. doi: 10.1109/TNSRE.2007.916303

Bianchini, M., & Scarselli, F. (2014). On the complexity of neural network classifiers: A comparison between shallow and deep architectures. *IEEE Transactions on Neural Networks and Learning Systems*. doi: 10.1109/TNNLS.2013.2293637

Billionnet, A., & Calmels, F. (1996). Linear programming for the 0-1 quadratic knapsack problem. *European Journal of Operational Research*. doi: 10.1016/0377-2217(94)00229-0

Borgheai, S. B., Deligani, R. J., McLinden, J., Zisk, A., Hosni, S. I., Abtahi, M., Mankodiya, K., & Shahriari, Y. (2019). Multimodal exploration of non-motor neural functions in ALS patients using simultaneous EEG-fNIRS recording. *Journal of Neural Engineering*, *16*(6). doi: 10.1088/1741-2552/ab456c

Borgheai, S. B., Mclinden, J., Zisk, A. H., Hosni, S. I., Deligani, R. J., Abtahi, M., Mankodiya, K., & Shahriari, Y. (2020). Enhancing Communication for People in Late-Stage ALS Using an fNIRS-Based BCI System. *IEEE Transactions on Neural Systems and Rehabilitation Engineering*, *28*(5). doi: 10.1109/TNSRE.2020.2980772

Brown, G., Pocock, A., Zhao, M. J., & Luján, M. (2012). Conditional likelihood maximisation: A unifying framework for information theoretic feature selection. *Journal of Machine Learning Research*.

Brunner, C., Delorme, A., & Makeig, S. (2013). Eeglab – an Open Source Matlab Toolbox for Electrophysiological Research. *Biomedical Engineering / Biomedizinische Technik*. doi: 10.1515/bmt-2013-4182

Buccino, A. P., Keles, H. O., & Omurtag, A. (2016). Hybrid EEG-fNIRS asynchronous brain-computer interface for multiple motor tasks. *PLoS ONE*. doi: 10.1371/journal.pone.0146610

Cernadas, E., Fernández-Delgado, M., González-Rufino, E., & Carrión, P. (2017). Influence of normalization and color space to color texture classification. *Pattern Recognition*. doi: 10.1016/j.patcog.2016.07.002

Cheng, L., Li, D., Yu, G., Zhang, Z., Li, X., & Yu, S. (2020). A motor imagery EEG feature extraction method based on energy principal component analysis and deep belief networks. *IEEE Access*. doi: 10.1109/ACCESS.2020.2969054

Chiarelli, A. M., Croce, P., Merla, A., & Zappasodi, F. (2018). Deep learning for hybrid EEG-fNIRS brain-computer interface: Application to motor imagery classification. *Journal of Neural Engineering*. doi: 10.1088/1741-2552/aaaf82

Dahl, G. E., Sainath, T. N., & Hinton, G. E. (2013). Improving deep neural networks for LVCSR using rectified linear units and dropout. *ICASSP, IEEE International Conference on Acoustics, Speech and Signal Processing - Proceedings*. doi: 10.1109/ICASSP.2013.6639346

Deligani, R. J., Borgheai, S. B., McLinden, J., & Shahriari, Y. (2021). Multimodal

fusion of EEG-fNIRS: a mutual information-based hybrid classification framework. *Biomedical Optics Express*.

Deriche, M., & Al-Ani, A. (2001). A new algorithm for EEG feature selection using mutual information. *2001 IEEE International Conference on Acoustics, Speech, and Signal Processing. Proceedings (Cat. No. 01CH37221) (Vol. 2)*, 4.

Erdoĝan, S. B., Özsarfati, E., Dilek, B., Kadak, K. S., Hanoĝlu, L., & Akin, A. (2019). Classification of motor imagery and execution signals with population-level feature sets: Implications for probe design in fNIRS based BCI. *Journal of Neural Engineering*. doi: 10.1088/1741-2552/aafdca

Fazli, S., Mehnert, J., Steinbrink, J., Curio, G., Villringer, A., Müller, K. R., & Blankertz, B. (2012). Enhanced performance by a hybrid NIRS-EEG brain computer interface. *NeuroImage*. doi: 10.1016/j.neuroimage.2011.07.084

Ghonchi, Hamidreza, et al. (2020). Spatio-temporal deep learning for EEG-fNIRS brain computer interface. *42nd Annual International Conference of the IEEE Engineering in Medicine & Biology Society (EMBC). IEEE*.

Hajinoroozi, M., Jung, T. P., Lin, C. T., & Huang, Y. (2015). Feature extraction with deep belief networks for driver's cognitive states prediction from EEG data. *2015 IEEE China Summit and International Conference on Signal and Information Processing, ChinaSIP 2015 - Proceedings*. doi: 10.1109/ChinaSIP.2015.7230517

Hennrich, J., Herff, C., Heger, D., & Schultz, T. (2015). Investigating deep learning for fNIRS based BCI. *Proceedings of the Annual International Conference of the IEEE Engineering in Medicine and Biology Society, EMBS*. doi: 10.1109/EMBC.2015.7318984

Hong, K. S., Khan, M. J., & Hong, M. J. (2018). Feature Extraction and Classification Methods for Hybrid fNIRS-EEG Brain-Computer Interfaces. In Frontiers in Human Neuroscience. doi: 10.3389/fnhum.2018.00246

Hong, K. S., Naseer, N., & Kim, Y. H. (2015). Classification of prefrontal and motor cortex signals for three-class fNIRS-BCI. *Neuroscience Letters*. doi: 10.1016/j.neulet.2014.12.029

Hosni, S. M., Deligani, R. J., Zisk, A., McLinden, J., Borgheai, S. B., & Shahriari, Y. (2020). An exploration of neural dynamics of motor imagery for people with amyotrophic lateral sclerosis. *Journal of Neural Engineering*, *17*(1). doi: 10.1088/1741-2552/ab4c75

Hua, J., Xiong, Z., Lowey, J., Suh, E., & Dougherty, E. R. (2005). Optimal number of features as a function of sample size for various classification rules. *Bioinformatics*. doi: 10.1093/bioinformatics/bti171

Jain, A. K., Duin, R. P. W., & Mao, J. (2000). Statistical pattern recognition: A review. *IEEE Transactions on Pattern Analysis and Machine Intelligence*. doi: 10.1109/34.824819

Jirayucharoensak, S., Pan-Ngum, S., & Israsena, P. (2014). EEG-Based Emotion

Recognition Using Deep Learning Network with Principal Component Based Covariate Shift Adaptation. *Scientific World Journal*. doi: 10.1155/2014/627892

Kingma, D. P., & Ba, J. L. (2015). Adam: A method for stochastic optimization. *3rd International Conference on Learning Representations, ICLR 2015 - Conference Track Proceedings*.

Ko, L. W., Lu, Y. C., Bustince, H., Chang, Y. C., Chang, Y., Ferandez, J., Wang, Y. K., Sanz, J. A., Pereira Dimuro, G., & Lin, C. T. (2019). Multimodal fuzzy fusion for enhancing the motor-imagery-based brain computer interface. *IEEE Computational Intelligence Magazine*. doi: 10.1109/MCI.2018.2881647

Kocak, O., Beytar, F., Firat, H., Telatar, Z., & Erogul, O. (2017). *Comparison of non-parametric PSD detection methods in the anaylsis of EEG signals in sleep apnea*. doi: 10.1109/tiptekno.2016.7863133

Kocsis, L., Herman, P., & Eke, A. (2006). The modified Beer-Lambert law revisited. *Physics in Medicine and Biology*. doi: 10.1088/0031-9155/51/5/N02

Krizhevsky, A., Sutskever, I., & Hinton, G. E. (2012). ImageNet classification with deep convolutional neural networks. *Advances in Neural Information Processing Systems*. doi: 10.1061/(ASCE)GT.1943-5606.0001284

Lecun, Y., Bengio, Y., & Hinton, G. (2015). Deep learning. In Nature. doi: 10.1038/nature14539

Li, M. A., Wang, Y. F., Jia, S. M., Sun, Y. J., & Yang, J. F. (2019). Decoding of motor imagery EEG based on brain source estimation. *Neurocomputing*. doi: 10.1016/j.neucom.2019.02.006

Li, R., Potter, T., Huang, W., & Zhang, Y. (2017). Enhancing performance of a hybrid EEG-fNIRS system using channel selection and early temporal features. *Frontiers in Human Neuroscience*. doi: 10.3389/fnhum.2017.00462

Lin, X., Sai, L., & Yuan, Z. (2018). Detecting Concealed Information with Fused Electroencephalography and Functional Near-infrared Spectroscopy. *Neuroscience*. doi: 10.1016/j.neuroscience.2018.06.049

Liu, K., Yu, Z. L., Wu, W., Gu, Z., & Li, Y. (2020). Imaging brain extended sources from EEG/MEG based on variation sparsity using automatic relevance determination. *Neurocomputing*. doi: 10.1016/j.neucom.2020.01.038

Liu, Y., Ayaz, H., & Shewokis, P. A. (2017). Mental workload classification with concurrent electroencephalography and functional near-infrared spectroscopy. *Brain-Computer Interfaces*. doi: 10.1080/2326263X.2017.1304020

Ma, Z., Tan, Z. H., & Guo, J. (2016). Feature selection for neutral vector in EEG signal classification. *Neurocomputing*. doi: 10.1016/j.neucom.2015.10.012

McFarland, D. J., McCane, L. M., David, S. V., & Wolpaw, J. R. (1997). Spatial filter selection for EEG-based communication. *Electroencephalography and Clinical Neurophysiology*. doi: 10.1016/S0013-4694(97)00022-2

Meyer, P. E., Schretter, C., & Bontempi, G. (2008). Information-theoretic feature selection in microarray data using variable complementarity. *IEEE Journal on Selected Topics in Signal Processing*. doi: 10.1109/JSTSP.2008.923858

Mikolov, T., Karafiát, M., Burget, L., Jan, C., & Khudanpur, S. (2010). Recurrent neural network based language model. *Proceedings of the 11th Annual Conference of the International Speech Communication Association, INTERSPEECH 2010*.

Mu, Z., & Hu, J. (2009). Research of EEG identification computing based on AR model. *FBIE 2009 - 2009 International Conference on Future BioMedical Information Engineering*. doi: 10.1109/FBIE.2009.5405847

Nasihatkon, B., Boostani, R., & Jahromi, M. Z. (2009). An efficient hybrid linear and kernel CSP approach for EEG feature extraction. *Neurocomputing*. doi: 10.1016/j.neucom.2009.07.012

Nguyen, T., Ahn, S., Jang, H., Jun, S. C., & Kim, J. G. (2017). Utilization of a combined EEG/NIRS system to predict driver drowsiness. *Scientific Reports*. doi: 10.1038/srep43933

Peng, H., Li, C., Chao, J., Wang, T., Zhao, C., Huo, X., & Hu, B. (2019). A novel automatic classification detection for epileptic seizure based on dictionary learning and sparse representation. *Neurocomputing*. doi: 10.1016/j.neucom.2019.12.010

Pisinger, D. (2006). Upper bounds and exact algorithms for p-dispersion problems. *Computers and Operations Research*. doi: 10.1016/j.cor.2004.09.033

Putze, F., Hesslinger, S., Tse, C. Y., Huang, Y. Y., Herff, C., Guan, C., & Schultz, T. (2014). Hybrid fNIRS-EEG based classification of auditory and visual perception processes. *Frontiers in Neuroscience*. doi: 10.3389/fnins.2014.00373

Saadati, M., Nelson, J., & Ayaz, H. (2020a). Convolutional neural network for hybrid fNIRS-EEG mental workload classification. *Advances in Intelligent Systems and Computing*. doi: 10.1007/978-3-030-20473-0_22

Saadati, M., Nelson, J., & Ayaz, H. (2020b). Multimodal fNIRS-EEG classification using deep learning algorithms for brain-computer interfaces purposes. *Advances in Intelligent Systems and Computing*. doi: 10.1007/978-3-030-20473-0_21

Scarpa, F., Cutini, S., Scatturin, P., Dell'Acqua, R., & Sparacino, G. (2010). Bayesian filtering of human brain hemodynamic activity elicited by visual short-term maintenance recorded through functional near-infrared spectroscopy (fNIRS). *Optics Express*. doi: 10.1364/oe.18.026550

Schalk, G., McFarland, D. J., Hinterberger, T., Birbaumer, N., & Wolpaw, J. R. (2004). BCI2000: A general-purpose brain-computer interface (BCI) system. *IEEE Transactions on Biomedical Engineering*. doi: 10.1109/TBME.2004.827072

Sur, S., & Sinha, V. (2009). Event-related potential: An overview. *Industrial Psychiatry Journal*. doi: 10.4103/0972-6748.57865

Tanveer, M. A., Khan, M. J., Qureshi, M. J., Naseer, N., & Hong, K. S. (2019).

Enhanced drowsiness detection using deep learning: An fNIRS Study. *IEEE Access*. doi: 10.1109/ACCESS.2019.2942838

Thanh Hai, N., Cuong, N. Q., Dang Khoa, T. Q., & Van Toi, V. (2013). Temporal hemodynamic classification of two hands tapping using functional near-infrared spectroscopy. *Frontiers in Human Neuroscience*. doi: 10.3389/fnhum.2013.00516

Wu, C. W., Tsai, P. J., Chen, S. C. J., Li, C. W., Hsu, A. L., Wu, H. Y., Ko, Y. T., Hung, P. C., Chang, C. Y., Lin, C. P., Lane, T. J., & Chen, C. Y. (2019). Indication of dynamic neurovascular coupling from inconsistency between EEG and fMRI indices across sleep–wake states. *Sleep and Biological Rhythms*. doi: 10.1007/s41105-019-00232-1

Yang, M., Li, J., Li, Z., Yao, D., Liao, W., & Chen, H. (2017). Whole-brain functional connectome-based multivariate classification of post-stroke aphasia. *Neurocomputing*. doi: 10.1016/j.neucom.2016.10.094

Yin, X., Xu, B., Jiang, C., Fu, Y., Wang, Z., Li, H., & Shi, G. (2015). A hybrid BCI based on EEG and fNIRS signals improves the performance of decoding motor imagery of both force and speed of hand clenching. *Journal of Neural Engineering*. doi: 10.1088/1741-2560/12/3/036004

Zhang, P., Wang, X., Chen, J., & You, W. (2017). Feature weight driven interactive mutual information modeling for heterogeneous bio-signal fusion to estimate mental workload. *Sensors (Switzerland)*. doi: 10.3390/s17102315

CHAPTER 5: DEEP LEARNING BASED MULTIMODAL EEG-FNIRS CLASSIFICATION: AN APPLICATION TO MOTOR IMAGERY

In preparation for submission to the Journal of *Neurocomputing*

Roohollah Jafari Deligani[1], Seyyed Bahram Borgheai[1], John McLinden[1], and Yalda Shahriari[1,2]

[1]Department of Electrical, Computer and Biomedical Engineering; University of Rhode Island, Kingston, RI 02881, USA

[2]Interdisciplinary Neuroscience Program; University of Rhode Island, Kingston, RI 02881, USA

Email: yalda_shahriari@uri.edu

ABSTRACT

Deep learning-based approaches recently have reached unprecedented complex classification outcomes through increased computational power and efficient learning algorithms to fill the crucial gap of accurate brain state classification from a multimodal signal dataset. In this work, we proposed a novel deep learning-based approach for automatic feature extraction from multimodal EEG-fNIRS data to enhance motor imagery classification which is a major processing step in BCI applications. The results demonstrated that our deep learning-based classification approaches outperformed conventional classification methods. Moreover, the automatic feature extraction strategy that was implemented using a dual convolutional neural network for multimodal EEG-fNIRS improved classification accuracy compared to other approaches based on manual feature extraction. These outcomes suggest promising improvements in BCI performances using multimodal EEG-fNIRS deep learning based classifiers with automatic feature extraction, which can be utilized in clinical applications for people with neurological disorders including ALS patients.

5.1 BACKGROUND

Two main processing steps are involved in brain computer interfaces (BCI), specifically feature extraction and classification. Through these steps, BCIs aim to accurately classify brain states. Conventionally, different features were extracted from electroencephalography (EEG) and functional near infrared spectroscopy (fNIRS) signals and were then fed to different types of classifiers.

Extracting the optimal features from EEG-fNIRS data for a conventional classifier to obtain the highest classification accuracies remains an area of research (Tanveer et al., 2019). Most studies use a variety of features for this purpose, including signal power in specific EEG frequency bands (i.e. delta, theta, alpha and beta) and temporal features computed from oxy-, and deoxy-hemoglobin (HbO and HbR respectively) variations in the brain for fNIRS (i.e. mean, signal peak, slope, sum of peaks, integral of the signal and etc). A variety of feature extraction methods have been used, including autoregression models (Mu et al., 2009), wavelet transforms (Hosni et al., 2020), common spatial patterns (Nasihatkon et al., 2009), and power spectral densities (Kocak et al., 2017).

Feeding too many features to a classifier is another concern which can degrade classification performance due to the effects of redundant features (Deligani et al., 2021) or due to overfitting especially, especially when there are a limited number of data points for training (Hua et al., 2005). Different studies have used prior knowledge to obtain the most relevant features or have used feature selection techniques to provide an optimal number of features for the classifier. For example, in a motor imagery (MI) classification study conducted by Fazli et al. (Fazli et al., 2012), alpha and beta EEG band-powers, which are as established MI associated features, along with HbO and HbR, were extracted from the data. However, HbR has been reported as a non-contributing signal for MI classification in other studies (Abdalmalak et al., 2017). Putze et al. (Putze et al., 2014) used ERP temporal features in addition to spectral features from EEG to perform classification based on auditory and visual perception. Another hybrid classification study (Ko et al., 2019) integrated the temporal and spectral features of EEG for MI

classification. In another study (Al-Shargie et al., 2016), a set of EEG temporal features was integrated with a set of fNIRS spatial features, and then features were selected using a joint temporal and spatial independent component analysis. In another study (Besio et al., 2008), the authors used a hardware based approach to extract more effective EEG features, improving classification accuracy using tripolar electrode disks in recording. Other studies have used a variety of different feature selection techniques to select the optimal subset of features from the original set of manually extracted features (Deligani et al., 2021; Hong et al., 2018; R. Li et al., 2017). However, all these algorithms require manual feature extraction, leaving it up to each study to ensure that the extracted features are appropriate for the classification task.

Despite the manual feature extraction requirement for conventional classification algorithms, deep learning approaches can be designed in a way that do not require manual feature extraction (Tanveer et al., 2019). In the simplest architecture, deep learning refers to neural networks (NN) composed of many layers (Lecun et al., 2015). Deep NNs (DNNs) use a set of layers of nonlinear processing units called neurons. Each successive layer uses the output from the previous layer as input, and some set of neurons from consecutive layers are connected. If all of the consecutive layers are connected to each other, the resulting network is called a fully connected network (FCN). Recently, increased computation power and technological development has facilitated the evolution of deep learning in several domains, including the implementation of efficient learning algorithms that avoid local minima in the objective function and poor generalization (Kingma et al., 2015), the development of new neuron activation functions to add non-linearity to the network such as rectified linear unit (ReLU) function (Dahl et

al., 2013), the implementation of neural networks where neurons are connected to portions of signals and or images such as convolutional neural networks (Krizhevsky et al., 2012), and the development of recursive neural networks where outputs are fed back into the network in a sequential manner to allow information storage such as recurrent neural networks RNNs (Mikolov et al., 2010).

DNNs can perform very complex and non-linear classifications, by increasing the number of layers in a shallow NN, which improve classifiers' performances (Bianchini et al., 2014). Specifically, when the neurons are connected to portions of signals that are close in time or space or frequency, the NN architecture is called a convolutional neural network (CNN) (Krizhevsky et al., 2012), which can encode temporal and spectral information even though the standard FCN cannot encode any spectro-temporal information (Chiarelli et al., 2018). Exploiting a CNN in a DNN can not only provide a completely automatic feature extraction/encoder framework from the raw data, but also can retain better features by eliminating redundant information and ultimately achieve higher classification accuracy (Cheng et al., 2020).

Deep learning approaches have been successfully applied to both EEG and fNIRS BCI classification, separately. In (An et al., 2014), left/right MI classification was performed by DNN using limited EEG recording channels, and the authors reported an average accuracy of 80%. In (Jirayucharoensak et al., 2014), a DNN was used to classify different levels of valence and arousal based on EEG power spectral density features and the authors reported a maximum classification accuracy of 83%. Using a DNN on EEG signals, the authors in (Hajinoroozi et al., 2015) classified driver's cognitive states and reported a maximum classification accuracy of 80%. In (Bashivan et al., 2016), the

authors fed EEG power in three different frequency bands of interest to a CNN and reported a maximum classification accuracy of 92%. In (Hennrich et al., 2015), the authors used a DNN for classification of a mental task based on fNIRS recordings and reported no accuracy improvement compared to conventional classification algorithms (such as LDA and SVM). In another study (Thanh Hai et al., 2013) the authors classified left/right MI fNIRS activity with an average accuracy of 85%. All of these studies have applied deep learning approaches to only one modality for BCI classification.

To the best of our knowledge, there are only a few studies implementing deep learning algorithms for BCI classification in a combined EEG-fNIRS framework. In (Chiarelli et al., 2018), the authors used a DNN with four hidden layers to perform MI classification. They used averaged event-related synchronization/event-related desynchronizations (ERD/ERS) over 1s windows as EEG features and averaged HbO and HbR as fNIRS features, and they found an 8% classification accuracy improvement over classification with LDA. In a similar study (Saadati et al., 2020b) with the same extracted features and the same DNN architecture, a 6% classification accuracy improvement over SVM was reported. They investigated the effect of window size for feature extraction from EEG and FNIRS data and reported a window of 3s length as the optimal size for both modalities. In another study by Ghonchi et al (Ghonchi, Hamidreza, 2020), the authors down-sampled the EEG data and up sampled the fNIRS data to obtain the same sampling rate for both signals, concatenate them, and feed them to the NN. Notably, they used RNN and CNN to extract the temporal and spatial features respectively, providing a 14% classification accuracy improvement over LDA. Overall, defining a fixed proper window size to capture the fast and slow dynamics of both EEG

and fNIRS respectively in a single feature remains an important research question to address.

In this chapter, using a dual CNN for EEG and fNIRS recorded activity of MI BCI, we have investigated an automatic deep learning-based feature extraction framework for a hybrid classification in which the results were compared with single modalities and conventional classification algorithms.

5.2 METHODS

Ten subjects (4 males, age: 60.7 ± 8.5), with no reported history of neurological or psychiatric disease were recruited for this study. The study protocol was approved by the URI institutional review board (IRB), and all subjects provided informed consent in writing.

EEG signals were recorded from 13 Ag/AgCl electrodes referenced to the left earlobe. The electrodes covered the pre-motor (FC3, FC4), primary motor (C1, C3, Cz, C2, C4), sensorimotor (CP1, CP3, CP2, CP4), and parietal (P3, P4) areas of the brain according to the 10–20 system. An additional electrode was placed at FCz as the ground electrode. Data acquisition was handled using BCI2000 software (Schalk et al., 2004). The signals were amplified using a g.USBamp amplifier (g.tec medical engineering), digitized at 256 Hz and zero-phase bandpass filtered (1–45 Hz). The impedance of the EEG electrodes was kept below 5 KΩ. fNIRS data were recorded with NIRScout (NIRx Inc.) at two near-infrared light wavelengths (760 nm and 850 nm) to acquire the HbR and HbO responses, respectively. The signals were digitized at 15.6 Hz, and the optode montage was configured using 16 probes, eight sources, and eight detectors mounted on

a standard EEG cap, with a separation distance of ~3 cm to maintain acceptable signal quality and sensing depth. This probe layout provided 14 channels. The sources were located according to the 10–5 electrode placement system as follows—AF3 (S1), AF4 (S5), FCC5h (S3), FCC1h (S2), FCC2h (S6), FCC6h (S7), CCP3h (S4), and CCP4h (S8)—while the detectors were placed at AFF1 (D2), AFF2 (D6), F5 (D1), F6 (D5), FCC3h (D3), FCC4h (D7), CCP1h (D4), and CCP2h (D8). Four fNIRS channels covered the pre/frontal cortex (CH1, CH2, CH8, and CH9) associated with the pre/supplementary motor area (pre/SMA), involved in motor preparation. In the proximity of the primary motor cortex, ten channels (CH3, CH4, CH5, CH6, CH7, CH10, CH11, CH12, CH13, and CH14) were positioned to surround the standard C1, C2, C3, and C4 areas as reference points for hand MI-related activation of the motor cortex.

The task was designed using the BCI2000 stimulus presentation module for MI (Schalk et al., 2004). Participants completed three recording runs, each separated by approximately 5 min of rest. During each run, the subject was instructed to attend to three types of visual cues presented on-screen and respond accordingly with one of three types of mental activity: (a) left-hand MI (LMI) when the cue appears on the left side of the screen, (b) right-hand MI (RMI) when the cue appears on the right side of the screen, and (c) rest when the cue appears in the middle of the screen (Figure 5.1). The imagination cue was the image of a hand, and participants were instructed to imagine moving their own hand, for example, to imagine squeezing a stress ball. The rest cue was a green circle positioned in the middle of the screen to help them relax and not think about any movement. The subjects sat comfortably in an armchair and were instructed to relax their arms and avoid movement. A total of ten trials for each type of MI per run randomly

alternated with rest trials in between each MI task. We followed a simple alternation between rest and imagination, where the participant was intuitively pacing and preparing for the next imagination task at the end of each preceding rest block (Fig. 5.1).

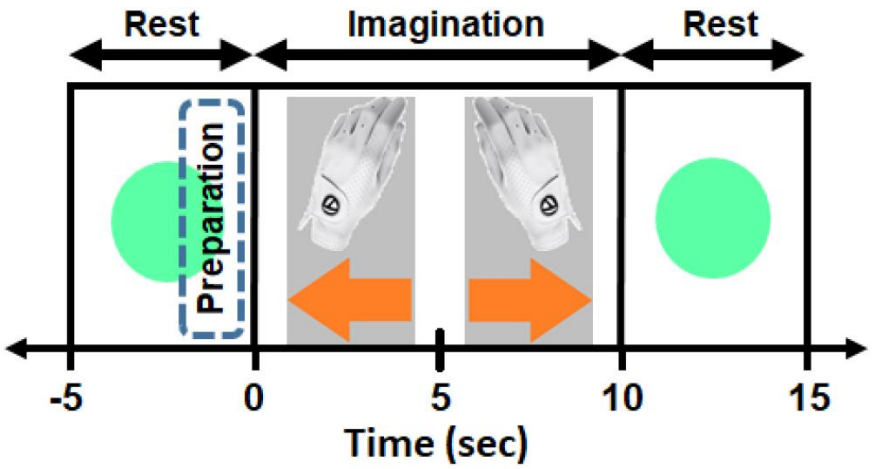

Figure 5.1. Overview of task blocks and timing. At each imagination block, either the left-hand or right-hand picture was shown to participants, but not both.

Offline preprocessing and analysis were performed in MATLAB (MathWorks Inc.). The EEG data were spatially filtered using common average referencing (CAR) filter (McFarland et al., 1997). CAR involves re-referencing the EEG data to the average of all the channels in order to filter out any global artifacts that appear simultaneously in all channels. Eye movements and fNIRS-interfered artifacts were removed using the extended Infomax Independent Component Analysis (ICA) algorithm (Brunner et al., 2013). These artifactual components were identified through visual inspection of the independent components' spatial topographies and the spectral analysis of their time courses. Time-frequency analysis of the EEG data was performed via complex Morlet wavelet convolution. A wavelet family was created ranging from 1 to 30 Hz in 30 linear frequency steps and a variable number of cycles (3 to 10). Individual 10 s trials were convolved with the set of complex wavelets, normalized with uniform scale energy. The

time-frequency power maps for each channel were obtained by squaring the magnitude of the convolution result for each individual trial, which yielded the input data for non-feature-based classification. For feature-based classification, the time-frequency power maps were averaged over all time points and over the alpha and beta frequency bands, which yielded 26 EEG features (number of frequency bands × number of channels). For fNIRS data, the modified Beer-Lambert Law was used to calculate changes in the concentrations of HbO and HbR using recorded alterations in the reflected light attenuation. fNIRS data were then band-pass filtered at 0.01-0.09 Hz to eliminate physiological noises caused by respiration (~0.3 Hz), cardiac activities (~1 Hz), and Mayer waves (~0.1 Hz). fNIRS data were initially segmented into 10-sec trials of LMI, RMI, and Rest, according to the stimulus presentation time, similar to the segmentation of the EEG data for non-feature-based classification. For feature-based classification, various features were extracted from fNIRS including the maximum peak, maximum peak delay, area under the curve, and slope. These features were combined into various feature sets and the best feature set was determined based on classification accuracy with LDA. The HbO maximum peak provided the highest accuracy and was therefore used, providing 14 (number of channels—one feature per channel) manually extracted fNIRS features. MI trials were then separated into 60 MI-Rest and 60 MI-Active (30 MI-Left, 30 MI-Right) trials for each subject.

The FCN employed was a fully connected feed-forward NN with two hidden layers, one input layer, and one output layer. Each neuron in the hidden layers performed a nonlinear transformation of a linear combination of all the outputs from the previous layer. As a non-linear processing function, we decided to employ the rectified linear unit

(ReLU) function, which was proven to mitigate the vanishing gradient problem, providing better performance than other non-linear functions (such as the hyperbolic tangent or the sigmoid function) (Dahl et al., 2013). The formula for ReLU function is shown in equation 5.1.

$$y = \begin{cases} 0, & wx + b \leq 0 \\ wx + b, & wx + b > 0 \end{cases} \tag{5.1}$$

In this formula, x is the input, w is the matrix of multiplied weights that will be updated during optimization, b is the bias, and y is the output. The softmax function for the two neurons in the output layer is the predicted probability of being in either of the classes (i.e. right or left/rest or motor imagery states). The formula for the softmax function is shown in equation 5.2.

$$\begin{bmatrix} P_{Right/Active} \\ P_{Left/Rest} \end{bmatrix} = \begin{bmatrix} \frac{e^{w_1 x}}{\sum_{k=1}^{2} e^{w_k x}} \\ \frac{e^{w_2 x}}{\sum_{k=1}^{2} e^{w_k x}} \end{bmatrix} \tag{5.2}$$

In this formula, the predicted probability of being in the right/motor imagery class is shown by $P_{Right/Active}$ and the probability of being in the left/rest class is shown by $P_{Left/Rest}$. Here, x is the input vector to the softmax layer, and w_1 and w_2 are the weight vectors for the neurons. The number of hidden layers and neurons were selected to approximately decrease the number of processing units (thus compressing information) by a factor of 2 between successive layers. The weights were initialized in a pseudo-random approach employing a truncated normal distribution (0 mean, 0.1 SD), and the biases were initialized to 0. The objective function measures the error between the output values and the desired values. We used the cross-entropy error as the objective function. Cross-entropy is defined as:

$$Cross - Entropy = -\sum_{i} y_i' \ln y_i \tag{5.3}$$

In this formula, y is the output vector of the FCN and y' is the known state ([1 0] for right/active motor imagery or [0 1] for left/rest motor imagery). For the optimization algorithm we employed the Adam Optimizer (Kingma et al., 2015). The Adam Optimizer is a state-of the art learning algorithm that differs from the classical stochastic gradient descent since it computes individual adaptive learning rates from estimates of the first and second moments of the gradients, mitigating slow learning rates and/or local minima issues. The Adam Optimizer learning rate was set to 0.01.

The CNNs used in this study are basically feedforward DNNs with local connections and non-linear ReLU activation functions. For the EEG data, the wavelet maps were fed to the first layer of the architecture. The l-th convolutional layer has a 3D array with CH (CH= number of recording channels) 2-dimensional feature maps of size $T_{EEG} \times f$ (number of time points in a trial × frequency) as its input. Each map is denoted by z_{ijk}^{l-1} $(i = 0,\cdots, T_{EEG} - 1, j = 0,\cdots, f - 1, k = 0,\cdots, CH - 1)$. A filter bank consists of M kernels and is denoted by $h_{pqkm}(p = 0,\cdots, H1 - 1, q = 0,\cdots, H2 - 1, k = 0,\cdots, CH - 1, m = 0,\cdots, M - 1)$. Each kernel additionally has CH channels, so its size is $H1 \times H2 \times CH$. Parallel calculations for each kernel provide u_{ijm}. Then an activation function $ReLU(.)$ is applied to u_{ijm} to get z_{ijk}^{l}, which the output of the l-th convolutional layer, and feed it to the next layer. The whole operation for each layer can be written as below:

$$u_{ijm} = \sum_{k=0}^{CH-1} \sum_{p=0}^{H_1-1} \sum_{q=0}^{H_2-1} z_{i+p,j+q,k}^{l-1} h_{pqkm} + b_{ijm} \tag{5.4}$$

$$z_{ijk}^{l} = ReLU(u_{ijm}) \tag{5.5}$$

Then, considering the fNIRS data, the HbO signals were fed to the first layer of the CNN architecture. The input of the l-th convolutional layer is a 2D array with CH (CH= number of recording channels) 1-dimensional feature maps of size T_{fNIRS} (number of time points in a trial). Each input is denoted by z_{ik}^{l-1} ($i = 0,\cdots, T_{EEG} - 1, k = 0,\cdots, CH - 1$). A filter bank consists of M kernels is denoted by h_{pkm}($p = 0,\cdots, H1 - 1, k = 0,\cdots, CH - 1, m = 0,\cdots, M - 1$). Each kernel and its corresponding input have CH channels, so its size is $H1 \times CH$. Parallel calculation with respect to each kernel yields u_{im}. Then an activation function $ReLU(.)$ is applied to u_{im} to get the output of the l-th convolutional layer, z_{ik}^{l}, and feed it to the next layer. The whole operation for each layer can be written as below:

$$u_{im} = \sum_{k=0}^{CH-1} \sum_{p=0}^{H_1-1} z_{i+p,k}^{l-1} h_{pkm} + b_{im} \tag{5.6}$$

$$z_{ik}^{l} = ReLU(u_{im}) \tag{5.7}$$

More details about the inputs, outputs, dimension size, kernel size and stride (overlapping size of each convolutional operation) for each layer of the CNNs are provided in figure 5.2.

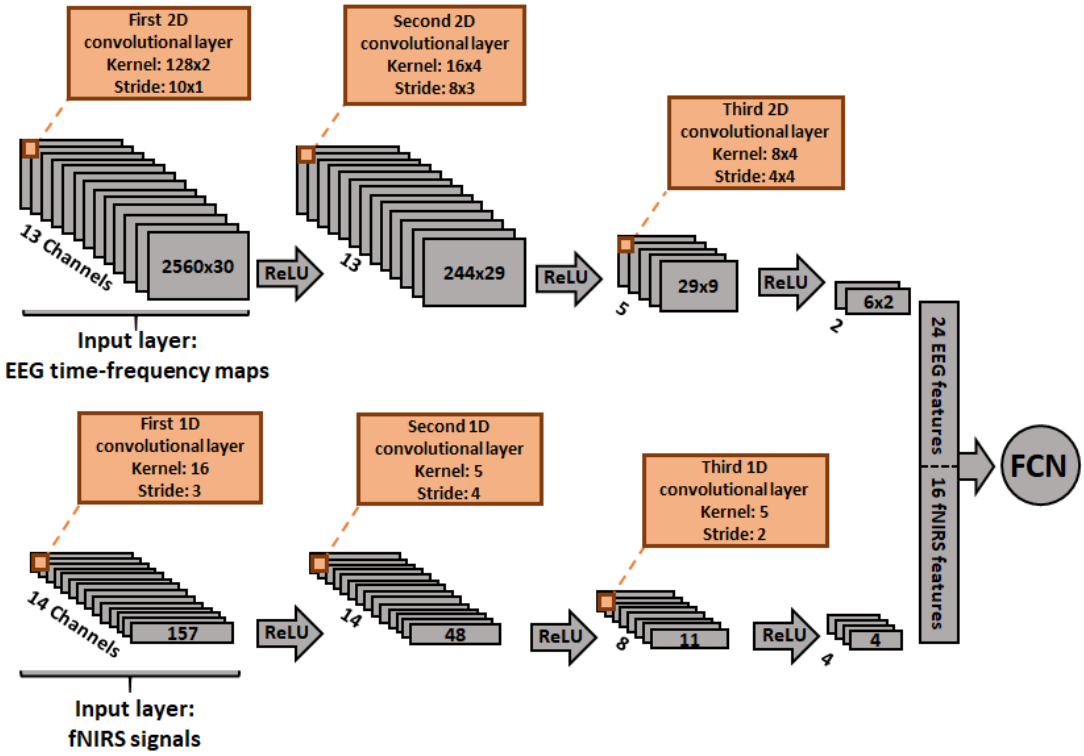

Figure 5.2. Block diagram of the dual CNN for EEG and FNIRS. Automatically extracted features are merged at the output layer of the CNN and fed to an FCN.

Three methods of classification were implemented in this study including LDA, FCN, and CNN+FCN. The first two classifiers were fed manually extracted features from the EEG and fNIRS trials, and the last classifier was fed HbO whole trial fNIRS data and whole trial time-frequency decomposed EEG data. All three classification methods were tested with three different modality sets: EEG only, fNIRS only, and hybrid EEG- fNIRS data. A five-fold cross validation strategy was used by shuffling the whole data and dividing it into five equal size folds. Test accuracy was averaged across folds, and finally a non-parametric Wilcoxon signed rank statistical test was used to compare modalities and classification methods, with the alpha, or type I error rate, set to α=0.01. The false discovery rate was further used for multiple comparison correction and adjusted *p*-values were reported.

5.3 RESULTS

Figures 5.3 through 5.5 show the averaged test accuracy across the five folds for each subject obtained from the three different methods of MI-state versus resting-state classification, specifically 1) conventional classification algorithm (LDA) using manually extracted features, 2) FCN using manually extracted features, and 3) CNN+FCN with no manual feature extraction. Figure 5.3 shows the results using only EEG data, figure 5.4 shows the results using only fNIRS data, and figure 5.5 shows the results using hybrid EEG-fNIRS data. Figures 5.6 through 5.8 show similar results, but for left MI versus right MI classification.

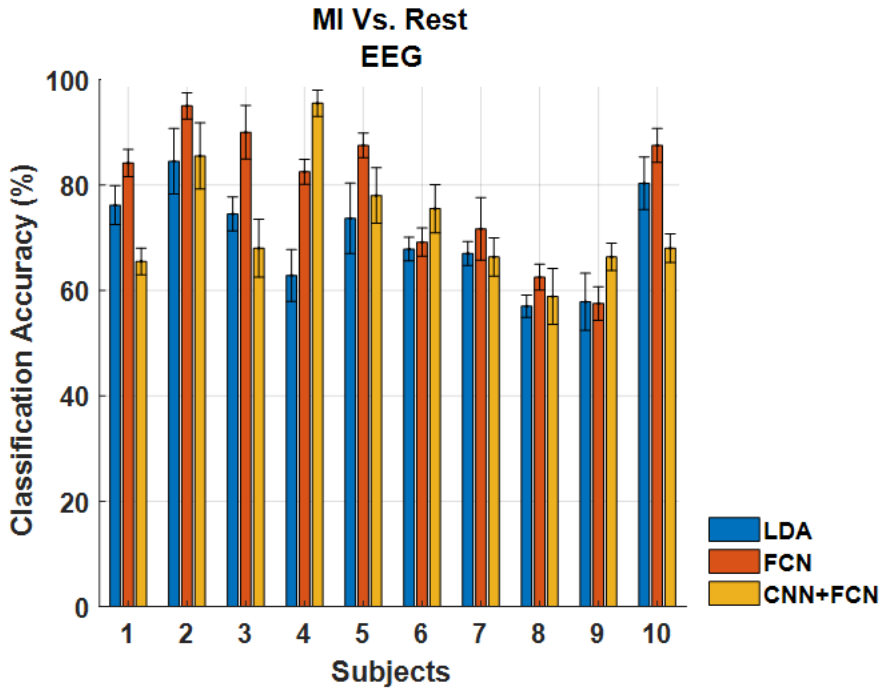

Figure 5.3. Classification results for MI versus rest using LDA, FCN, and CNN+FCN for each subject on EEG data alone. Error bars show the standard deviation of the test accuracies across the five folds.

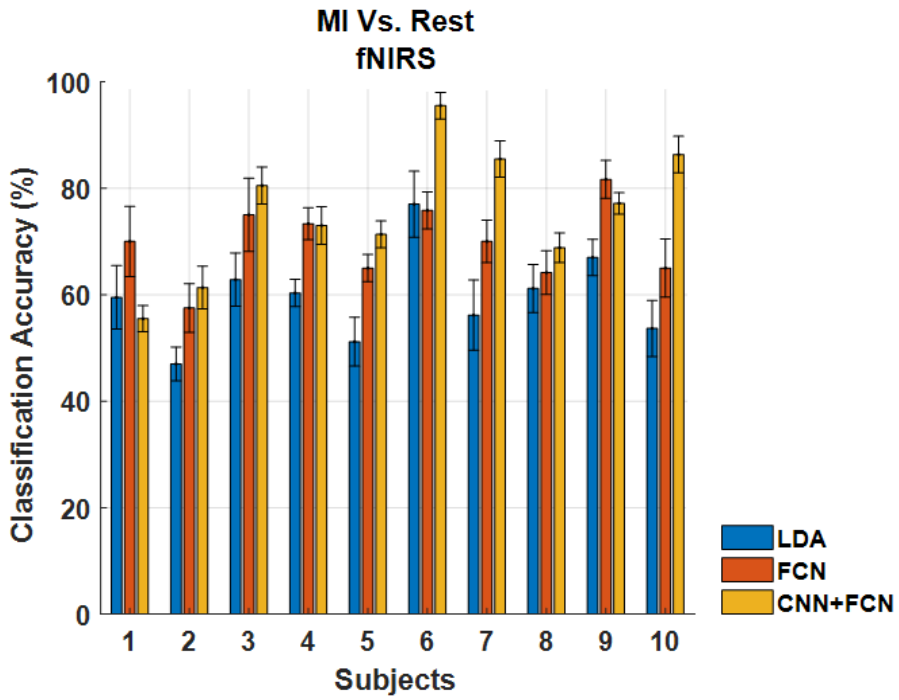

Figure 5.4. Classification results for MI versus rest using LDA, FCN, and CNN+FCN for each subject on fNIRS data alone. Error bars show the standard deviation of the test accuracies across the five folds.

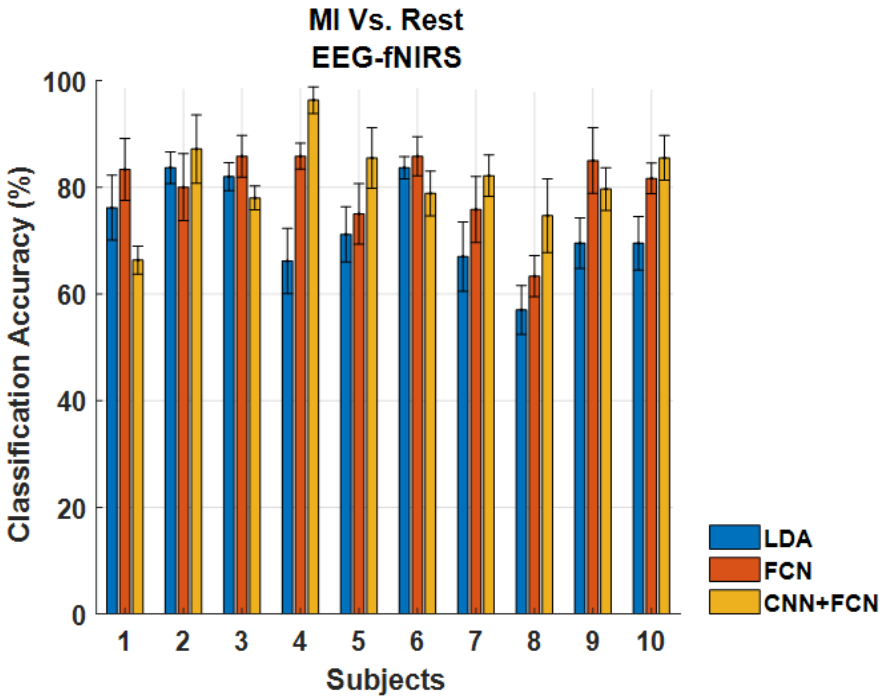

Figure 5.5. Classification results for MI versus rest using LDA, FCN, and CNN+FCN for each subject on hybrid EEG-fNIRS data. Error bars show the standard deviation of the test accuracies across the five folds.

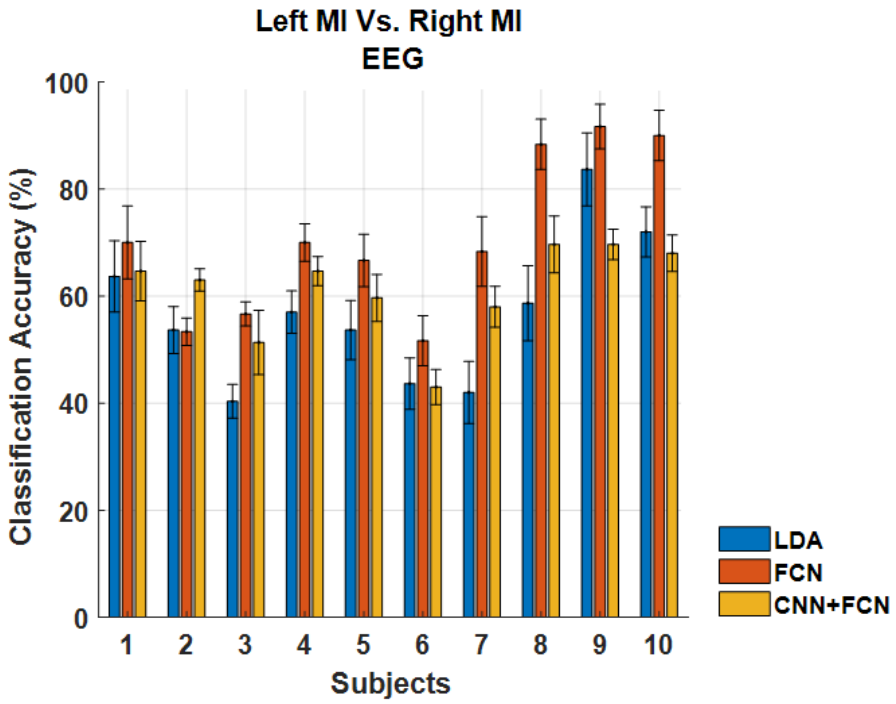

Figure 5.6. Classification results for left versus right MI using LDA, FCN, and CNN+FCN for each subject on EEG data alone. Error bars show the standard deviation of the test accuracies across the five folds.

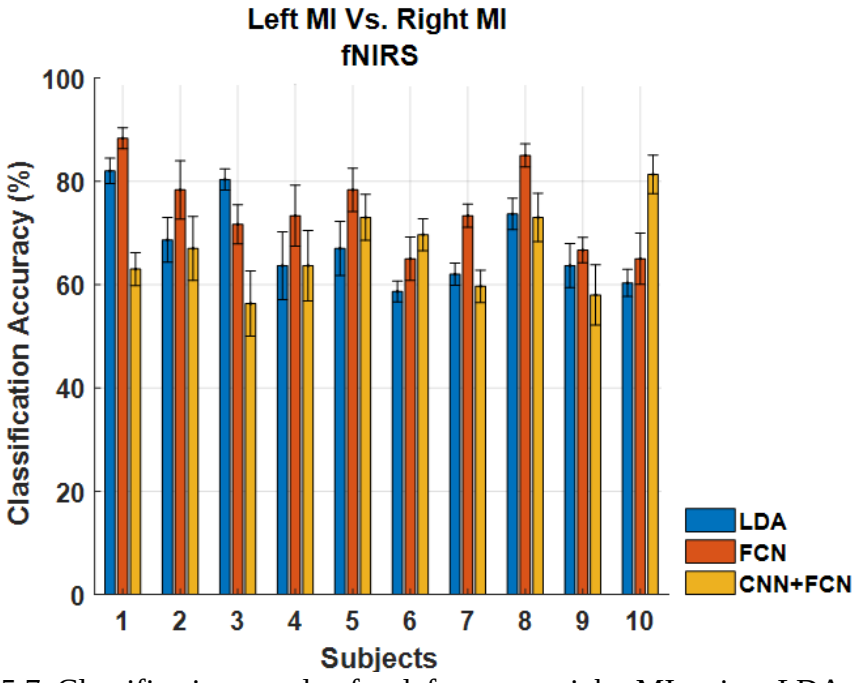

Figure 5.7. Classification results for left versus right MI using LDA, FCN, and CNN+FCN for each subject on fNIRS data alone. Error bars show the standard deviation of the test accuracies across the five folds.

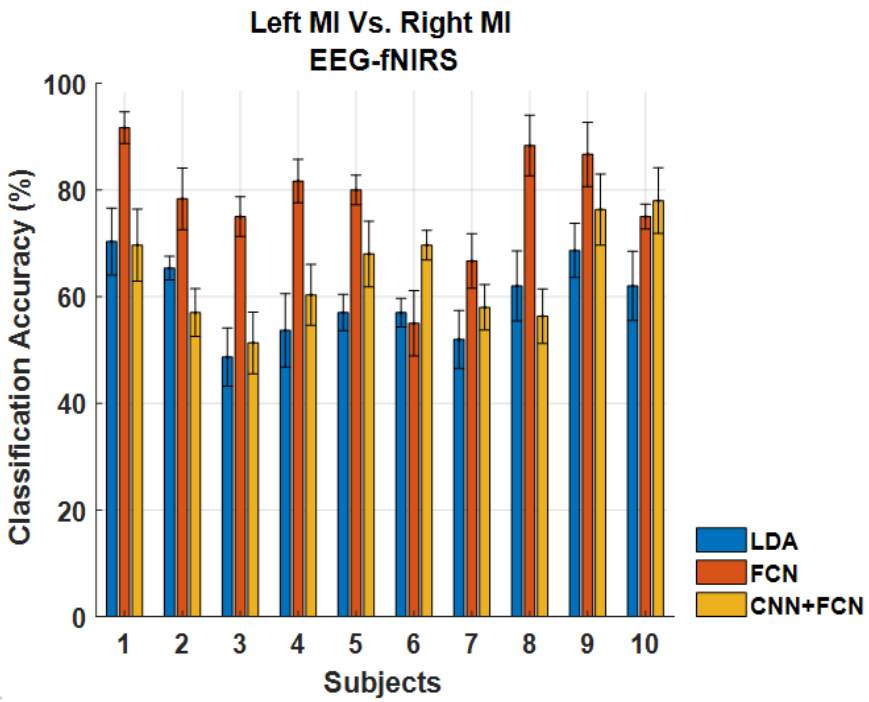

Figure 5.8. Classification results for left versus right MI using LDA, FCN, and CNN+FCN for each subject on hybrid EEG-fNIRS data. Error bars show the standard deviation of the test accuracies across the five folds.

Table 5.1 shows three classification performance metrics: accuracy, sensitivity, and specificity, for MI-state versus resting-state classification and for left MI versus right MI classification for the three aforementioned approaches. The results are shown for EEG alone, fNIRS alone, and hybrid EEG- fNIRS. Averages and standard deviations over all subjects are shown. The highest test accuracy for left MI versus right MI classification was 77.8$\pm$9.3, achieved by classifying hybrid EEG-fNIRS data with the FCN. The highest test accuracy for MI-state versus resting-state classification was 81.4$\pm$7.6, achieved by classifying hybrid EEG-fNIRS data with the CNN+FCN. For left MI versus right MI classification, statistical analysis showed that using the FCN with hybrid EEG-fNIRS data provided significant improvements over the other two classification methods and over using the FCN with EEG data alone. For MI-state versus resting-state classification, statistical analysis showed that using the CCN+FCN with

hybrid EEG-fNIRS data provided significant improvements over fNIRS data alone with all classification methods and EEG data alone with the CCN+FCN. In addition, both FCN and CNN+CNN results showed significant improvements over LDA in all single and hybrid modalities. All the *p*-values obtained for significant results were below 0.01 *(*$p < 0.01$).

Table 5.1. Classification performance metrics for MI-state versus resting-state classification and for left MI versus right MI classification obtained from LDA, FCN, and CNN+FCN methods using single and hybrid modalities.

		Left Vs. Right Classification			**MI Vs. Rest Classification**		
		EEG	**fNIRS**	**EEG-fNIRS**	**EEG**	**fNIRS**	**EEG-fNIRS**
LDA	Sensitivity	62.2±16.6	72±15.9	62.7±8.4	78.6±8.1	64.4±10	79.1±9.9
	Specificity	34.4±12.9	39.3±9.3	33.5±4.5	34.6±13.6	32.7±9	37.5±8.3
	Accuracy	56.8±13	68±7.7	59.7±6.8	70.2±8.8	59.6±8	72.6±8.3
FCN	Sensitivity	79.6±9.2	82.5±7.5	85.9±8.1	87.3±10.4	77.2±8.4	88.8±11.2
	Specificity	60.3±10.7	65.3±7.6	69.5±6.8	70.5±8.2	59.8±7.7	72.7±9.7
	Accuracy	70.7±14.2	74.5±7.6	**77.8±9.3**	78.7±12	69.7±6.7	80.2±6.8
CNN+ FCN	Sensitivity	69.1±8.8	73.9±11.8	71.9±12.8	78.4±8.6	81.8±7.7	89.9±9.6
	Specificity	53.8±11.6	59.2±10.8	56.3±14.8	66.3±7.9	70.1±9.6	74.5±7.1
	Accuracy	61.7±8.1	66.5±7.5	64.5±8.6	72.7±10.4	75.5±11.5	**81.4±7.6**

5.4 DISCUSSION

Comparing the results for different modalities and classification methods, NN based classification approaches significantly outperformed conventional classification methods (LDA and SVM were implemented in this study but only LDA results were reported in this study since they outperformed the SVM) for both left/right and rest/MI datasets. Moreover, a deep learning based automatic feature extraction strategy was implemented using a dual-CNN, which yielded the best classification accuracy for the rest/ MI dataset. In addition, significant improvement was observed using hybrid EEG-fNIRS modality compared to single modalities.

The small number of MI trials per subject meant sample size was a limitation for this study. Using bigger datasets in the future could improve the generalizability of the classifier and further validate the performance improvements from the proposed classification methods. Moreover, examining the proposed methods for datasets recorded from people with neurological disorders including ALS patients, major targets of BCI design, can provide a basis for clinical applications of our study in the future.

Results reported in this study suggest potentially high BCI performance with combined hybrid EEG-fNIRS recordings and deep learning classifiers with convolutional layers for automatic feature extraction. The higher performance of the multimodal data with respect to single-modality EEG or fNIRS highlights the higher information content available by combining both hemodynamic and electrical brain activity recordings. The higher performances of FCN and FCN+CNN compared to LDA additionally suggest the non-linearity involved in MI classification, which supports further utilization of NN based classification. Moreover, the marginally higher performances of CNN classification compared to FCN results using the previously reported most distinguishing features shows the capabilities of our dual-CNN learning procedures with automatic feature extraction, which do not require prior knowledge about the data.

REFERENCES

Abdalmalak, A., Milej, D., Diop, M., Shokouhi, M., Naci, L., Owen, A. M., & St. Lawrence, K. (2017). Can time-resolved NIRS provide the sensitivity to detect brain activity during motor imagery consistently? *Biomedical Optics Express*. doi: 10.1364/boe.8.002162

Abtahi, M., Bahram Borgheai, S., Jafari, R., Constant, N., Diouf, R., Shahriari, Y., & Mankodiya, K. (2020). Merging fNIRS-EEG Brain Monitoring and Body Motion Capture to Distinguish Parkinsons Disease. *IEEE Transactions on Neural Systems and Rehabilitation Engineering*. doi: 10.1109/TNSRE.2020.2987888

Ahn, S., & Jun, S. C. (2017). Multi-modal integration of EEG-fNIRS for brain-computer interfaces – Current limitations and future directions. In Frontiers in Human Neuroscience. doi: 10.3389/fnhum.2017.00503

Akhonda, M. A. B. S., Levin-Schwartz, Y., Bhinge, S., Calhoun, V. D., & Adali, T. (2018). Consecutive Independence and Correlation Transform for Multimodal Fusion: Application to EEG and Fmri Data. *ICASSP, IEEE International Conference on Acoustics, Speech and Signal Processing - Proceedings*. doi: 10.1109/ICASSP.2018.8462031

Al-Shargie, Fares, Hasan Al-Nashash, and T. B. T. (2019). Assessment of Mental Stress among Undergraduate Students Using Novel Fusion Method on EEG and fNIRS Features. *Frontiersin*, 1.

Al-Shargie, F., Kiguchi, M., Badruddin, N., Dass, S. C., Hani, A. F. M., & Tang, T. B. (2016). Mental stress assessment using simultaneous measurement of EEG and fNIRS. *Biomedical Optics Express*. doi: 10.1364/boe.7.003882

Al-Shargie, F., Tang, T. B., & Kiguchi, M. (2017a). Assessment of mental stress effects on prefrontal cortical activities using canonical correlation analysis: an fNIRS-EEG study. *Biomedical Optics Express*. doi: 10.1364/boe.8.002583

Al-Shargie, F., Tang, T. B., & Kiguchi, M. (2017b). Stress Assessment Based on Decision Fusion of EEG and fNIRS Signals. *IEEE Access*. doi: 10.1109/ACCESS.2017.2754325

An, X., Kuang, D., Guo, X., Zhao, Y., & He, L. (2014). A deep learning method for classification of eeg data based on motor imagery. *Lecture Notes in Computer Science (Including Subseries Lecture Notes in Artificial Intelligence and Lecture Notes in Bioinformatics)*. doi: 10.1007/978-3-319-09330-7_25

Baillet, S., Garnero, L., Marin, G., & Hugonin, J. P. (1999). Combined MEG and EEG source imaging by minimization of mutual information. *IEEE Transactions on Biomedical Engineering*. doi: 10.1109/10.759053

Bashivan, P., Rish, I., Yeasin, M., & Codella, N. (2016). Learning representations from EEG with deep recurrent-convolutional neural networks. *4th International Conference on Learning Representations, ICLR 2016 - Conference Track Proceedings*.

Besio, W. G., Cao, H., & Zhou, P. (2008). Application of tripolar concentric electrodes and prefeature selection algorithm for brain-computer interface. *IEEE Transactions on Neural Systems and Rehabilitation Engineering*. doi: 10.1109/TNSRE.2007.916303

Bianchini, M., & Scarselli, F. (2014). On the complexity of neural network classifiers: A comparison between shallow and deep architectures. *IEEE Transactions on Neural Networks and Learning Systems*. doi: 10.1109/TNNLS.2013.2293637

Billionnet, A., & Calmels, F. (1996). Linear programming for the 0-1 quadratic knapsack problem. *European Journal of Operational Research*. doi: 10.1016/0377-2217(94)00229-0

Borgheai, S. B., Deligani, R. J., McLinden, J., Zisk, A., Hosni, S. I., Abtahi, M.,

Mankodiya, K., & Shahriari, Y. (2019). Multimodal exploration of non-motor neural functions in ALS patients using simultaneous EEG-fNIRS recording. *Journal of Neural Engineering*, *16*(6). doi: 10.1088/1741-2552/ab456c

Borgheai, S. B., Mclinden, J., Zisk, A. H., Hosni, S. I., Deligani, R. J., Abtahi, M., Mankodiya, K., & Shahriari, Y. (2020). Enhancing Communication for People in Late-Stage ALS Using an fNIRS-Based BCI System. *IEEE Transactions on Neural Systems and Rehabilitation Engineering*, *28*(5). doi: 10.1109/TNSRE.2020.2980772

Brown, G., Pocock, A., Zhao, M. J., & Luján, M. (2012). Conditional likelihood maximisation: A unifying framework for information theoretic feature selection. *Journal of Machine Learning Research*.

Brunner, C., Delorme, A., & Makeig, S. (2013). Eeglab – an Open Source Matlab Toolbox for Electrophysiological Research. *Biomedical Engineering / Biomedizinische Technik*. doi: 10.1515/bmt-2013-4182

Buccino, A. P., Keles, H. O., & Omurtag, A. (2016). Hybrid EEG-fNIRS asynchronous brain-computer interface for multiple motor tasks. *PLoS ONE*. doi: 10.1371/journal.pone.0146610

Cernadas, E., Fernández-Delgado, M., González-Rufino, E., & Carrión, P. (2017). Influence of normalization and color space to color texture classification. *Pattern Recognition*. doi: 10.1016/j.patcog.2016.07.002

Cheng, L., Li, D., Yu, G., Zhang, Z., Li, X., & Yu, S. (2020). A motor imagery EEG feature extraction method based on energy principal component analysis and deep belief networks. *IEEE Access*. doi: 10.1109/ACCESS.2020.2969054

Chiarelli, A. M., Croce, P., Merla, A., & Zappasodi, F. (2018). Deep learning for hybrid EEG-fNIRS brain-computer interface: Application to motor imagery classification. *Journal of Neural Engineering*. doi: 10.1088/1741-2552/aaaf82

Dahl, G. E., Sainath, T. N., & Hinton, G. E. (2013). Improving deep neural networks for LVCSR using rectified linear units and dropout. *ICASSP, IEEE International Conference on Acoustics, Speech and Signal Processing - Proceedings*. doi: 10.1109/ICASSP.2013.6639346

Deligani, R. J., Borgheai, S. B., McLinden, J., & Shahriari, Y. (2021). Multimodal fusion of EEG-fNIRS: a mutual information-based hybrid classification framework. *Biomedical Optics Express*.

Deriche, M., & Al-Ani, A. (2001). A new algorithm for EEG feature selection using mutual information. *2001 IEEE International Conference on Acoustics, Speech, and Signal Processing. Proceedings (Cat. No. 01CH37221) (Vol. 2)*, 4.

Erdoĝan, S. B., Özsarfati, E., Dilek, B., Kadak, K. S., Hanoĝlu, L., & Akin, A. (2019). Classification of motor imagery and execution signals with population-level feature sets: Implications for probe design in fNIRS based BCI. *Journal of Neural Engineering*. doi: 10.1088/1741-2552/aafdca

Fazli, S., Mehnert, J., Steinbrink, J., Curio, G., Villringer, A., Müller, K. R., &

Blankertz, B. (2012). Enhanced performance by a hybrid NIRS-EEG brain computer interface. *NeuroImage*. doi: 10.1016/j.neuroimage.2011.07.084

Ghonchi, Hamidreza, et al. (2020). Spatio-temporal deep learning for EEG-fNIRS brain computer interface. *42nd Annual International Conference of the IEEE Engineering in Medicine & Biology Society (EMBC). IEEE*.

Hajinoroozi, M., Jung, T. P., Lin, C. T., & Huang, Y. (2015). Feature extraction with deep belief networks for driver's cognitive states prediction from EEG data. *2015 IEEE China Summit and International Conference on Signal and Information Processing, ChinaSIP 2015 - Proceedings*. doi: 10.1109/ChinaSIP.2015.7230517

Hennrich, J., Herff, C., Heger, D., & Schultz, T. (2015). Investigating deep learning for fNIRS based BCI. *Proceedings of the Annual International Conference of the IEEE Engineering in Medicine and Biology Society, EMBS*. doi: 10.1109/EMBC.2015.7318984

Hong, K. S., Khan, M. J., & Hong, M. J. (2018). Feature Extraction and Classification Methods for Hybrid fNIRS-EEG Brain-Computer Interfaces. In Frontiers in Human Neuroscience. doi: 10.3389/fnhum.2018.00246

Hong, K. S., Naseer, N., & Kim, Y. H. (2015). Classification of prefrontal and motor cortex signals for three-class fNIRS-BCI. *Neuroscience Letters*. doi: 10.1016/j.neulet.2014.12.029

Hosni, S. M., Deligani, R. J., Zisk, A., McLinden, J., Borgheai, S. B., & Shahriari, Y. (2020). An exploration of neural dynamics of motor imagery for people with amyotrophic lateral sclerosis. *Journal of Neural Engineering*, *17*(1). doi: 10.1088/1741-2552/ab4c75

Hua, J., Xiong, Z., Lowey, J., Suh, E., & Dougherty, E. R. (2005). Optimal number of features as a function of sample size for various classification rules. *Bioinformatics*. doi: 10.1093/bioinformatics/bti171

Jain, A. K., Duin, R. P. W., & Mao, J. (2000). Statistical pattern recognition: A review. *IEEE Transactions on Pattern Analysis and Machine Intelligence*. doi: 10.1109/34.824819

Jirayucharoensak, S., Pan-Ngum, S., & Israsena, P. (2014). EEG-Based Emotion Recognition Using Deep Learning Network with Principal Component Based Covariate Shift Adaptation. *Scientific World Journal*. doi: 10.1155/2014/627892

Kingma, D. P., & Ba, J. L. (2015). Adam: A method for stochastic optimization. *3rd International Conference on Learning Representations, ICLR 2015 - Conference Track Proceedings*.

Ko, L. W., Lu, Y. C., Bustince, H., Chang, Y. C., Chang, Y., Ferandez, J., Wang, Y. K., Sanz, J. A., Pereira Dimuro, G., & Lin, C. T. (2019). Multimodal fuzzy fusion for enhancing the motor-imagery-based brain computer interface. *IEEE Computational Intelligence Magazine*. doi: 10.1109/MCI.2018.2881647

Kocak, O., Beytar, F., Firat, H., Telatar, Z., & Erogul, O. (2017). *Comparison of non-*

parametric PSD detection methods in the anaylsis of EEG signals in sleep apnea. doi: 10.1109/tiptekno.2016.7863133

Kocsis, L., Herman, P., & Eke, A. (2006). The modified Beer-Lambert law revisited. *Physics in Medicine and Biology*. doi: 10.1088/0031-9155/51/5/N02

Krizhevsky, A., Sutskever, I., & Hinton, G. E. (2012). ImageNet classification with deep convolutional neural networks. *Advances in Neural Information Processing Systems*. doi: 10.1061/(ASCE)GT.1943-5606.0001284

Lecun, Y., Bengio, Y., & Hinton, G. (2015). Deep learning. In Nature. doi: 10.1038/nature14539

Li, M. A., Wang, Y. F., Jia, S. M., Sun, Y. J., & Yang, J. F. (2019). Decoding of motor imagery EEG based on brain source estimation. *Neurocomputing*. doi: 10.1016/j.neucom.2019.02.006

Li, R., Potter, T., Huang, W., & Zhang, Y. (2017). Enhancing performance of a hybrid EEG-fNIRS system using channel selection and early temporal features. *Frontiers in Human Neuroscience*. doi: 10.3389/fnhum.2017.00462

Lin, X., Sai, L., & Yuan, Z. (2018). Detecting Concealed Information with Fused Electroencephalography and Functional Near-infrared Spectroscopy. *Neuroscience*. doi: 10.1016/j.neuroscience.2018.06.049

Liu, K., Yu, Z. L., Wu, W., Gu, Z., & Li, Y. (2020). Imaging brain extended sources from EEG/MEG based on variation sparsity using automatic relevance determination. *Neurocomputing*. doi: 10.1016/j.neucom.2020.01.038

Liu, Y., Ayaz, H., & Shewokis, P. A. (2017). Mental workload classification with concurrent electroencephalography and functional near-infrared spectroscopy. *Brain-Computer Interfaces*. doi: 10.1080/2326263X.2017.1304020

Ma, Z., Tan, Z. H., & Guo, J. (2016). Feature selection for neutral vector in EEG signal classification. *Neurocomputing*. doi: 10.1016/j.neucom.2015.10.012

McFarland, D. J., McCane, L. M., David, S. V., & Wolpaw, J. R. (1997). Spatial filter selection for EEG-based communication. *Electroencephalography and Clinical Neurophysiology*. doi: 10.1016/S0013-4694(97)00022-2

Meyer, P. E., Schretter, C., & Bontempi, G. (2008). Information-theoretic feature selection in microarray data using variable complementarity. *IEEE Journal on Selected Topics in Signal Processing*. doi: 10.1109/JSTSP.2008.923858

Mikolov, T., Karafiát, M., Burget, L., Jan, C., & Khudanpur, S. (2010). Recurrent neural network based language model. *Proceedings of the 11th Annual Conference of the International Speech Communication Association, INTERSPEECH 2010*.

Mu, Z., & Hu, J. (2009). Research of EEG identification computing based on AR model. *FBIE 2009 - 2009 International Conference on Future BioMedical Information Engineering*. doi: 10.1109/FBIE.2009.5405847

Nasihatkon, B., Boostani, R., & Jahromi, M. Z. (2009). An efficient hybrid linear and kernel CSP approach for EEG feature extraction. *Neurocomputing*. doi: 10.1016/j.neucom.2009.07.012

Nguyen, T., Ahn, S., Jang, H., Jun, S. C., & Kim, J. G. (2017). Utilization of a combined EEG/NIRS system to predict driver drowsiness. *Scientific Reports*. doi: 10.1038/srep43933

Peng, H., Li, C., Chao, J., Wang, T., Zhao, C., Huo, X., & Hu, B. (2019). A novel automatic classification detection for epileptic seizure based on dictionary learning and sparse representation. *Neurocomputing*. doi: 10.1016/j.neucom.2019.12.010

Pisinger, D. (2006). Upper bounds and exact algorithms for p-dispersion problems. *Computers and Operations Research*. doi: 10.1016/j.cor.2004.09.033

Putze, F., Hesslinger, S., Tse, C. Y., Huang, Y. Y., Herff, C., Guan, C., & Schultz, T. (2014). Hybrid fNIRS-EEG based classification of auditory and visual perception processes. *Frontiers in Neuroscience*. doi: 10.3389/fnins.2014.00373

Saadati, M., Nelson, J., & Ayaz, H. (2020a). Convolutional neural network for hybrid fNIRS-EEG mental workload classification. *Advances in Intelligent Systems and Computing*. doi: 10.1007/978-3-030-20473-0_22

Saadati, M., Nelson, J., & Ayaz, H. (2020b). Multimodal fNIRS-EEG classification using deep learning algorithms for brain-computer interfaces purposes. *Advances in Intelligent Systems and Computing*. doi: 10.1007/978-3-030-20473-0_21

Scarpa, F., Cutini, S., Scatturin, P., Dell'Acqua, R., & Sparacino, G. (2010). Bayesian filtering of human brain hemodynamic activity elicited by visual short-term maintenance recorded through functional near-infrared spectroscopy (fNIRS). *Optics Express*. doi: 10.1364/oe.18.026550

Schalk, G., McFarland, D. J., Hinterberger, T., Birbaumer, N., & Wolpaw, J. R. (2004). BCI2000: A general-purpose brain-computer interface (BCI) system. *IEEE Transactions on Biomedical Engineering*. doi: 10.1109/TBME.2004.827072

Sur, S., & Sinha, V. (2009). Event-related potential: An overview. *Industrial Psychiatry Journal*. doi: 10.4103/0972-6748.57865

Tanveer, M. A., Khan, M. J., Qureshi, M. J., Naseer, N., & Hong, K. S. (2019). Enhanced drowsiness detection using deep learning: An fNIRS Study. *IEEE Access*. doi: 10.1109/ACCESS.2019.2942838

Thanh Hai, N., Cuong, N. Q., Dang Khoa, T. Q., & Van Toi, V. (2013). Temporal hemodynamic classification of two hands tapping using functional near-infrared spectroscopy. *Frontiers in Human Neuroscience*. doi: 10.3389/fnhum.2013.00516

Wu, C. W., Tsai, P. J., Chen, S. C. J., Li, C. W., Hsu, A. L., Wu, H. Y., Ko, Y. T., Hung, P. C., Chang, C. Y., Lin, C. P., Lane, T. J., & Chen, C. Y. (2019). Indication of dynamic neurovascular coupling from inconsistency between EEG and fMRI indices across sleep–wake states. *Sleep and Biological Rhythms*. doi: 10.1007/s41105-019-00232-1

Yang, M., Li, J., Li, Z., Yao, D., Liao, W., & Chen, H. (2017). Whole-brain functional connectome-based multivariate classification of post-stroke aphasia. *Neurocomputing*. doi: 10.1016/j.neucom.2016.10.094

Yin, X., Xu, B., Jiang, C., Fu, Y., Wang, Z., Li, H., & Shi, G. (2015). A hybrid BCI based on EEG and fNIRS signals improves the performance of decoding motor imagery of both force and speed of hand clenching. *Journal of Neural Engineering*. doi: 10.1088/1741-2560/12/3/036004

Zhang, P., Wang, X., Chen, J., & You, W. (2017). Feature weight driven interactive mutual information modeling for heterogeneous bio-signal fusion to estimate mental workload. *Sensors (Switzerland)*. doi: 10.3390/s17102315

VITA

Roohollah Jafari Deligani
Electrical, Computer and Biomedical Engineering Department
University of Rhode Island, Kingston, RI
Email: rjafari@uri.edu**, Cell:** +1 (734) 846-3261

PhD. Electrical, Computer and Biomedical Engineering, Neural processing and control lab, University of Rhode Island
M. Sc. in Biomedical Engineering, Bio-Electrics, University of Tehran
B. Sc. in Electrical Engineering, Communications, Isfahan University of Technology (IUT)

Selected publications:

R. J. Deligani, B. Borgheai, J. McLinden, Y. Shahriari. Multimodal fusion of EEG-fNIRS: A mutual information-based hybrid classification framework. Biomedical Optics Express; 2021; 12(3) (16 pp).

R. J. Deligani, S. I. Hosni, S. B. Borgheai, J. McLinden, A. H. Zisk, K. Mankodiya, Y. Shahriari. Electrical and Vascular Neural Functions in People with ALS: An EEG-fNIRS Resting-State Study. IEEE Transactions on Neural Systems and Rehabilitation Engineering; 2020; 1558-0210 (10pp).

B. Borgheai, **R. J. Deligani**, J. McLinden, A. Zisk, S. I. Hosni, M. Abtahi, K. Mankodiya, Y. Shahriari. Multimodal Exploration of Non-motor Neural Functions in ALS Patients Using Simultaneous EEG-fNIRS Recording. Journal of Neural Engineering; 2019; 16:066036 (15pp) (co-first authors).

J. McLinden**, R. J. Deligani**, M. R. Abtahi, U. Akbar, K. Mankodiya, Y. Shahriari. Disruptions of Cortico-Kinematic Interactions in Parkinson's Disease. Behavioral Brain Research; 2021; 404:113153 (9 pp).

A. H. Zisk, S. B. Borgheai, J. McLinden, S. I. Hosni, **R. J. Deligani**, Y. Shahriari. Latency Jitter and its Correlates in People with Amyotrophic Lateral Sclerosis. Clinical Neurophysiology Journal; 2020, 132(2) (11 pp).

S. I. Hosni, **R. J. Deligani**, A. Zisk, J. McLinden, S. B. Borgheai, Y. Shahriari. An Exploration of Neural Dynamics of Motor Imagery for People with Amyotrophic Lateral Sclerosis. Journal of Neural Engineering; 2019; 17:016005 (15pp).

S.B. Borgheai, S. I. Hosni, **R. J. Deligani**, A. Zisk, J. McLinden, M. Abtahi, K. Mankodiya, Y. Shahriari. Enhancing Communication for People in Late Stage ALS Using a fNIRS-Based BCI System. IEEE Transactions on Neural Systems and Rehabilitation Engineering; 2020; 28 (10 pp).

R. J. Deligani, S. I. Hosni, T. M. Vaughan, L. M. McCane, D. J. Zeitlin, D. J. McFarland, D. J. Krusienski, Y. Shahriari, "Neural Alterations During Use of a P300-based BCI by Individuals with Amyotrophic Lateral Sclerosis", In Neural Engineering, 8th IEEE/EMBS Conference, 2019